**UNIVERSIDAD DE SALAMANCA**
**FACULTAD DE CIENCIAS**
**Departamento de Física Aplicada**
**Área de Óptica**

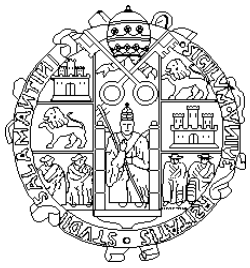

# On the generation and propagation of harmonics in ionizing media

**Enrique Conejero Jarque**

**Salamanca, April 1998**

**UNIVERSIDAD DE SALAMANCA**
**FACULTAD DE CIENCIAS**
**Departamento de Física Aplicada**
**Área de Óptica**

# On the generation and propagation of harmonics in ionizing media

Memoria que presenta Enrique Conejero Jarque ante la Facultad de Ciencias de la Universidad de Salamanca para optar al Grado de Doctor en Ciencias Físicas

**Salamanca, Abril 1998**

LUIS PLAJA RUSTEIN, AYUDANTE DE FACULTAD DEL AREA DE OPTICA DE LA UNIVERSIDAD DE SALAMANCA, CERTIFICA:

Que la presente Memoria, "**Sobre la generación y propagación de armónicos en medios ionizables**" ha sido realizada bajo su dirección en el Área de Óptica del Departamento de Física Aplicada de la Universidad de Salamanca por el Licenciado Enrique Conejero Jarque y constituye su Tesis para optar al grado de Doctor en Ciencias Físicas.

Salamanca, Abril de mil novecientos noventa y ocho.

A todos los que me han hecho reír

*Maiorum more rite secuto in cuiuslibet operis capite locus*
*ex scriptis alicuius illustris auctoris depromptus interdum imponitur.*
*Quae quidem sententia ad rem expositam saepius nihil prorsus refert,*
*sed tantummodo ad scriptoris scientiam ostendendam eruditionemque*
*eius ingentem uindicandam adlatam esse comperimus.*
*Cui rei populi uox accedit opportuna:*
*quae de te gloriose praedicas, ipsis indiges.*

CAIUS FACETUS

## List of publications

Publications upon which this report is based:

- E. Conejero Jarque and L. Plaja, "Effect of time-dependent ionization on the harmonics generated by bound-bound transitions", J. Opt. Soc. Am. B **13**, 2724 (1996).

- E. Conejero Jarque and L. Plaja, "Harmonic generation with ionizing two-level atoms", J. Phys. B: At. Mol. Opt. Phys. **31**, 1687 (1998).

- L. Plaja and E. Conejero Jarque, "Introduction of the Liénard-Wiechert correction to the particle simulation of relativistic plasmas", accepted for publication in Phys. Rev. E.

- V. Malyshev, E. Conejero Jarque and L. Roso, "Self-reflection of an intense ultrahort laser pulse by tunnel ionization on a solid surface", J. Opt. Soc. Am. B **14**, 163 (1997).

- E. Conejero Jarque, V. Malyshev and L. Roso, "Self-reflection and high-order harmonic generatin due to plasma effect on the surface of a solid insulator: normal incidence", J. Mod. Opt. **44**, 563 (1997).

- E. Conejero Jarque and L. Plaja, "Harmonic generation during the ionization of a thin target irradiated by a strong laser field", submitted to J. Opt. Soc. Am. B.

- E. Conejero Jarque and L. Plaja, "Harmonic filtering in a laser generated thin plasma", submitted to Phys. Rev. E.

Other work carried out in the predoctoral period and not mentioned in this report:

- V. Malyshev and E. Conejero Jarque, J. Opt. Soc. Am. B **12**, 1868 (1995).
- V. Malyshev and E. Conejero Jarque, J. Opt. Soc. Am. B **14**, 1167 (1997).
- E. Conejero Jarque and V. Malyshev, Opt. Comm. **142**, 66 (1997).
- V. A. Malyshev and E. Conejero Jarque, Opt. and Spectr. **82**, 582 (1997).
- V. Malyshev and E. Conejero Jarque, J. Lumin. **72-74**, 822 (1997).
- L. Plaja, E. Conejero Jarque and L. Roso, submitted to Astrophys. J. Suppl.
- E. Conejero Jarque and L. Plaja, in *Superstrong fields in plasmas*, M. Lontano, G. Mourou, F. Pegoraro and E. Sindoni, eds., AIP Conf. Proc. **426**, 360 (1998).
- F. Cornolti, A. Macchi and E. C. Jarque, in *Superstrong fields in plasmas*, M. Lontano, G. Mourou, F. Pegoraro and E. Sindoni, eds., AIP Conf. Proc. **426**, 55 (1998).

# Agradecimientos y demás

Tentado estoy de omitir estas páginas, tan importantes o más que las conclusiones en una tesis. Y no es la ingratitud la que me mueve a ello sino el hecho de que si tuviera que agradecer todo lo que debo, esto parecería el listín telefónico y la memoria simple apéndice suyo. La fuerza de la costumbre y, como digo, el miedo a parecer ingrato, me empujan a cumplimentar este requisito. Además, esto es lo único que no pasa censura, así que ahí va la letanía.

Comenzando por el terreno científico, debo agradecer la labor de las tres personas con las que tengo el honor de firmar los artículos en los que se basa este trabajo. Ellas han conseguido la incomparable hazaña de que un holgazán, ametódico, descreído, somnoliento, irracionalista, aficionado al fútbol y telespectador compulsivo, amén de otros muchos calificativos que pueden aplicárseme y que no vienen al caso, han conseguido, digo, que pueda presentar este trabajo, esperando, con la venia del tribunal, obtener el grado de doctor.

En primer lugar, y vergüenza me da decirlo puesto que él es el principal autor de lo que de bueno tiene este trabajo y yo simple escribano, agradezco al director de la tesis la arriesgada elección de su primer discípulo, tal vez, todo hay que decirlo, por falta de otro (discípulo) mejor en ese momento. Durante el tiempo que ha llevado la realización de esta tesis el único enfrentamiento reseñable que hemos tenido ocurrió el pasado verano en Varenna, tranquilo pueblecillo a la vera del lago de Como, cuando dos simpáticas conserjes de nuestro hotel me abordaron en un ascensor para sonsacarme si mi estudiante tenía novia. Yo les contesté que en realidad era él el maestro, que tenía

la edad de Cristo, dos hijos y estaba divorciado. En aquel mismo instante me di cuenta de lo viejo que soy y lo joven que parece. Las chicas no se creyeron nada pero él las rechazó porque no eran demasiado agraciadas. Juró venganza, eso sí.

También soy, creo, el primer discípulo del ex-capitán del Ejército Rojo que se atrevió a dirigirme la tesina y me enseñó que para inventar la bicicleta hace falta pensar mucho. Nunca le agradeceré lo suficiente todo lo que ha hecho por desasnarme científicamente. Espero que lo siga haciendo.

Poco puedo decir del dilectísimo y adoradísimo gran jefe. Le agradezco no sólo el dinero que consigue para ordenadores sino sus sabios y ponderados consejos en todos los terrenos y la oportunidad que me dio de unirme a un grupo entonces pequeño pero muy prometedor. Es tan entrañable que ahora incluso se preocupa por mi deteriorada salud mental.

A continuación agradezco a todos los que han sido y son miembros del grupo subversivo *El fotón charro* especialmente por aguantarme cuando invado su territorio profiriendo blasfemias en alta voz. No nombro a todos por si me dejo alguno. Mención especial merece aquél que me ha proporcionado los programas del hidrógeno y su propia tesis, sobre la que he escrito esta. Es una de las pocas personas con las que he compartido cama, en su caso por obligación. También la merece el otro que ha compartido conmigo habitación y lavabo, pero no cama, durante tres largos años en el Bartolo, aparte de dieciséis en las aulas, y sin el cual me temo que todavía estaría intentando ejecutar mi primer programa (el famoso *Hello, world!*) en una máquina UNIX. Debo recordar también a las dos personas que me abrieron las puertas de la óptica antes incluso de que hubiera acabado la carrera, cuando aún no sabía qué quería ser de mayor. Ellos y mi compañera de despacho, que escucha paciente mis diarias imprecaciones por los cuelgues de *blas.usal.es* y me deja el diccionario de inglés, han soportado y soportan con resignación mi ineptitud experimental sin una mala queja.

Gracias también a ti, querido lector, por haber llegado al menos hasta

este punto de los agradecimientos. ¡Adelante, ya falta poco!

Por una vez, quiero agradecer públicamente al vicario del Magnífico en la Tierra, léase el Director de nuestro Departamento, la impagable ayuda prestada en aspectos administrativo-burocráticos. Es más, en su honor escribiré aquí las palabras *lentes* y *gafas*, que, creo, no vuelven a aparecer en toda la memoria.

Debo recordar también, porque me lo exigió expresamente, a ese exanarquista y ahora suspendedor de aprendices de optometría en tierras murcianas que se pasó seis horas de reloj fotocopiándome unas tablas de secciones eficaces de colisión en las frías tierras germanas. He cumplido.

No puedo dejar de hacer mención al amigo italiano, amantísimo padre de familia y gran estudioso de la receta del bacalao al pil-pil, a quien nunca perdonaré que nos metiera en el mundillo de los plasmas, en el que aún brilla más nuestra ignorancia. Y en este capítulo internacional, obligada es también la referencia al corrector de la versión inglesa de la tesis, quien prácticamente la ha reescrito con rotulador verde sobre un penoso borrador de mi cosecha que parecía producto de uno de esos abominables programas traductores con los que pretenden subdesarrollarnos.

Y en el terreno amistoso, aunque no se descarta alguna colaboración científica, me acuerdo también de mis coleguillas de francachelas y tertulias, por desgracia cada vez menos frecuentes a medida que crecen nuestros ingresos (de algunos) y disminuye nuestro pelo (de todos).

Finalmente, y no por ser lo menos importante sino todo lo contrario, paso a lo afectivo. Me refiero aquí a mi familia, tanto biológica como adquirida, porque, como decía don Vito Corleone, la familia es lo más importante en la vida. Todos ellos han soportado, e incluso han echado de menos, mi habitual desidia comunicativa, se han preocupado por mí más que yo mismo y hasta han llorado de vez en cuando por mi causa. Un beso para cada uno y dos, pues si no se queja, para Laura.

# Index

**2**

# Introduction

In recent decades there has been renewed interest in study of the interaction between electromagnetic fields and matter. The main reason is undoubtedly the availability of shorter and more intense laser pulses which are continuously improving in such a way that it takes only a few months to reduce their duration by a few femtoseconds and their intensity by some terawatts. Hence, theoretical assumptions that earlier seemed experimentally unfeasible, are now realized in laboratories in a fairly straightforward way. On the other hand, experiments are now so abundant that a better understanding of the physical phenomena involved is necessary to interpret the results obtained. This joint effort involves researchers who come from such different disciplines as optics, atomic and molecular physics, plasma physics, and, recently, even nuclear physics, quantum electrodynamics and astrophysics. The possibilities of such a broad subject are therefore unlimited.

One of the most attractive phenomena is harmonic generation because it has been shown to be a process able to provide us with coherent and relatively intense radiation sources with frequencies in the range of the ultraviolet and soft X-rays. The infrared and visible laser being so important in all aspects relating to atomic and molecular structure, we can expect that the X-ray laser will play a similar role regarding nuclear structure, relativistic phenomena, and perhaps other applications which are barely imagined today. As an example, the creation of electron-positron pairs has been observed in laser experiments, a phenomenon that will be more likely if the frequencies of the lasers are higher. Another possible application of

high harmonics currently under study is the achievement of trains of attosecond pulses, for which the name of "ultrashort" is really long.

The generation of high harmonics seems to be strongly linked to the ionization process. As we shall see, the ionization and subsequent recombination of electrons is the source of the harmonics in a low density gas. In a solid or plasma, harmonic radiation is generated by the motion of the electrons ionized either by the laser or by any other mechanism. Moreover, if we wish to obtain significant efficiencies we need much more than a single radiating atom or electron: we need an extended medium whose particles, the more the better, will emit radiation in a coherent way. This is the reason why the study of the propagation of harmonics is also crucial.

In this work, we wish to add our small contribution to the study of harmonic generation and propagation in ionizing media. Since we are not very good in the lab and computers are becoming cheaper and cheaper, our contribution will be theoretical, with a lot of numerical calculations because simulations are a very good tool not only for understanding the physical phenomena but also for contrasting the experimental results. The ionizing media we are referring to are mainly of two kinds. First, we have isolated atoms, which are relatively easy to study. The conclusions obtained from the study of isolated atoms can be extended to the case of rare gases in which atom-atom interactions can be neglected. However, if we raise the density of the medium as well as the laser intensity in such a manner that the ionization becomes noticeable, atom-atom (or ion-ion) and atom-free electron interactions dramatically change the phenomenology, rendering the radiation emitted completely different. This is why we also have to study other ionizing media such as solids, which rapidly generate a plasma when impinged by intense enough pulses. As we shall see below, plasmas are also able to generate high harmonics and they even have some advantages over gases in this respect.

To date, the problem of the interaction of an atom and an electromagnetic

field has only been exactly solved in the case of hydrogen-like atoms, which is the one we shall consider along this work. However, regarding harmonic generation the results can be extended without important changes to other kinds of atoms. The experimental results are quite similar with low pressure alkaline and noble gases. This is undoubtedly due to the fact that the processes involved in harmonic generation, in particular ionization, are qualitatively the same for all of them. The study of solid media is even more difficult because the number of particles involved in the interactions is practically infinite. Again, it has been experimentally observed that the harmonics generated by media as different as aluminum and plastic are similar in the case of short and intense enough pulses. The reason is that for such pulses a nearly complete ionization is achieved in very few optical cycles (sometimes less than one) and afterwards both of them only comprise a set of electrons and atoms moved by the field. We can therefore idealize our medium by representing it by a set of atoms, which again will be hydrogen-like for the sake of simplicity, and which -after ionization- become an ion plus an electron evolving according to the laws of classical electrodynamics.

With regard to the electric field, we shall always consider this to be linearly polarized. In this case, both the scientific interest (the generation of harmonics is more efficient with linearly polarized fields in gases and in solids) and the numerical simplicity (this permits us to reduce the dimensionality of the problem) coincide. Moreover, the incident pulses will have only one main frequency. Both elliptically polarized fields and several-colour pulses are currently being studied owing to their possible application in the generation of ultrashort pulses and in the control of the efficiency of the harmonics, but we shall not use them in the present work. We shall neglect the effect of the secondary field in the case of the interaction of the field with single atoms because it is expected to be very weak. By contrast, when dealing with extended media, this secondary field will be essential and the total

field will be calculated in a self-consistent way.

Regarding the structure of this report, we have split the contents into four chapters. The first one is introductory and we shall use it to establish the basis of our work as well as to make a brief summary of what is known up to now. We shall review non-linear atomic ionization phenomenology, especially in the tunnelling regime, which is the most interesting for high harmonics generation, recalling some of the models proposed to explain that generation; we shall recover the expressions for the ionization rates that we shall use; we shall define what we mean when we speak about the emission spectrum of a (classical or quantum) system; we shall also review the generation of harmonics by free electrons. Finally, we shall sketch some aspects of the generation and propagation of harmonics in ionizing (or ionized) media which will be used later. Chapter two is devoted to the study of the generation of harmonics in a very simple system composed of two bound levels whose population can be ionized into a continuum state and then rescatter back with the core. The aim of this chapter is to determine the influence of a time-dependent ionization and the transitions between bound states on harmonic generation. These two effects are usually neglected in existing models. In chapter three, we explain how we simulate the interaction of a plasma with a laser pulse, paying special attention to certain problems which crop up when the dynamics of the particles is relativistic and to the inclusion of the ionization process, which is not usual in most of the codes. In chapter four, we shall explain the results obtained in our study of the harmonics generated during the ionization of a solid by a laser, establishing the relative importance of the different processes that contribute to this generation; we shall also see the importance of propagation effects, such as phase mismatch, frequency shifts or frequency filtering, in the case of large enough media.

Before we start, it is also appropriate to make a comment about the units used

in this report. We have nearly always used atomic units, which are the most useful to study the interaction between atoms and electromagnetic fields. Recall that atomic units are defined from the identities $e = m = \hbar = 1$, $c \simeq 137$, where $e$ and $m$ are the absolute values of the charge of the electron and its mass, and $c$ is the speed of light in vacuum. In this system, since $\hbar = 1$, both the energy and frequency are expressed with the same variable $\omega$. In the sections in which purely classical issues are dealt with, we prefer to use Gaussian units because they are more usual in the literature. The expressions related to electromagnetic fields are almost identical in both unit systems. In addition, when we refer to experimental data such as wavelengths or laser intensities we shall give the equivalence in SI units for the better understanding of readers not familiar with atomic units.

# Chapter 1

# Preliminary concepts

## 1.1 Nonlinear atomic ionization

Atomic photoionization is a phenomenon that has drawn physicists' attention for almost a century and which is still very much alive. After being crucial for the introduction and acceptance of quantum theory, it is nowadays a clear example of the inadequacy of perturbative approaches to explain certain physical processes.

The ionization of a quantum system is nonlinear when the condition $\omega_0 < I_p$ is fulfilled, where $\omega_0$ is the frequency of the incident radiation and $I_p$ is the ionization potential, i.e. the energy necessary to extract the least bound electron of the system [1]. It is clear that such a process violates Einstein's expression for the photoelectric effect [2], but one can overcome this problem if a multiphoton ionization which satisfies $K\omega_0 > I_p$, $K$ being the integer number of photons absorbed by the system, is introduced. Multiphoton processes are of course not restricted to the case of ionization (which is a transition from a bound to a continuum level) but they can be extended to any transition between bound states, changing Bohr's third postulate from its initial form $\omega_0 = E_f - E_i$ to the multiphoton one $K\omega_0 = E_f - E_i$. Physically, the possibility of having multiphoton transitions is justified by the uncertainty principle for energy and time, $\delta\omega\delta t \geq 1$, which permits the system to pass through virtual states during a time $\delta t$ with an energy defect $\delta\omega$.

### 1.1.1 Kinds of nonlinear ionization

The nonlinear ionization process mainly depends on three parameters: the frequency $\omega_0$ and amplitude $E_0$ of the electromagnetic field and the ionization potential of the electron $I_p$. In fact, a combination of these parameters, the so-called Keldysh adiabaticity parameter [3] defined as

$$\gamma = \frac{\omega_0 (2I_p)^{1/2}}{E_0} = \sqrt{\frac{I_p}{2U_p}}, \tag{1.1}$$

separates the different regimes of nonlinear ionization in atoms. $U_p = E_0^2/4\omega_0^2$ is the ponderomotive energy, which is the mean energy absorbed by a free electron from the electromagnetic field in one optical cycle.

Let us now review the different kinds of ionization when the electromagnetic field amplitude is much lower than the atomic field (good reviews of the interaction of atoms with intense fields, including many references, can be found in [1, 4, 5, 6, 7]).

#### Multiphoton ionization

If the condition $\gamma \gg 1$ is fulfilled -that is, the ionization potential is much higher than the ponderomotive energy, which happens for relatively high frequencies (always below the ionization potential, of course) or weak fields- the most likely process is the so-called multiphoton ionization (MPI). In this case, we can graphically describe the process as the absorption of an integer number of photons $K$ by an electron, which passes to the continuum with a kinetic energy given by $\omega_f = K\omega_0 - I_p$. The ionization rate (probability of ionization in a time unit) for weak fields takes the form

$$w = \sigma^{(K)} \left( \frac{E_0^2}{\omega_0} \right)^K, \tag{1.2}$$

where $\sigma^{(K)}$ is the generalized cross section, which depends on the frequency and the polarization of the field and also on the atomic structure but not on the field

intensity. It is evident that for $K = 1$ we recover the well-known photoelectric effect formula, whose dependence on the field intensity is linear. However, when the field is intense enough, processes involving a number of photons higher than that strictly necessary can take place with a similar probability. In this case, we have above-threshold ionization (ATI), for which the final energy of the electron will be $\omega_f = (K + S)\omega_0 - I_p$, $S$ being the additional number of absorbed photons. The first experiments about multiphoton ionization were performed in 1977 by Lompré *et al.* [8], whilst above-threshold ionization was first reported by Pierre Agostini *et al.* in 1979 [9].

**Tunnelling ionization**

Let us now go to the case when the Keldysh parameter is smaller than unity, which happens for very low frequencies and moderately intense fields. We are then within the so-called tunnelling ionization (TI) regime, which will be the most interesting for us due to the peculiarity of the harmonics generated in it. In order to understand what happens in this regime, it is very useful to remember how an intense static field affects an atom. Let us think, for the sake of simplicity, of a hydrogen atom in its fundamental state. The wavepacket is then strongly bounded by the Coulomb barrier, as we can observe in figure 1.1a. When an external field that is linearly polarized in the $x$ direction is applied, the instantaneous potential is modified, taking the form $V = -1/r + Ex$ (figure 1.1b). The electron "sees" a potential barrier through which it can go via the tunnelling effect if the field is intense enough. The calculations used to obtain the ionization rate are relatively simple and yield the expression [10]

$$w = \frac{4}{E} \exp\left(-\frac{2}{3E}\right), \tag{1.3}$$

which, as expected, grows with the field intensity.

In the tunnelling regime we have no static field but the frequency is so small

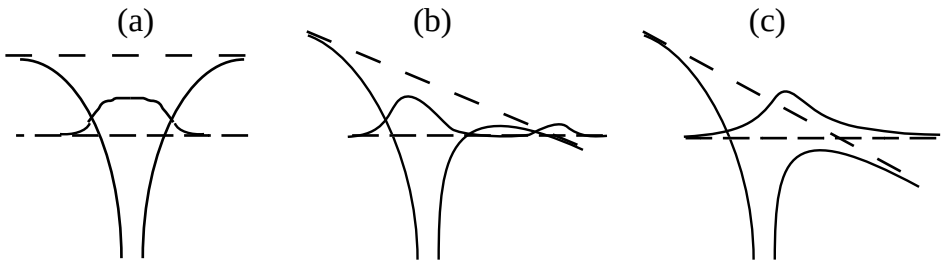


Figure 1.1: Scheme of the evolution of the atomic wavepacket in the absence of an external field (a), when the field permits tunnelling ionization (b) and when the field is so intense that there is barrier suppression.

that we can use an adiabatic approach, valid when the optical cycle is much longer than the tunnelling time. This tunnelling time can be estimated simply as the ratio of the distance between the points where the potential barrier crosses the unperturbed energy of the electron and the velocity of the electron inside the barrier [11, 12]. The result is $\tau_t \approx \sqrt{I_p}/E_0$. The electron can pass through the barrier when this time is shorter than one optical cycle, i.e., when the Keldysh parameter is smaller than unity. It can then be assumed that the electron "sees" a potential barrier which evolves so slowly that it permits the electron to cross via tunnelling. After half a cycle the field will change its sign and part of the ionized population will come back to the neighbourhood of the core. We shall later see the important effect of this population on the generation of harmonics.

### Barrier suppression ionization

The limiting case of tunnelling is the so-called barrier suppression ionization (BSI), which is depicted in figure 1.1c. This kind of ionization takes place when the field amplitude is so high that the potential barrier lies below the ionization potential level, the electron wavepacket being free to escape from the nucleus. For even higher intensities, and contrary to what one would expect intuitively, the ionization is not so fast, but a stabilization regime can be reached in which a large amount of the population is trapped in the bound states closest to the continuum (Rydberg

states) due to interference effects in the wavefunction. Both barrier suppression ionization and stabilization cannot be readily observed in the experimental setting because they require such intense fields that the atoms are first ionized either by tunnelling or by multiphoton channels during the first part of the pulses before they interact with the peak pulses.

## 1.2 Ionization rate in the tunnelling regime

We believe that it is convenient to sketch the deduction of the expression for the ionization rate in the tunnelling regime since it will be used quite frequently along this work [1, 14, 15].

Let us start with the expression which gives the probability amplitude of a transition between an initial bound state $|i\rangle$ and a final continuum state $|f\rangle$, which is given in the interaction picture by the S-matrix element [13]:

$$a_{if}(t) = -i \int_0^t \langle \Psi_f \mid V(\mathbf{r}, t') \mid \Psi_i^0 \rangle dt'. \tag{1.4}$$

where $V(\mathbf{r}, t)$ includes, in principle, both the Coulomb potential and the interaction with the external electromagnetic field.

The Keldysh-Faisal-Reiss approach [3, 16, 17] (KFR in the literature) consists in neglecting the Coulomb contribution to the continuum state. In this case, the interaction term in the momentum gauge takes the form

$$V(\mathbf{r}, t) = \frac{\mathbf{p} \cdot \mathbf{A}}{c} + \frac{\mathbf{A}^2}{2c^2} \tag{1.5}$$

and the final state is a Volkov wave:

$$\Psi_f^{(V)} = \exp\Big[-i\mathbf{p}\mathbf{r} + \frac{i}{2}\int (\mathbf{p} + \frac{\mathbf{A}}{c})^2 dt\Big]. \tag{1.6}$$

If we wish to take into account the effect of the atomic potential on the final state, we can use the perturbative theory and pass from $\Psi_f^{(V)}$ to $I\Psi_f^{(V)}$, where the

Coulomb correction is given by [14]

$$I = \exp\Big(-i\int \frac{-Z}{r}dt\Big), \tag{1.7}$$

where $Z$ is the atom or ion charge. This correction is determined by the moments of time during which the field is near its extreme values because then the probability of the electron crossing the barrier is maximum. The integral in (1.4) takes one or another value depending on the initial state and on the electromagnetic field polarization. For instance, when the initial state has a principal quantum number $n$ and an orbital number $l = 0$, and the field is linearly polarized, $\mathbf{E} = E_0 \cos\omega_0 t\ \hat{x}$, the transition amplitude, if the field is weak enough, is

$$a_{nf}(t) = \frac{2^n}{n!}\Big(\frac{C_I Z\pi}{n}\Big)^{1/2}\int_0^t \exp\left[ig(t')\right]dt', \tag{1.8}$$

where $C_I = (2Z^3/n^3E_0)^{2n}$ comes from the Coulomb interaction term $I$ and the function $g(t)$ is defined as

$$g(t) = \left(\frac{p^2}{2} + \frac{Z^2}{2n^2} + \frac{E_0^2}{4\omega_0^2}\right)t + \frac{p_x E_0}{\omega_0^2}\cos\omega_0 t - \frac{E_0^2}{8\omega_0^3}\sin 2\omega_0 t. \tag{1.9}$$

In order to solve (1.8), the different contributions of each field cycle must be added, and the following expression is obtained for the transition probability

$$W_{nf}(t) = |a_{nf}(t)|^2 = \left|a_{nf}\left(\frac{2\pi}{\omega_0}\right)\right|^2 \frac{\omega_0^2 t}{2\pi}\delta\left(\frac{p^2}{2} + \frac{Z^2}{2n^2} + \frac{E_0^2}{4\omega_0^2} - N\omega_0\right). \tag{1.10}$$

N is the number of photons absorbed in the process and the Dirac $\delta$ function stands for energy conservation. In order to find the angular and energy distribution of the ionized electrons in the $N$th-order process, it is sufficient to divide the previous expression by time, multiply the result by the final state density and integrate this over the momentum, obtaining

$$\frac{dw_N}{d\Omega} = \frac{2^{2n-1}p\omega_0^2 Z C_I}{(2\pi)^3 n n!^2}\ \Big|\int_0^{2\pi/\omega_0} \exp\left[ig(t)\right]dt\Big|^2, \tag{1.11}$$

where the momentum $p$ must fulfill the energy conservation law in equation (1.10). The integral in (1.11) is not easy to solve unless further approximations are done. In the tunnelling limit, when the field is below the barrier suppression value, the saddle-point or stationary phase method can be used (see, for instance, [18, 19]). In this method the only contributions to the integral that are taken into account are those coming from the most significant points, which are the classical turning points, i.e. those for which $\dot{g}(t) = 0$. Using this approximation and integrating over the angular momentum, it follows that

$$w_N = \frac{\omega_0^2 C_I 2^{2n}}{2\pi Z p} \exp\Big(-\frac{2Z^3}{3En^3} - \frac{p^2\gamma^3}{3\omega_0}\Big), \tag{1.12}$$

where $\gamma$ is the Keldysh parameter. Finally, summing up the number of photons we will have the total transition probability per unit of time

$$w = \frac{2^{2n} n C_I E}{4Z n!^2} \Big(\frac{3En^3}{\pi Z^3}\Big)^{1/2} \exp\Big(-\frac{2Z^3}{3n^3 E}\Big), \tag{1.13}$$

where we have used the condition that $\gamma << 1$ in the tunnelling regime. If we compare the previous expression with the one obtained for circular polarization, when the field amplitude always remains the same, we observe that

$$w_l = \Big(\frac{3En^3}{\pi Z^3}\Big)^{1/2} w_c, \tag{1.14}$$

where it is clear that this difference comes from averaging the electric field over one optical cycle in previous calculations. Hence, if we wish to use this expression for a time-dependent instantaneous field we must neglect the term $3En^3/\pi Z^3$.

It is also possible to perform the same calculations when the initial state has an angular momentum different from zero and for non-hydrogen-like atoms or ions. The general result is [20]

$$w(|E|) = C_I |C_{nl}|^2 f(l,m) \frac{Z^2}{2n^2} \Big(\frac{n^3|E|}{2Z^3}\Big)^{m+1} \exp\Big(-\frac{2Z^3}{3n^3|E|}\Big), \tag{1.15}$$

where $n$, $l$, $m$ are the effective quantum numbers and $f$ and $C_{nl}$ are defined as

$$f(l,m) = \frac{(2l+1)(l+|m|)!}{2^{|m|}(|m|)!(l-|m|)!}, \qquad |C_{nl}|^2 = \frac{2^{2n}}{n(n+l)!(n-l-1)!}. \tag{1.16}$$

In order to obtain averaged expressions, we have to substitute $|E|$ by $E_0$ and add the term $(3E_0n^3/\pi Z^3)^{1/2}$. It is trivial to check that in the case of the ground level of the hydrogen atom and a static field expression (1.15) reduces to (1.3).

The validity of the previous formulae is restricted, as we have mentioned, to the tunnelling regime. This imposes two restrictions on the field intensity. First, to ensure that the Keldysh parameter is smaller than one and that an adiabatic approach is valid, the field has to be intense enough (or its frequency very small, so that we should be within the infrared or even the microwaves regions in which tunnelling has been observed from Rydberg states [13, 21]). In this sense, when $\gamma \approx 1$ both tunnelling and multiphoton ionization coexist, although it has been observed that the obtained expressions are a good approximation in this borderline situation [22]. On the other hand, we know that to avoid the barrier suppression the field intensity cannot be too high. Calculation of the critical field value for which the potential barrier is exceeded is very simple if we assume that the electron escapes in the direction of the electric field. In this case, we only have to equate the bound energy $-I_p$ with the sum of the atomic and the interaction potential $-Z/x+Ex$, obtaining a critical field $E_{cr} = I_p^2/4Z$ [23]. For the hydrogen ground level its value is $E_{cr}^{1s} = 0.0625$ a.u., which means an intensity $I \simeq 1.4\times10^{14}\mathrm{W/cm}^2$. In fact, for a tridimensional system such as hydrogen, the critical value is higher because the motion of the electron is not restricted to the direction of the field polarization. The real barrier suppression occurs, in the case of the ground state, for a field $E_{cr}^{1s} \simeq 0.15$ a.u. ($I \simeq 10^{15}\mathrm{W/cm}^2$) [24, 25]. When the field amplitude is greater than this value, the expressions for the tunnelling ionization rate overestimate the real ionization rates in the barrier suppression regime [14].

In any case, these formulae are used in calculations dealing with atomic ioniza-

tion due to their simplicity and also because they have been tested experimentally with good results for different media [26]. We are especially interested in them because of their strong indirect dependence on time via the oscillating field.

## 1.3 Emission spectrum of a system. Harmonic generation

Harmonic generation is perhaps the most typical process of nonlinear optics. This phenomenon has been much studied since the appearance of the first experimental evidence of second harmonic generation in crystals [27, 28] due to the availability of more and more intense lasers. In rare gases, after the observation of low order harmonics, which could be explained with perturbative theories, higher order harmonics were soon detected whose intensity did not decrease exponentially with their order. Harmonics higher than the 150th order have recently been observed with neodymium ($\lambda = 1053$ nm) and titanium-sapphire ($\lambda = 800$ nm) lasers [29, 30]. Nowadays, the aim is not to break high frequencies records, since the soft X-ray range is easily reached, but rather to obtain better intensity efficiencies, as well as to gain a better understanding of the different mechanisms underlying coherent emission at such high frequencies.

Harmonic generation is therefore a general phenomenon. When we illuminate a medium with an intense electromagnetic field, both free and bound charges oscillate in a nonlinear way. This produces a secondary emission not only with the incident frequency but with other contributions, some of which are integer multiples of the initial one. These latter are the harmonics.

Before describing the generation of harmonics in real systems, it is convenient to recall what we mean when talking about the emission spectrum of a system. In this section we shall not use atomic but Gaussian units because the latter are more common in the literature.

### 1.3.1 Emission spectrum of classical particles

Liénard-Wiechert potentials are appropriate to find the energy radiated by a classical accelerated particle. We shall also use them when speaking about plasma simulations, so we think it useful to recall how they are calculated in 3D space. Let us start from the wave equations for the scalar and vector potentials [31]

$$\nabla^2\phi - \frac{1}{c^2}\frac{\partial^2}{\partial t^2}\phi = -4\pi\rho, \tag{1.17}$$

$$\nabla^2\mathbf{A} - \frac{1}{c^2}\frac{\partial^2}{\partial t^2}\mathbf{A} = -\frac{4\pi}{c}\mathbf{J}, \tag{1.18}$$

where $\rho$ and $\mathbf{J}$ are respectively the charge and current densities, and we have imposed the Lorentz gauge condition

$$\nabla\cdot\mathbf{A} + \frac{1}{c}\frac{\partial}{\partial t}\phi = 0. \tag{1.19}$$

The electric and magnetic field are given by

$$\mathbf{E} = -\nabla\phi - \frac{1}{c}\frac{\partial}{\partial t}\mathbf{A}, \tag{1.20}$$

$$\mathbf{B} = \nabla\times\mathbf{A}. \tag{1.21}$$

The Green's function technique is used to solve the wave equation. The retarded Green's function for the three-dimensional wave equation is [32]

$$G^+(\mathbf{r},t;\mathbf{r}',t') = \frac{\delta(t'-t+R/c)}{R};\quad t>t',\quad R=|\mathbf{r}-\mathbf{r}'|, \tag{1.22}$$

and the solution of the scalar potential is obtained simply as

$$\phi(\mathbf{r},t) = \int\int G^+(\mathbf{r},t;\mathbf{r}',t')\rho(\mathbf{r}',t')d\mathbf{r}'dt'. \tag{1.23}$$

The expression for the vector potential is obtained by replacing $\rho$ by $\mathbf{J}/c$. If we have only one particle whose charge is $q_m$, position $\mathbf{r}_m$ and velocity $\mathbf{v}_m$, the charge and current densities can be expressed as

$$\rho(\mathbf{r},t) = q_m\delta[\mathbf{r}-\mathbf{r}_m(t)] = q_m\delta\Big[\mathbf{r}-\mathbf{r}_m(0)-\int_0^t d\tau\mathbf{v}_m(\tau)\Big], \tag{1.24}$$

$$\mathbf{J}(\mathbf{r},t) = q_m\mathbf{v}_m(t)\delta[\mathbf{r}-\mathbf{r}_m(t)] = q_m\mathbf{v}_m(t)\delta\Big[\mathbf{r}-\mathbf{r}_m(0)-\int_0^t d\tau\mathbf{v}_m(\tau)\Big]. \tag{1.25}$$

Substituting (1.22) and (1.24) in (1.23) and performing the integral over $t'$ we arrive at

$$\phi_m(\mathbf{r},t) = q_m \int \frac{d\mathbf{r}'}{R}\delta\Big[\mathbf{r}' - \mathbf{r}_m(0) - \int_0^{t-R/c} d\tau \mathbf{v}_m(\tau)\Big], \tag{1.26}$$

and introducing the new variable

$$\mathbf{u} = \mathbf{r}' - \mathbf{r}_m(0) - \int_0^{t-R/c} d\tau\ \mathbf{v}_m(\tau); \quad d\mathbf{u} = (1-\beta_m\cdot\mathbf{n})|_{t-R/c}\ d\mathbf{r}', \tag{1.27}$$

with $\beta_m = \mathbf{v}_m/c$, $\mathbf{n} = (\mathbf{r}'-\mathbf{r})/R$ (the unit vector in the direction of observation). $|_{t-R/c}$ means that $\beta_m$ must be measured in the retarded time. The solution of (1.26) is quite simple with the new variable,

$$\phi_m(\mathbf{r},t) = \left.\frac{q_m}{R_n(1-\beta_m\cdot\mathbf{n}_m)}\right|_{ret}, \tag{1.28}$$

where $R_m = |\mathbf{r}-\mathbf{r}_m|$, $\mathbf{n}_m = (\mathbf{r}_m - \mathbf{r})/R_m$ and now the retarded time is $t'_m = t - R_m(t')/c$ and the position $\mathbf{r}_m(t'_m) = \mathbf{r}_m(0) + \int_0^{t'_m} d\tau \mathbf{v}_m(\tau)$. In a similar way the solution for the vector potential can be obtained,

$$\mathbf{A}_m(\mathbf{r},t) = \left.\frac{q_m\beta_m}{R_m(1-\beta_m\cdot\mathbf{n}_m)}\right|_{ret}. \tag{1.29}$$

Once we have the potentials, we can use (1.20) and (1.21) to obtain the electric and magnetic fields. The calculation is *slightly* tedious and the result is [31]

$$\mathbf{E}_m(\mathbf{r},t) = q_m\left.\left[\frac{\mathbf{n}_m-\beta_m}{\gamma_m^2 R_m^2(1-\beta_m\cdot\mathbf{n}_m)^3} + \frac{\mathbf{n}_m\times[(\mathbf{n}_m-\beta_m)\times\dot{\beta}_m]}{cR_m(1-\beta_m\cdot\mathbf{n}_m)^3}\right]\right|_{ret}, \tag{1.30}$$

$$\mathbf{B}_m(\mathbf{r},t) = \left.\mathbf{n}_m\right|_{ret} \times \mathbf{E}_m(\mathbf{r},t), \tag{1.31}$$

with $\dot{\beta}_m = d\beta_m/dt$ and $\gamma_m = (1-\beta_m^2)^{-1/2}$. It is clear that the electric (and magnetic) field includes two different contributions. The first part in (1.30), which will be written $\mathbf{E}_m^{(v)}$, varies as $R^{-2}$ and vanishes when we depart from the particle a long way. This is the velocity or near field. By contrast, the second one, which is called acceleration or far field, varies as $R^{-1}$. This is the most important one

and can propagate as a wave. It will be written $\mathbf{E}_m^{(a)}$. From now on we shall drop the subindices to unburden the notation.

The energy flux is given by the Poynting vector, $\mathbf{S} = c/4\pi\ \mathbf{E}\times\mathbf{B} = c/4\pi\ |\mathbf{E}|^2\mathbf{n}$, from which we can obtain the emitted power per unit solid angle

$$\frac{dP(t)}{d\Omega} = R^2|\mathbf{S}(t)|. \tag{1.32}$$

When the particle moves with a velocity much lower than $c$ in our reference frame, we can approximate the acceleration field by

$$\mathbf{E}^{(a)} = \frac{q}{c}\Big[\frac{\mathbf{n}\times\mathbf{n}\times\dot{\beta}}{R}\Big]\Big|_{ret}, \tag{1.33}$$

and hence

$$\frac{dP(t)}{d\Omega} = \frac{q^2}{4\pi c^3}|\dot{\mathbf{v}}|^2\sin^2\Theta, \tag{1.34}$$

where $\Theta$ is the angle between the direction of observation and the particle's acceleration. Integrating over the solid angle, we shall obtain the total power radiated by the charge, which is the well-known Larmor's expression in the non-relativistic regime [31]

$$P(t) = \frac{2}{3c^3}|\ddot{\mathbf{d}}(t)|^2, \tag{1.35}$$

where $\mathbf{d} = q\mathbf{r}$ is the dipole momentum of the particle. We shall always deal with signals which have finite duration because in our simulations (and also in the laboratory) an infinite time has no sense. Hence, we can define the power spectrum as

$$\sum_{n\geq 0}\mathcal{S}(\omega_n) = \frac{1}{T}\int_0^T P(t)\ dt, \tag{1.36}$$

where $T$ is the duration of the signal and $\omega_n = n\Delta\omega = 2\pi n/T$. Expanding the dipole acceleration in Fourier series,

$$\ddot{\mathbf{d}}(t) = \sum_{n=-\infty}^{\infty}\ddot{\tilde{\mathbf{d}}}(\omega_n)e^{-i\omega_n t} \tag{1.37}$$

and using Parseval's theorem

$$\frac{1}{T}\int_0^T |\ddot{\mathbf{d}}(t)|^2\, dt = 2\sum_{n=0}^{\infty} |\ddot{\tilde{\mathbf{d}}}(\omega_n)|^2, \tag{1.38}$$

we arrive at

$$\mathcal{S}(\omega_n) = \frac{4}{3c^3}|\ddot{\tilde{\mathbf{d}}}(\omega_n)|^2. \tag{1.39}$$

This expression, as we have said, is valid in the non-relativistic regime ($v \ll c$), which, in the case of a charge moving inside an external electromagnetic field, coincides with the dipole approximation, i.e. we can use it when the field wavelength is much longer than the dimensions of the system. With this approximation, the emission spectrum of a classical system is determined by its dipole acceleration.

By contrast, calculations are more difficult in the relativistic regime. The generalized Larmor's formula for the total emitted power has the form [33]

$$P(t) = \frac{2q^2}{3c^3}\gamma^6[\dot{\beta}^2 - (\beta \times \dot{\beta})^2]. \tag{1.40}$$

When the motion of the particle is periodic, the system emits only with frequencies which are integer multiples of the proper frequencies, i.e. it emits harmonics $\omega_l = l\omega_0$. In this case, if the observation point is very distant from the area in which the acceleration is produced, the power per unit solid angle radiated in each mode during an optical cycle is [31]

$$\frac{d\mathcal{S}(\omega_l)}{d\Omega} = \frac{q^2\omega_0^4 l^2}{(2\pi c)^3}\left|\int_0^{2\pi/\omega_0} dt\ \mathbf{n}\times(\mathbf{n}\times\mathbf{v})e^{il\omega_0(t-\mathbf{n}\cdot\mathbf{r}(t)/c}\right|^2, \tag{1.41}$$

which is an expression that can be used to calculate the power in each harmonic component emitted by free charges under relativistic motion. If we have charge and current densities instead of single charges, we shall replace $q\mathbf{v}$ by $\mathbf{J}$. In the case of extended media, we shall use the squared modulus of the Fourier transform of the field, measured at a sufficient distance from the medium, as the power spectrum. It is proportional to $d\mathcal{S}/d\Omega$.

### 1.3.2 Quantum system spectrum

In the case of a quantum system, things are rather more complicated and an in-depth study is out of the scope of this work. Here we shall sketch a very simple scheme which will permit us to relate the quantum spectrum with the classical one [34, 35, 36]. Thorough studies on classical and quantum spectra can be found, for instance, in references [37, 38].

Let us start with the Hamiltonian describing the interaction between the atom system and the external field,

$$H = H_A + H_F - \mathbf{d} \cdot \mathbf{E}. \tag{1.42}$$

$H_A$ and $H_F$ are the corresponding atom and field Hamiltonians and $-\mathbf{d} \cdot \mathbf{E}$ is the interaction term. The field Hamiltonian, neglecting the zero-point energy, is $H_F = \sum_{\mathbf{k},\lambda} \hbar\omega_k a^\dagger_{\mathbf{k},\lambda} a_{\mathbf{k},\lambda}$, with $\omega_k = kc$. The electric field operator in the dipole approximation takes the form

$$\mathbf{E} = i \sum_{\mathbf{k},\lambda} \Big( \frac{2\pi\hbar\omega_k}{V_0} \Big)^{1/2} (a_{\mathbf{k},\lambda} - a^\dagger_{\mathbf{k},\lambda}) \hat{\epsilon}_{\mathbf{k},\lambda}, \tag{1.43}$$

where $a_{\mathbf{k},\lambda}$ and $a^\dagger_{\mathbf{k},\lambda}$ are the creation and annihilation operators of a plane wave with wave vector $\mathbf{k}$ and polarization $\lambda$, $V_0$ is the quantization volume and the real unitary vectors $\hat{\epsilon}_{\mathbf{k},\lambda}$ form a linear polarization basis. The Hamiltonian (1.42) is therefore written as

$$H = H_A + \sum_{\mathbf{k},\lambda} \hbar\omega_k a^\dagger_{\mathbf{k},\lambda} a_{\mathbf{k},\lambda} - i\hbar \sum_{\mathbf{k},\lambda} C_{\mathbf{k},\lambda} d_{k,\lambda} (a_{\mathbf{k},\lambda} - a^\dagger_{\mathbf{k},\lambda}), \tag{1.44}$$

with $C_{\mathbf{k},\lambda} = (2\pi\omega_k/\hbar V_0)^{1/2}$ and $d_{k,\lambda} = \mathbf{d} \cdot \hat{\epsilon}_{\mathbf{k},\lambda}$. We obtain the evolution of the annihilation operator by using Heisenberg's equations of motion,

$$i\hbar \frac{da_{\mathbf{k},\lambda}}{dt} = [a_{\mathbf{k},\lambda}, H], \tag{1.45}$$

which yields

$$\dot{a}_{\mathbf{k},\lambda} = -i\omega_k a_{\mathbf{k},\lambda} + C_{\mathbf{k},\lambda} d_{\mathbf{k},\lambda}, \tag{1.46}$$

which can be formally solved to obtain

$$a_{\mathbf{k},\lambda}(t) = a_{\mathbf{k},\lambda}(0)e^{-i\omega_k t} + C_{\mathbf{k},\lambda}\int_0^t d_{k,\lambda}(t')e^{i\omega_k(t'-t)}dt'. \tag{1.47}$$

The corresponding equation for the creation operator is obtained by complex conjugates of the previous equation. The energy exchange between the system and the field during the interaction time is given by

$$\frac{1}{T}\int_0^T dt\ P(t) = \frac{1}{T}\sum_{\mathbf{k},\lambda}\hbar\omega_k\langle a^\dagger_{\mathbf{k},\lambda}(t)a_{\mathbf{k},\lambda}(t)\rangle. \tag{1.48}$$

The number of photons in mode $(\mathbf{k},\lambda)$ is calculated using (1.47),

$$\begin{aligned}\langle a^\dagger_{\mathbf{k},\lambda}(t)a_{\mathbf{k},\lambda}(t)\rangle &= \langle a^\dagger_{\mathbf{k},\lambda}(0)a_{\mathbf{k},\lambda}(0)\rangle \\ &+ 2\mathrm{Re}\Big[C_{\mathbf{k},\lambda}\int_0^t\langle a^\dagger_{\mathbf{k},\lambda}(0)d_{\mathbf{k},\lambda}(t')\rangle e^{-i\omega_k t'}dt'\Big] \\ &+ |C_{\mathbf{k},\lambda}|^2\int_0^t dt'\int_0^t dt''\langle d^\dagger_{\mathbf{k},\lambda}(t')d_{\mathbf{k},\lambda}(t'')\rangle e^{i\omega_k(t''-t')}. \end{aligned}\tag{1.49}$$

It is evident that the first term represents the number of photons at the initial time and will be null if the corresponding modes are not excited at the beginning of the interaction. Regarding the second summand, this stands for the absorption or the stimulated emission in mode $(\mathbf{k},\lambda)$, i.e. with the same frequency and polarization as the external field. If that mode is initially a coherent state $|\alpha_{\mathbf{k},\lambda}\rangle$, we shall have $\alpha_{\mathbf{k},\lambda}|\alpha_{\mathbf{k},\lambda}\rangle = \alpha^{(\mathbf{k},\lambda)}|\alpha_{\mathbf{k},\lambda}\rangle$ and then

$$2\mathrm{Re}\Big[C_{\mathbf{k},\lambda}\int_0^t\langle\alpha^\dagger_{\mathbf{k},\lambda}(0)d_{k,\lambda}(t')\rangle e^{-i\omega_k t'}dt'\Big] = 2\mathrm{Re}\Big[\alpha^{(\mathbf{k},\lambda)}C_{\mathbf{k},\lambda}\int_0^t\langle d_{k,\lambda}(t')\rangle e^{-i\omega_k t'}dt'\Big]. \tag{1.50}$$

Thus, the expected value of the dipole projection in the field polarization direction gives us the absorption or stimulated emission spectrum. Obviously, this term also vanishes if the mode $|a_{\mathbf{k},\lambda}\rangle$ is not initially excited and hence the third term is the only one of interest for us. It comes from scattering and spontaneous emission and depends on the dipole correlation function,

$$\langle a^\dagger_{\mathbf{k},\lambda}(t)a_{\mathbf{k},\lambda}(t)\rangle^{(S)} = |C_{\mathbf{k},\lambda}|^2\int_0^t dt'\int_0^t dt''\langle d^\dagger_{\mathbf{k},\lambda}(t')d_{\mathbf{k},\lambda}(t'')\rangle e^{i\omega_k(t''-t')} \tag{1.51}$$

Frequently, the approximation $\langle \mathbf{d}^\dagger(t') \cdot \mathbf{d}(t) \rangle \simeq \langle \mathbf{d}^\dagger(t') \rangle \cdot \langle \mathbf{d}(t) \rangle$ is done and hence the spectrum is calculated as

$$\langle a^\dagger_{\mathbf{k},\lambda}(t) a_{\mathbf{k},\lambda}(t) \rangle^{(S)} \approx |C_{\mathbf{k},\lambda}|^2 \Big| \int_0^t dt' \langle d_{\mathbf{k},\lambda}(t') \rangle e^{i\omega_k t'} \Big|^2. \tag{1.52}$$

The validity of this approximation is only guaranteed when dealing with a set of $N$ atoms instead of a single one. In that case $d_{\mathbf{k},\lambda} = \sum_i d_{\mathbf{k},\lambda,i}$ and (1.51) becomes

$$\langle a^\dagger_{\mathbf{k},\lambda}(t) a_{\mathbf{k},\lambda}(t) \rangle^{(S)} = |C_{\mathbf{k},\lambda}|^2 \sum_{i=1}^{N} \sum_{j=1}^{N} \int_0^t dt' \int_0^t dt'' \langle d^\dagger_{\mathbf{k},\lambda,i}(t') d_{\mathbf{k},\lambda,j}(t'') \rangle e^{i\omega_k (t''-t')}. \tag{1.53}$$

If the atoms are far enough apart from each other, the interactions among them can be neglected, having $\langle d^\dagger_{\mathbf{k},\lambda,i}(t') d_{\mathbf{k},\lambda,j}(t'') \rangle = \langle d^\dagger_{\mathbf{k},\lambda,i}(t') \rangle \langle d_{\mathbf{k},\lambda,j}(t'') \rangle$ if $i \neq j$. We shall have $\langle a^\dagger_{\mathbf{k},\lambda}(t) a_{\mathbf{k},\lambda}(t) \rangle^{(S)} = C_N^{(S)} + I_N^{(S)}$, with

$$\begin{aligned} C_N^{(S)} &= |C_{\mathbf{k},\lambda}|^2 \sum_{i,j=1, i\neq j}^{N} \int_0^t dt' \int_0^t dt'' \langle d^\dagger_{\mathbf{k},\lambda,i}(t') \rangle \langle d_{\mathbf{k},\lambda,j}(t'') \rangle e^{i\omega_k (t''-t')} \\ &\simeq N^2 |C_{\mathbf{k},\lambda}|^2 \Big| \int_0^t dt' \langle d^\dagger_{\mathbf{k},\lambda,i}(t') \rangle e^{-i\omega_k t'} \Big|. \end{aligned} \tag{1.54}$$

$$\begin{aligned} I_N^{(S)} &= |C_{\mathbf{k},\lambda}|^2 \sum_{i=1}^{N} \int_0^t dt' \int_0^t dt'' \langle d^\dagger_{\mathbf{k},\lambda,i}(t') d_{\mathbf{k},\lambda,i}(t'') \rangle e^{i\omega_k (t''-t')} \\ &\simeq N |C_{\mathbf{k},\lambda}|^2 \int_0^t dt'' \langle d^\dagger_{\mathbf{k},\lambda,i}(t') d_{\mathbf{k},\lambda,i}(t'') \rangle e^{i\omega_k (t''-t')}, \end{aligned} \tag{1.55}$$

where we have assumed that all the atoms experience the same field, i.e. the dipole approximation is still valid. When the number of photons is large, the coherent contribution $C_N^{(S)}$ is much greater than the incoherent one, $I_N^{(S)}$, and it makes sense to calculate the spectrum from the expected value of the dipole moment instead of its correlation. The importance of the incoherent term has been studied for two-level [39] and hydrogen-like [40] atoms, but we shall not study this here. With this approximation and using (1.48), we shall have

$$\frac{1}{T} \int_0^T dt \; P(t)^{(S)} = \sum_{\mathbf{k},\lambda} \frac{2\pi\omega_k^2}{V_0} \int_0^T dt' \int_0^T dt'' \langle d^\dagger_{\mathbf{k},\lambda}(t') \rangle \langle d_{\mathbf{k},\lambda}(t'') \rangle e^{i\omega_k (t''-t')}. \tag{1.56}$$

If we define the Fourier components of the dipole as

$$\tilde{\mathbf{d}}_{\mathbf{k},\lambda}(\omega_k) = \frac{1}{T}\int_0^T dt\ e^{-i\omega_k t}\langle \mathbf{d}_{\mathbf{k},\lambda}(t)\rangle, \tag{1.57}$$

and transform the sum over the wave vectors in the k-space in a sum over frequencies by integrating over the solid angle

$$\sum_{\mathbf{k}} = \sum_n \int \frac{k^2\ d\Omega}{\left(\frac{2\pi}{L_0}\right)^2}, \tag{1.58}$$

we obtain

$$\frac{1}{T}\int_0^T dt\ P(t)^{(S)} = \sum_{n\geq 0}\frac{\omega_n^2}{2\pi c^3}\int d\Omega \sum_{\lambda}|\tilde{\mathbf{d}}_{n,\lambda}(\omega_n)|^2, \tag{1.59}$$

where we have used the fact that the quantization length is $L_0 = V_0^{1/3} = cT$ because $\Delta k = \Delta\omega/c$. If we perform the integral and sum over both polarizations, we have

$$\frac{1}{T}\int_0^T dt\ P(t)^{(S)} = \sum_{n\geq 0}\mathcal{S}(\omega_n) = \sum_{n\geq 0}\frac{4}{3c^3}\omega_n^4|\tilde{\mathbf{d}}(\omega_n)|^2. \tag{1.60}$$

In the case of a harmonic signal the equality $\ddot{\tilde{\mathbf{d}}}(\omega) = \omega^2\tilde{\mathbf{d}}(\omega)$ is fulfilled and we obtain the classical expression (1.39). In the general case, since it is not possible in practice to integrate over an infinite time but only up to a maximum time $T$, it is clear that

$$\int_0^T e^{-i\omega t}\ddot{\mathbf{d}}(t)dt = e^{-i\omega T}\dot{\mathbf{d}}(T) + i\omega e^{i\omega T}\mathbf{d}(T) - \omega^2\int_0^T e^{-i\omega t}\mathbf{d}(t)dt, \tag{1.61}$$

and hence when both the dipole and its velocity vanish at $t = T$, the difference between the spectrum calculated using the dipole acceleration and the dipole momentum will be the $\omega^4$ factor, but it will not be the same in general, especially if there is a noticeable ionization because in this case the dipole does not vanish at all at the end of the calculation, except if we use an immense grid. That is why dipole acceleration is used instead of dipole momentum, making use of Ehrenfest's theorem [41, 42, 43] and calculating the dipole acceleration with

$$\ddot{\mathbf{d}}(t) = \langle -\nabla H\rangle. \tag{1.62}$$

In the present work, when we speak about atomic spectra, we refer to the expression analogous to the classical one (1.39) (without the prefactor). In the two-level system case it is very easy to calculate. When making comparisons with hydrogen spectra, dipole acceleration will be calculated by means of equation (1.62).

## 1.4 Harmonic generation in atoms

Let us now review the main characteristics of the harmonic spectrum generated by an atom irradiated by an intense laser pulse. We choose hydrogen for a simple reason: it is the only *real* system which to date has been exactly simulated by solving the time-dependent Schrödinger equation. Recently, attempts have been made to solve helium, the following system in complexity but for a restricted range of field parameters and not without difficulties [44, 45]. The results for hydrogen can be automatically extended to the rest of hydrogen-like ions by rescaling the atomic variables and indeed to any atomic system for which the one active electron approximation works correctly (especially alkaline elements). In any case, the main characteristics of the harmonic spectrum of hydrogen have also been observed in many experiments with different gases. The spectra to be shown here were calculated with a ten-cycle long trapezoidal pulse as shown in figure 1.2. When we refer to the field amplitude we mean the flat envelope part, which is the only one considered to calculate the spectra.

We begin with the case of a very weak field for which ionization is negligible. In this situation, only the transitions between bound levels are relevant. Harmonics are generated when the electron absorbs $K$ photons and moves from an initial state $|i\rangle$ to a final one $|f\rangle$ passing through virtual intermediate states, as was explained in section 1.1 and is depicted in figure 1.3. Since the final state is not stable, the electron will come back to the initial one, emitting a photon with

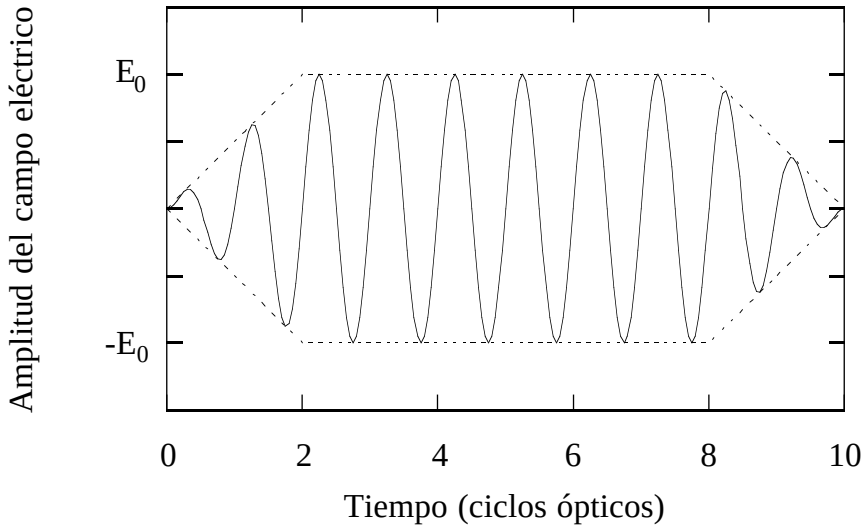


Figure 1.2: Scheme of the laser pulse used to calculate the spectra.

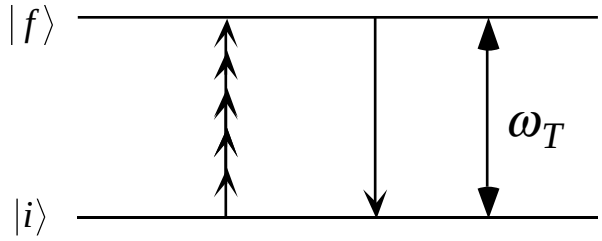


Figure 1.3: Scheme of the harmonic generation process in transitions between bound states.

energy $K\omega_0$. $K$ must be an odd number because of the symmetry of the Coulomb potential. Transitions involving an even number of photons are not permitted in this case. The relative intensity of the harmonics will decrease depending on the field parameters, but the existence of intermediate (or final) resonant states with the laser frequency can make things different.

In figure 1.4 we see a harmonic spectrum which is typical of the transitions among bound states. A few harmonics are visible together with other relevant frequencies determined by the different resonances

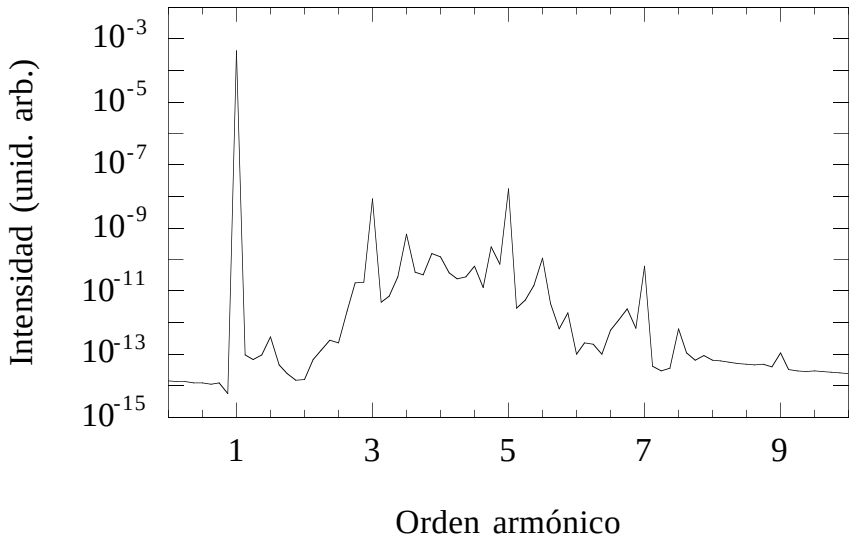


Figure 1.4: Harmonic spectrum of hydrogen for a pulse with frequency $\omega_0 = 0.1$ a.u. and amplitude $E_0 = 0.02$ a.u.

In the multiphoton ionization regime, the mechanism is very similar, but in this case the transition energy will be greater than the ionization potential and thus the final state will not be bound but will lie inside the continuum. The scheme is represented in figure 1.5. In this case the number of visible harmonics as well as their intensities basically depend on the amplitude of the electric field: the higher the amplitude, the more likely the different channels of above-threshold ionization and the higher the harmonics. In figure 1.6 we see an example of a multiphoton spectrum. The shape is quite similar to the bound-bound transition case, but the peaks are more intense and the relative importance of resonances is lower. Harmonics higher than the seventh correspond to above-threshold processes and are less and less probable.

As we already know, the atom dynamics in the tunnelling ionization regime is different from the multiphoton case and this will have great bearing on the harmonic yield. The spectrum has certain peculiar features which have been observed

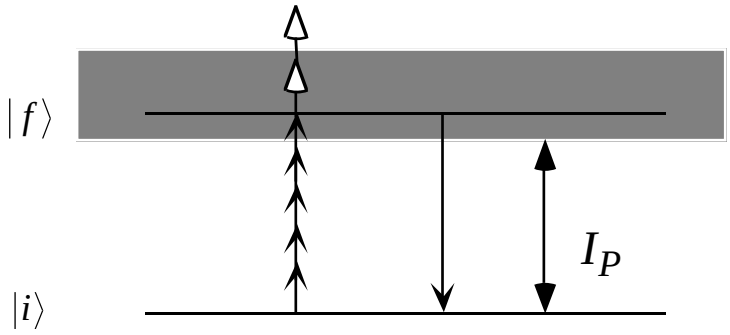


Figure 1.5: Scheme of the process of harmonic generation in the multiphoton ionization regime. Photons represented with white arrows indicate the possibility of above-threshold ionization.

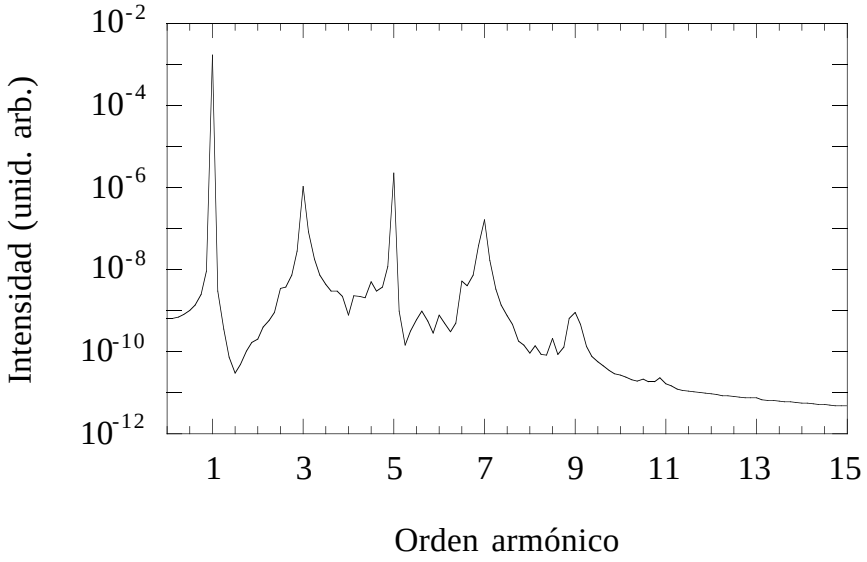


Figure 1.6: Harmonic spectrum of hydrogen for a pulse with frequency $\omega_0 = 0.1$ a.u. and amplitude $E_0 = 0.04$ a.u.

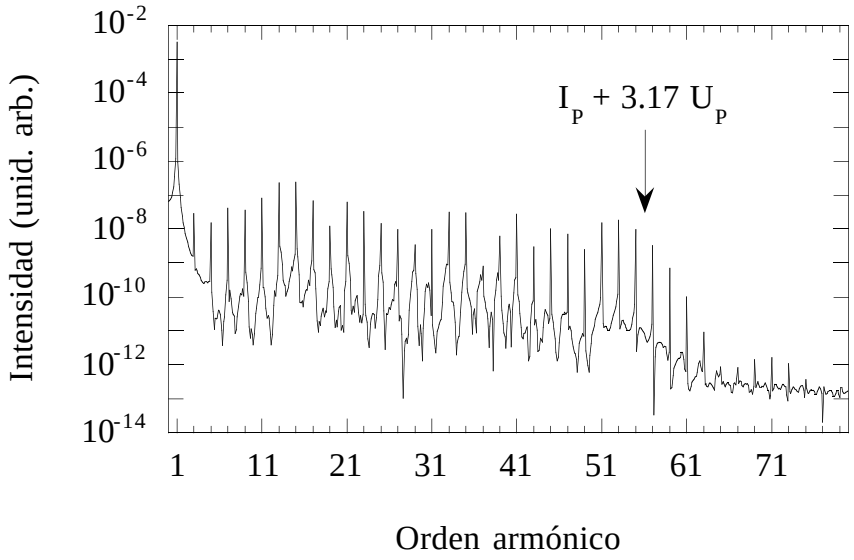


Figure 1.7: Harmonic spectrum of hydrogen when the pulse has a frequency $\omega_0 = 0.04$ a.u. and amplitude $E_0 = 0.06$ a.u. The arrow points to the frequency given by equation (1.63).

in experiments and also in the first computer simulations performed by Krause *et al.* [42]. There are usually a few low order harmonics whose intensities decrease exponentially following the perturbative laws. Then, a wide region of harmonics with similar intensities appears, called a plateau. This plateau ends sharply at a cutoff frequency given by the empirical law

$$\omega_{co} = I_p + 3.17U_p. \tag{1.63}$$

Beyond this frequency, the intensity of the harmonics decreases quickly and higher order harmonics are hardly visible. In figure 1.7 we see a typical spectrum corresponding to the tunnelling ionization regime. The differences with the previous ones need no additional comment.

It is clear from expression (1.63) that the maximum frequency can be made higher by decreasing the frequency of the field and raising its intensity. In fact, as has been previously mentioned, harmonics with orders greater than the 150th have

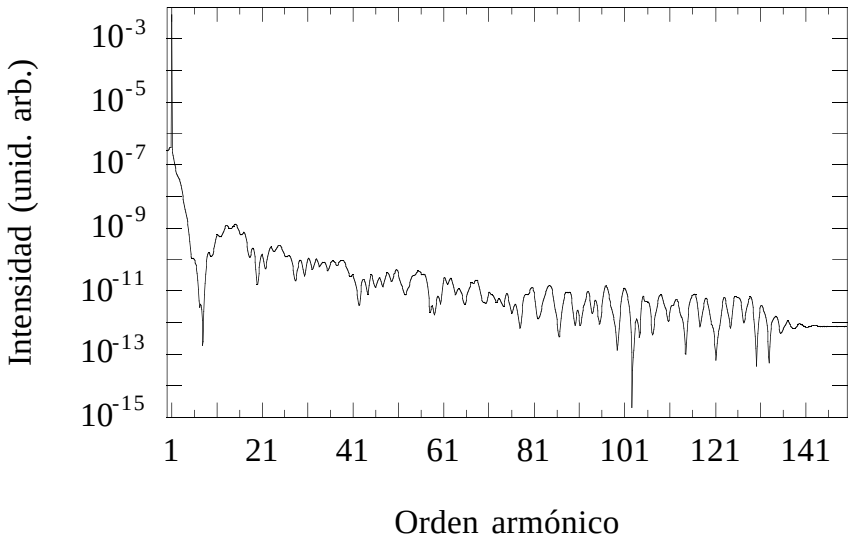


Figure 1.8: Harmonic spectrum for a pulse with frequency $\omega_0 = 0.04$ a.u. and amplitude $E_0 = 0.15$ a.u. The maximum frequency is scarcely $1.6U_p$.

been observed when the incident wavelengths are in the visible range. In spite of this, this process is not the panacea. First, if we try to use much more intense lasers, we move to the barrier suppression regime. In this case, the maximum frequency does not follow the law (1.63) and, what is even worse, the visibility of the harmonics is seriously damaged, as we can see in figure 1.8. Second, but no less important, the harmonics emitted by each atom will not add coherently but will be lost during propagation due to phase mismatch effects. We shall see how these mismatch effects will be more important when the medium is denser. This is why high harmonics are only observed in very rare media and thus with low efficiency.

Several theories have been advanced in recent years to explain this strange behaviour of the harmonics generated in the tunnelling regime. Let us recall the two most successful ones, which are very useful for understanding the physical phenomena and which have been "patched up" on many occasions. We shall use both them when studying the effect of bound-bound transitions in the tunnelling

regime.

### 1.4.1 The classical model

This is usually known as the *simpleman's model* and it is really the simplest of all. It assumes that once the wavepacket has become ionized, it behaves as a classical particle that evolves in the external electromagnetic field, both the effect of the Coulomb potential and the typical phenomenology of a quantum wavepacket (diffusion, coherent effects, etc.) being neglected. This model was proposed by van Linden and Muller [46], and Gallagher [47] to study above-threshold ionization and used by Corkum [48] and Kulander and Schafer [49] to explain the plateau in the harmonic spectrum in the tunnelling regime.

Let us assume that we have a particle which ionizes at the instant $t_0$ and evolves under a monochromatic external field which is linearly polarized in the $x$ direction. Its classical equations of motion are

$$\frac{\mathrm{d}^2x}{\mathrm{d}t^2} = -E_0\sin(\omega_0 t) \tag{1.64}$$

$$\frac{\mathrm{d}x}{\mathrm{d}t} = \frac{E_0}{\omega_0}[\cos(\omega_0 t) - \cos(\omega_0 t_0)] + v_0(t_0) \tag{1.65}$$

$$\begin{aligned} x &= -\frac{E_0}{{\omega_0}^2}[\omega_0(t-t_0)\cos(\omega_0 t_0) + \sin(\omega_0 t_0) - \sin(\omega_0 t)] \\ &+ v_0(t_0)(t-t_0) + x_0(t_0). \end{aligned} \tag{1.66}$$

Here, we have neglected relativistic effects (magnetic field and inertial mass correction) because the field intensity is so small in the tunnelling regime that they are not relevant. We can see that the velocity includes two distinct terms, a drift term, $v_d = v_0(t_0) - E_0/\omega_0\cos(\omega_0 t_0)$, and a ponderomotive term, $v_p = E_0/\omega_0\cos(\omega_0 t)$, which describes the oscillation in the external field. This is why the trajectory depends strongly on the initial phase of the electric field $\omega_0 t_0$. Some particles come back to the core position once, several times, or never. Those which return acquire some kinetic energy from the electric field. This model proposes

that there exists the probability that the returning particles will recombine and go back to the ground state during rescattering. At that moment, the electron emits a photon whose energy equals the particle's energy: kinetic plus ionization potential. In order to calculate the kinetic energy at the instant of recollision, we can assume that the initial velocity in the tunnelling regime is zero because it is an adiabatic process and because zero is the mean value of the velocity in the initial state. The initial position, $x_0(t_0)$, depends on the shape of the potential barrier but we can assume in first approximation that it is also very small as compared with the excursion suffered by the electron and hence $x_0(t_0) \simeq 0$. In this case, we have to look for solutions of $x(t) = 0$, $t > t_0$ in equation (1.66) and find $T(t) = v^2(t)/2$.

In figure 1.9a we have depicted the trajectories of the ionized particles in half a cycle as a function of the initial phase. The returning particles are those which left the atom with initial phases $\omega_0 t_0 \in [\pi/2, \pi] \cup [3\pi/2, 2\pi]$. We see the kinetic energy of the particles that return at the instant of the first recollision in figure 1.9b. The maximum energy takes a well-known value, $T_M = 3.17U_p$, precisely when $\omega_0 t_0 \simeq 107°, 287°$. Further recollisions do not raise this maximum energy.

We notice, therefore, that a very simple classical picture provides us with the first explanation of the reason why high harmonics are generated in the tunnelling regime. This model can be extended to different regimes. In the case of multi-photon ionization, the important difference is that we can no longer consider the initial velocity to be null because it will be given by the energy excess taken from the field in the ionization process; i.e. $v_0(t_0) = [2(K\omega_0 - I_p - U_p)]^{1/2}$. This new contribution to the drift velocity shifts the trajectories and hence fewer particles with high kinetic energy return to the core. Moreover, the ponderomotive energy measured in photon numbers is also lower in this regime, which is another reason preventing us from obtaining high order harmonics. The only possibility to get them would be to raise the field intensity such that the probability of high order

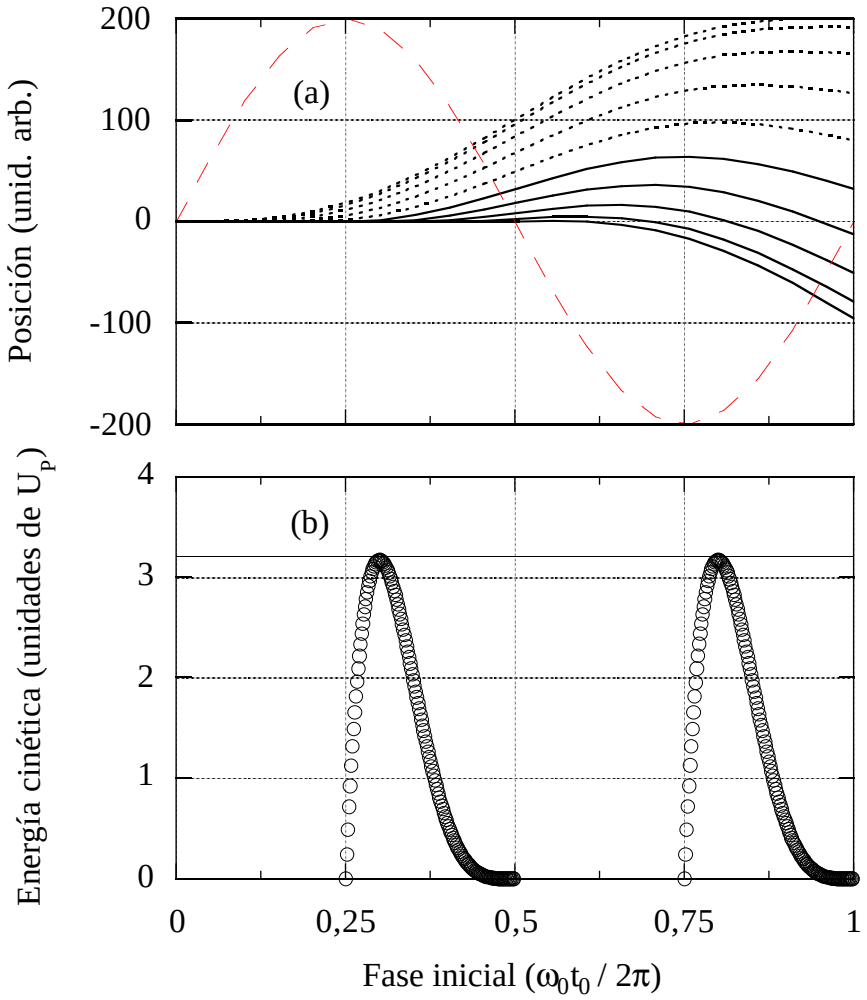


Figure 1.9: Trajectories of the ionized particles as a function of the initial phase (a). Solid lines represent the trajectories which recross $x = 0$; dotted lines represent those which never cross again. Dashed line represents the amplitude of the electric field. Graph (b) represents the kinetic energies of the returning particles at the instant of their first recollision with the core.

above-threshold processes is relevant However, in this case, too, the probability of the electrons coming back to the core decreases. Regarding the barrier suppression regime, the electrons that are ionized before the field lowers the potential barrier to the rest energy of the electron (whether by tunnelling or multiphoton absorption) behave in the same way we as have explained above. From this point on, the rest of electrons are instantaneously released and have a negligible probability of coming back to the atom again. This explains the decrease in the intensity and number of harmonics in the barrier suppression regime [50].

### 1.4.2 Quantum model

There is no doubt about the importance of the *simpleman's model*, which provides us with a natural and meaningful explanation of the mechanism underlying harmonic generation during atomic ionization. Notwithstanding, we cannot forget the limitations arising from its purely classical nature, which somehow render it unsatisfactory. A more convincing quantum model was proposed in 1994 by Lewenstein *et al* [51]. This model solves the time-dependent Schrödinger equation taking into account four assumptions: (a) the only relevant bound state is the ground one, the effect of the rest of them being neglected; (b) the depletion of the ground state due to ionization is negligible; (c) the electron in the continuum behaves as a free wavepacket moving in the electric field, the effect of the atomic potential being neglected; and (d) the effect of transitions between continuum states with different energies can also be neglected. To a certain extent, these four assumptions limit the validity of the model. Regarding the third assumption, this is equivalent to the above-mentioned Keldysh-Faisal-Reiss approach and can be accepted whenever the ponderomotive energy is high enough; for instance, in the tunnelling regime. If we restrict ourselves to that regime, the fourth one makes sense, but is no longer acceptable in the above-threshold ionization case. Assumption (a) is

questionable and later we shall attempt to offer an answer to it. The same is the case of (c), which in principle does not seem to be justified since we are studying ionization regimes, for which the depletion is important. In the original work, the model is corrected by introducing a constant ionization rate and observing that the generation of harmonics does not change relevantly. We shall also study this aspect later on. To begin, however, let us accept the four assumptions and posit that the electronic wavefunction can be expressed as

$$|\psi(t)\rangle = e^{iI_p t}\Big(a(t)|0\rangle + \int d\mathbf{v}\; b(\mathbf{v},t)|\mathbf{v}\rangle\Big), \tag{1.67}$$

where $a(t) \simeq 1$ is the ground state amplitude, $b(\mathbf{v},t)$ the continuum ones, and the exponential factor stands for the oscillations of the ground state with its proper frequency $I_p$. The Schrödinger equation in the dipole approximation takes the form

$$i\frac{\partial}{\partial t}|\psi(t)\rangle = \Big[-\frac{1}{2}\nabla^2 + V(\mathbf{r}) - E\sin(t)x\Big]|\psi(t)\rangle, \tag{1.68}$$

where we are assuming that the field is linearly polarized in the $x$ direction and the units of frequency and energy are those of the field. Using (1.67) in (1.68) we arrive at

$$\dot{b}(\mathbf{v},t) = -i\Big(\frac{\mathbf{v}^2}{2} + I_p\Big)b(\mathbf{v},t) - E\sin(t)\frac{\partial b(\mathbf{v},t)}{\partial v_x} + iE\sin(t)d_x(\mathbf{v}), \tag{1.69}$$

where $\mathbf{d}(\mathbf{v}) = \langle\mathbf{v}|\mathbf{r}|0\rangle$ is the dipole matrix element corresponding to the transition whose projection along the polarization direction of the field is $d_x(\mathbf{v})$, which gives us all the information we need to have about the atom. Equation (1.69) can be solved in a formal manner, to obtain

$$\begin{aligned} b(\mathbf{v},t) &= i\int_0^t dt' E\sin(t')d_x(\mathbf{v}+\mathbf{A}(t)-\mathbf{A}(t')) \\ &\times \exp\Big\{-i\int_{t'}^t dt''\Big[(\mathbf{v}+\mathbf{A}(t)-\mathbf{A}(t''))^2/2 + I_p\Big]\Big\}. \end{aligned} \tag{1.70}$$

$\mathbf{A}(t) = E\cos(t)\hat{x}$ is the vector potential. Introducing (1.70) in (1.68) and using assumption (d) we can find the dipole momentum

$$x(t) = \langle\psi(t)|x|\psi(t)\rangle = 2Re\int d\mathbf{v} d_x^*(\mathbf{v}) b(\mathbf{v},t)$$
$$= 2Re\left[i\int_0^t dt' \int d\mathbf{p} E\sin(t') d_x(\mathbf{p}-\mathbf{A}(t')) d_x^*(\mathbf{p}-\mathbf{A}(t)) e^{[-iS(\mathbf{p},t,t')]}\right], \quad (1.71)$$

Here, $\mathbf{p} = \mathbf{v} + \mathbf{A}(t)$ is the canonical momentum and the quasiclassical action is

$$S(\mathbf{p},t,t') = \int_{t'}^{t} dt''\left(\frac{[\mathbf{p}-\mathbf{A}(t'')]^2}{2} + I_p\right). \quad (1.72)$$

We can interpret (1.71) in the following way: $E\sin(t')d_x(\mathbf{p}-\mathbf{A}(t'))$ is the probability amplitude for the electron to make a transition from the ground level to the continuum with canonical momentum $\mathbf{p}$ at time $t'$. The wavepacket is then propagated in the field, acquiring a phase given by the complex exponential of the action $S(\mathbf{p},t,t')$, its momentum remaining unchanged (here we are neglecting the effect of the atomic potential). Finally, the electron recombines at time $t'$ with a probability amplitude given by $d_x^*(\mathbf{p}-\mathbf{A}(t))$.

In order to solve the integral over the momentum in (1.71), we can again use the saddle-point method. We can justify this approach because the dipole momenta vary much more slowly than the quasiclassical action and the integral can be well approximated by the contributions of those points in which the gradient (in $\mathbf{p}$) of the action vanishes; i.e., precisely those in which the electron ionized at time $t'$ comes back to the original position at $t$:

$$\nabla_{\mathbf{p}} S(\mathbf{p},t,t') = \mathbf{r}(t) - \mathbf{r}(t') = 0. \quad (1.73)$$

It is also clear that $\mathbf{r}(t)$ must be close to the origin if the transitions take place. This can be checked by taking the dipole momentum $d_x(\mathbf{p}-\mathbf{A}(t'))$ calculated for the Coulomb potential and observing that its Fourier transform is localized close to the nucleus in the scale of Bohr's radius. We then recover the result of the

*simpleman's model*: the contribution of the electrons which are ionized and come back to the core after moving in the external electric field is the most important one to the dipole momentum, and hence to harmonic generation. With this in mind, the result for the dipole is

$$x(t) = 2Re\Big[i\int_0^\infty d\tau\Big(\frac{\pi}{\epsilon + i\tau/2}\Big)^{3/2} d_x^*(p_{est}(t,\tau) - A_x(t))$$
$$d_x(p_{est}(t,\tau) - A_x(t-\tau))E\sin(t-\tau)\exp[-iS_{est}(t,\tau)]\Big]. \quad (1.74)$$

Here $\tau = t - t'$ is the returning point, and we have also defined the stationary values of the $x$ component of the momentum

$$p_{est}(t,\tau) = E[\sin(t) - \sin(t-\tau)]/\tau \quad (1.75)$$

and the quasiclassical action

$$\begin{aligned} S_{est}(t,\tau) &= \frac{1}{2}\int_{t-\tau}^{t} dt''(\mathbf{p}_{est} - \mathbf{A}(t'')) \\ &= (I_p + U_p)\tau - 2U_p[1-\sin(\tau)]/\tau - U_p C(\tau)\sin(2t-\tau), \quad (1.76) \end{aligned}$$

where $C(\tau) = \cos(\tau) - 4\cos^2(\tau/2)/\tau$. The factor $[\pi/(\epsilon + i\tau/2)]^{3/2}$ expresses the effect of diffusion of the wavepacket during its excursion in the continuum. As we already know, to study the emission spectrum of the atom we have to calculate the Fourier components of the dipole, defined as

$$x_{2K+1} = \frac{1}{2\pi}\int_{t_0}^{t_0+2\pi} dt\ x(t)e^{(2K+1)it}. \quad (1.77)$$

Even components are zero because of the symmetry of the Coulomb potential. We have to solve a two-fold integral over variables $t$ and $\tau$ -see (1.74) and (1.77)- to find each component. Those integrals can be calculated using the saddle-point method again, which will become a better and better approximation as the ponderomotive energy, the ionization potential and the harmonic order $K$ become

higher. Using this method, we obtain two additional conditions apart from (1.73)

$$\frac{\partial S(\mathbf{p},t,\tau)}{\partial \tau} = \frac{[\mathbf{p}-\mathbf{A}(t-\tau)]^2}{2} + I_p = 0, \tag{1.78}$$

$$\frac{\partial S(\mathbf{p},t,\tau)}{\partial t} = \frac{[\mathbf{p}-\mathbf{A}(t)]^2}{2} - \frac{[\mathbf{p}-\mathbf{A}(t-\tau)]^2}{2} = 2K+1. \tag{1.79}$$

The first of these conditions, if $I_p$ were zero, tells us that the initial velocity of the electron when it escapes from the atom must be zero, $v(t-\tau) = p_{est}(t,\tau) - A(t-\tau) = 0$. In fact, the ionization potential is not null, which means that the electron must have a negative kinetic energy at time $t-\tau$ in order to cross the potential barrier. This problem is solved if we permit $\tau$ to be complex. Its imaginary part is the tunnelling time, which has been previously introduced. In any case, the ionization potential in the tunnelling regime is much lower than the ponderomotive energy and we can assume the velocity of the particle to be very small, thus recovering another condition of the classical model, which assumed a null initial velocity of the ionized electrons. As regards equation (1.79), this is simply the energy conservation condition, as is evident using (1.78). This expression therefore tells us that the maximum emitted frequency is given by the maximum kinetic energy of the rescattering electron, exactly as proposed by the classical model. In fact, to obtain the exact law which gives the cutoff frequency it is necessary to solve the set of equations (1.73), (1.78) and (1.79) exactly. It is a difficult task to solve them analytically but it can be done numerically. The result is slightly different to the phenomenological one:

$$(2K+1)_{max} = 3.17U_p + F(I_p/U_p)I_p. \tag{1.80}$$

The $F(I_p/U_p)$ factor takes the value 1.32 when $I_p/U_p \simeq 0$ and decreases when that ratio grows. The difference with the classically predicted value is then very small and can be linked to several factors. First, the electron is not exactly ionized at $x = 0$ because it has to cross the potential barrier. Moreover, the wavepacket

spreads, reducing the contribution of the fastest electrons to the spectrum. Finally, the atomic dipole momentum is not regular in the saddle-point for the Coulomb potential and some additional corrections are needed to solve the integrals. This also lowers the cutoff frequency to values closer to the classical one.

We can see that this quantum model is much more refined and consistent than the *simpleman's* one. However, it has some problems related to the initial assumptions which need to be solved.

### 1.4.3 Solution of the time-dependent Schrödinger equation

The most straightforward way to study the interaction between a hydrogen-like atom and an intense laser pulse is to solve the time-dependent Schrödinger equation. This option cannot be considered as another model comparable to the previous ones since we assume that the evolution of an atomic system in the non-relativistic regime is perfectly described by the Schrödinger equation, whose results are exact in this sense. The only problem, apart from the purely numerical ones because the equation has not been solved analytically up to now, is that it is difficult to clear the results to draw out the information about the physical mechanisms which generate them, because all the possible couplings between the external field and the atomic structure are included. In any case, in order to check the validity of any simple model, it is essential to compare its results with the *reality* given by the Schrödinger equation (in the real world it is not at all easy to irradiate an isolated hydrogen atom with an intense field and to observe the consequences, leaving aside the interaction with the rest of the universe).

The Schrödinger equation for a hydrogen atom in the dipole approximation and length gauge is

$$i\frac{\partial}{\partial t}\psi(\mathbf{r},t) = \Big[-\frac{1}{2}\nabla^2 - \frac{1}{r} - E(t)x\Big]\psi(\mathbf{r},t), \tag{1.81}$$

where, as usual, we have chosen a field linearly polarized in the $x$ direction. The

earliest numerical solutions of this equation date from the last decade [52, 53, 54, 55]. Several methods can be used to solve it. The most common one consists in splitting the wavefunction into its angular and radial parts, thus reducing the problem to a set of partial derivative equations in time and the radial coordinate for each angular component. In principle, this set is infinite, but one can see that with a reduced number of angular momenta the results obtained are satisfactory. There is no fixed rule for determining which is the maximum angular momentum to be considered and, usually, it is a question of trial and error until we find that nearly the whole population is included in the levels we are considering. In our case, we have taken $l_{max} = 70$, which is a sufficient limit for our purposes. The way to solve the equations for each angular momentum is not unique, but there are several possible algorithms. We shall not study this problem in detail here because we solve this equation merely to compare its results with those coming from our models and, moreover, this is a widely debated issue in many publications (see, for instance, [4, 7]). Here, we shall use the scheme developed by our group and explained in reference [56].

Hence, the solution of the 3-dimensional Schrödinger equation for hydrogen is currently relatively simple, but it does require considerable computing time, especially when the field is very intense and one needs a huge spatial grid to follow the evolution of the wavefunction far away from the core. This is why 1-dimensional models have been used which reproduce, better or worse, the 3-dimensional results. It is clear that a 1-dimensional calculation only makes sense if the field is linearly polarized and all the relevant dynamics is restricted to the direction of polarization, which happens for intense fields. The 1-dimensional equation takes the form

$$i\frac{\partial}{\partial t}\psi(x,t) = \Big[-\frac{1}{2}\frac{\partial^2}{\partial x^2} + V(x) - E(t)x\Big]\psi(x,t). \tag{1.82}$$

The most important problem is to find an atomic potential which replaces the Coulomb potential. The most obvious choice is $V(x) = -1/|x|$, but, as usual,

what seems easy at first glance is not the best because that potential involves problems arising from its singularity at the origin that cannot be avoided as in the 3-dimensional case. This singularity causes a degeneracy of the energy levels and considerable instability [57]. This is why a non-singular potential called the soft-core or Rochester potential [58, 59, 60, 61], which has the form $V(x) = -Z/\sqrt{a_0^2 + x^2}$, has been widely used. The most important advantage of this potential is that it behaves asymptotically like the Coulomb potential and that it is regular at the origin. It reproduces the ionization process quite well and has a Rydberg series similar to that of hydrogen. In addition, the energy and parity have the same eigenvalues, which is an advantage in the study of dipole electric transitions. By contrast, the most negative counterpart is that the energy eigenvalues of bound states are not equal to those of hydrogen, although we can adjust the $Z$ and $a_0$ parameters to drive the depth and width of the potential well, thus choosing the ground state level. In particular, when $Z = 1$ a.u. and $a_0 = 1.412$ a.u. we recover an ionization potential of 0.5 a.u.

The numerical solution of the 1-dimensional Schrödinger equation is also well documented and we shall not reproduce it here. All the details can be found in the above-mentioned references and in Q. Su's PhD thesis [62].

## 1.5 Harmonic generation by free electrons

Let us return for a moment to the classical world (and hence to Gaussian units). As we have already stated, once the electron is ionized, it is a good approximation to consider it as a classical particle subject to Newton's equations of motion, especially if the field is very intense and the effect of the core is negligible. We can then recover the old problem of the motion of a charged particle in an electromagnetic field in order to study its emission spectrum. This problem has been approached many times in the literature, the classical work by Sarachik and Schappert in 1970 [63]

perhaps being the most famous example. Here we shall give a simplified treatment [64] since we are only interested in the case of a linearly polarized monochromatic wave.

The motion of an electron in an electromagnetic field is governed by the Newton-Lorentz equation

$$\frac{d\mathbf{p}}{dt} = -e\Big(\mathbf{E} + \frac{\mathbf{v}}{c} \times \mathbf{B}\Big), \tag{1.83}$$

from which, by performing the scalar product with the linear momentum, the equation of the evolution of the kinetic energy follows

$$mc^2 \frac{d\gamma}{dt} = -e\mathbf{E} \cdot \mathbf{v}, \tag{1.84}$$

where $\gamma = (1 + p^2/m^2c^2)^{1/2}$ and $\mathbf{p} = \gamma m\mathbf{v}$. Let us assume that the vector potential is a monochromatic wave linearly polarized along $y$ axis, $\mathbf{A} = A_0 \cos\eta\ \hat{y}$, with $\eta = \omega_0 t - k_0 x$ as phase. Here we neglect the effect of the radiation field on its own dynamics, which is reasonable whenever the field wavelength is much longer than the electron radius [10]. A recent study on the effect of the radiation field on the spectrum emitted by a relativistic particle can be found in [65]. The electric and magnetic fields are then $\mathbf{E} = A_0 k_0 \sin\eta\ \hat{y}$, $\mathbf{B} = A_0 k_0 \sin\eta\ \hat{z}$. From the evolution equations we find two conservation laws

$$mc\gamma - p_x = \alpha, \tag{1.85}$$

$$p_y - e/cA_y = p_{y_0}, \tag{1.86}$$

where $\alpha$ and $p_{y_0}$ are constants of motion given by the initial conditions. We notice that on replacing $\gamma$ by its value, (1.85) can be written as

$$p_x = (m^2c^2 - \alpha^2 + p_y^2)/2\alpha. \tag{1.87}$$

There are two useful reference frames in this problem. The first one is the laboratory frame (L), in which the particle is initially at rest. In this frame, the

constants of motion are $p_{y_0}^{(L)} = 0$, $\alpha^{(L)} = mc$. The other interesting frame is the rest frame (R), defined as that in which, on average, the particle is at rest. In this frame, the constants take values $p_{y_0}^{(R)} = 0$, $\alpha^{(R)} = mc(1 + a_0^2/2)^{1/2} \equiv mc\gamma_0$, which easily follow from (1.86) and (1.87). $a_0 = eA_0/mc^2$ is the adimensional parameter proportional to the field amplitude which drives the motion of the particle. Solving the equations of motion, we arrive at the following expressions for the momentum components in the R frame

$$p_x^{(R)} = \frac{mca_0^2}{4\gamma_0} \cos 2\eta, \tag{1.88}$$

$$p_y^{(R)} = mca_0 \cos\eta. \tag{1.89}$$

In order to find the electron orbits, we notice that $\mathbf{p} = k_0\alpha/c \; d\mathbf{r}/d\eta$, which is evident from (1.85) and $d\eta/dt = \omega_0(1 - v_x/c)$. Integrating (1.88) and (1.89) we obtain

$$(kx)^{(R)} = \frac{a_0^2}{8\gamma_0} \sin 2\eta, \tag{1.90}$$

$$(ky)^{(R)} = \frac{a_0}{\gamma_0} \sin\eta. \tag{1.91}$$

and in the laboratory frame

$$p_x^{(L)} = \frac{mca_0^2}{2} \cos^2\eta, \tag{1.92}$$

$$p_y^{(L)} = mca_0 \cos\eta, \tag{1.93}$$

$$(kx)^{(L)} = \frac{a_0^2}{4}\Big(\eta + \frac{\sin 2\eta}{2}\Big), \tag{1.94}$$

$$(ky)^{(L)} = a_0 \sin\eta. \tag{1.95}$$

We observe that the R frame moves with respect to the laboratory one with a drift velocity $v_D = ca_0^2(4+a_0^2)^{-1}$. Using the fact that the phase is Lorentz-invariant, we also observe that the frequencies in both systems are related by the well-known expression for the Doppler shift $\omega_L = \gamma_0\omega_R$, where we have used the expression for the drift velocity

The orbit solutions are obviously implicit since we cannot find the trajectory $\mathbf{r}(t)$ explicitly because the $x$ coordinate is included in $\eta$. However, we do notice that the motion in R frame is periodic, both in the field and in the propagation directions, with double frequency in the latter case. We obtain the orbit eliminating the phase in parametric equations (1.90) and (1.91)

$$16(kx^{(R)})^2 = (ky^{(R)})^2((a_0/\gamma_0)^2 - (ky^{(R)})^2), \tag{1.96}$$

which gives the well-known eight-shaped figure. In the laboratory frame, the trajectory is not periodic due to the non-zero drift velocity. Figure 1.10 shows the orbit of the electron in the rest frame (a) and the laboratory frame (b) for three values of $a_0$. We observe that the *eight* is broadened and the trajectory in the laboratory frame is more peaked.

The calculations necessary to obtain the emitted radiation are easier in the R frame because of the periodicity, which implies that the spectrum is only composed of harmonics of the fundamental frequency, which can be even and odd depending on the direction of observation because the oscillation frequency is different in both directions. Expression (1.41) is used to calculate this spectrum. Once the emission spectrum of the system is known in the R frame we can find it in the observer's frame by means of a Lorentz transformation. The calculations are quite complex and the interested reader can find them in the original work [63], but here we can recall some general conclusions. First, the spectrum is not composed of harmonics of the initial frequency in the laboratory frame but rather of multiples of another frequency that depends on the direction of observation and the field intensity, which has the form $\omega_0[1 + 1/2a_0^2 \sin^2(\theta/2)]^{-1}$. The frequencies shift towards the red for very intense fields and large angles. In addition, a large part of the angular distribution tends towards the direction of propagation due to the increase in drift velocity. The total radiated power integrated over the whole space can be expressed as an expansion in the parameter $a_0^2$ when $a_0 < 1$. For the $k$th harmonic $P_k \propto a_0^{2k}$,

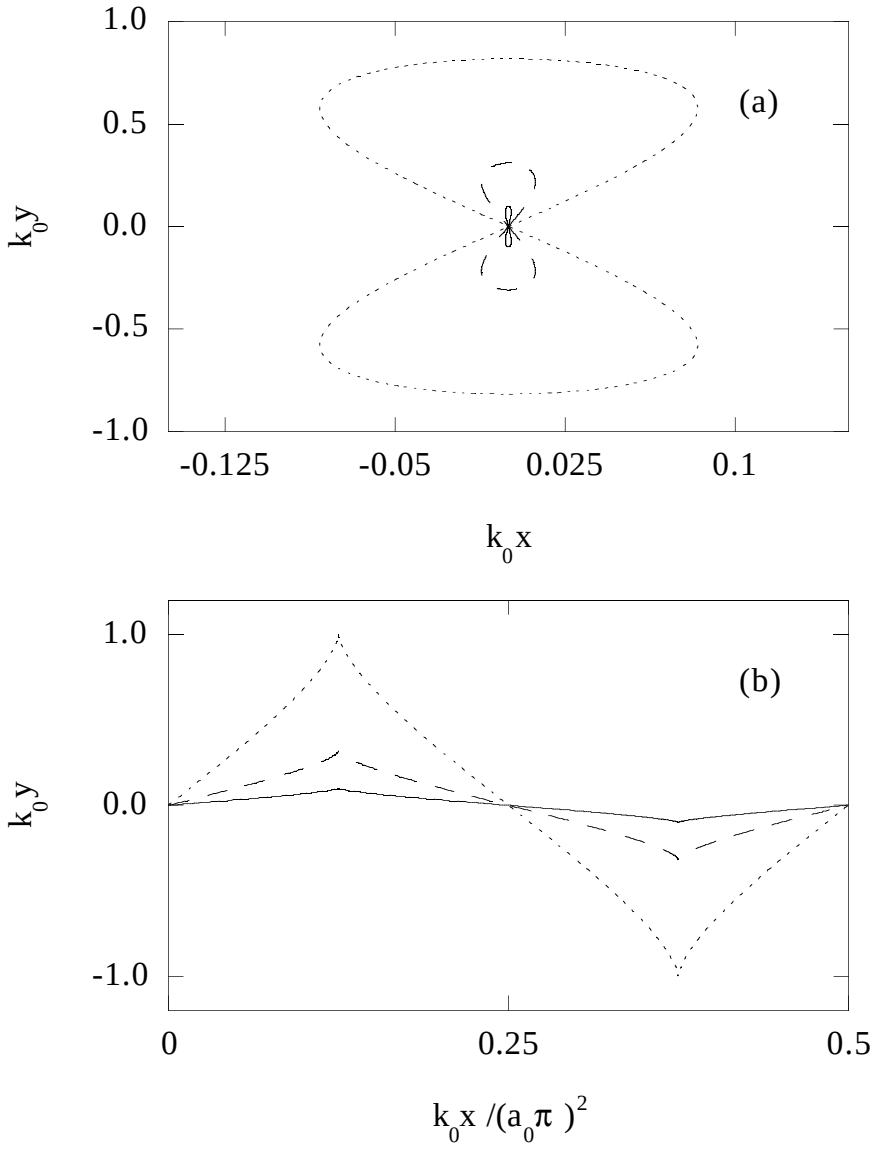


Figure 1.10: Orbits of an electron subject to a linearly polarized plane wave in the rest (a) and laboratory (b) frames. The solid line corresponds to $a_0^2 = 0.01$; the dashed line to $a_0^2 = 0.1$, and the dotted line to $a_0^2 = 1$.

such that it rapidly decreases with the harmonic order.

The reader may wonder if this mechanism, apparently so simple, is used in practice to generate harmonics now that ultraintense lasers are available. The answer is no. Experimental evidence of harmonic generation by free electrons is very rare. The reason is that the radiation emitted by a single electron is too weak and, as soon as many electrons are considered, the spectrum changes dramatically due to the effects of propagation that we shall now explain.

## 1.6 Harmonic propagation in extended media. Phase mismatch

Up to now we have tackled the generation of harmonics in single atoms or electrons, assuming that the results can be extended to more complex systems. This idea is supported by the experimental results, which roughly follow the theoretical predictions. Nevertheless, the processes involved in the generation and propagation of harmonics in extended media are much more complicated than what we have explained and many other important factors are involved. Perhaps the most important ones are phase mismatch effects, because of the damage caused by them to the visibility of harmonics.

### 1.6.1 Phase mismatch effects in neutral media

This problem has been specially studied By Anne L'Huillier's group [66, 67, 68, 69] for the case of rare gases and strong enough fields that prevent a perturbative approach. Here we shall follow their approach and explain their main conclusions. The aim is to find the resulting field of the coherent sum of the dipoles in an extended medium. Let us think of a linearly polarized beam focused on an isotropic slightly dense medium (it can be a low-pressure gas jet). The field inside the

medium is described by the wave equation

$$\nabla^2 E - \frac{1}{c^2}\frac{\partial^2 E}{\partial t^2} = \frac{4\pi}{c^2}\frac{\partial^2 P}{\partial t^2}, \tag{1.97}$$

where $P$ is the macroscopic polarization. If the incident field is monochromatic with frequency $\omega_0$, we can expand both the field and the polarization as Fourier series

$$E(\mathbf{r},t) = \frac{1}{2}\Big[\sum_q E_q(\mathbf{r})e^{-iq\omega_0 t} + c.c.\Big]; \quad P(\mathbf{r},t) = \frac{1}{2}\Big[\sum_q P_q(\mathbf{r})e^{-iq\omega_0 t} + c.c.\Big]; \tag{1.98}$$

and the Fourier transform of (1.97) yields the set of equations

$$\nabla^2 E_q + \Big(\frac{q\omega_0}{c}\Big)^2 E_q = -4\pi\Big(\frac{q\omega_0}{c}\Big)^2 P_q. \tag{1.99}$$

The polarization can be split into two contributions, $P_q = P_q^L + P_q^{NL}$, where the linear polarization $P_q^L$ stands for the response of the medium to the field propagated with frequency $q\omega_0$ and can be regarded as the product of the $q$th component of the field, multiplied by the susceptibility and by the density of atoms, $P_q^L = N\chi(-q\omega_0, q\omega_0)E_q$. We are thus neglecting the dependence of susceptibility on the field intensity and the other higher order contributions. The non-linear polarization includes all the processes which result from couplings between the main frequency and lower order harmonics which generate a $q$th order oscillation. Here we shall only consider the contribution of the fundamental field, $E_1$ to higher order polarizations. This approach is not valid in dense media, where the effect of couplings among high order harmonics cannot be neglected [70]. In that case, the problem of propagation is completely different because one needs to take into account effects such as the local field, absorption saturation, etc. The wavenumbers of the different modes are defined as

$$k_q = q\frac{\omega_0}{c}n_q = q\frac{\omega_0}{c}\sqrt{1 + 4\pi N\chi(-q\omega_0, q\omega_0)}, \tag{1.100}$$

where $n_q$ are the refractive indices for each mode. Equation (1.99) reduces to

$$\nabla^2 E_q + k_q^2 E_q = -4\pi\Big(\frac{q\omega_0}{c}\Big)^2 P_q^{NL}. \tag{1.101}$$

The right hand side term is by definition null in the case of the fundamental harmonic. Equation (1.101) can alternatively be written in its integral form. In this case, the Green function is $G(\mathbf{r},\mathbf{r}') = e^{ik_qR}/R$ [32], with $R = |\mathbf{r}-\mathbf{r}'|$ and the equation takes the form

$$E_q(\mathbf{r}) = \Big(\frac{q\omega_0}{c}\Big)^2 \int \frac{e^{ik_qR}}{R} P_q^{NL}(\mathbf{r}')d\mathbf{r}'. \tag{1.102}$$

We can use the paraxial approximation to simplify the problem if we assume a beam propagating along the $x$ axis and we neglect the possibility of reflection in the medium. Since we are interested in the far field radiation, we will have that $R \simeq x - x' + R_\perp^2/2(x-x')$, with $R_\perp^2 = (y-y')^2 + (z-z')^2$. We then arrive at

$$e_q(\mathbf{r}) = \Big(\frac{q\omega_0}{c}\Big)^2 \int \frac{e^{-i\Delta k_q x}}{x-x'} \exp\left(\frac{ik_qR_\perp^2}{2(x-x')}\right) p_q^{NL}(\mathbf{r}')d\mathbf{r}', \tag{1.103}$$

$e_q(\mathbf{r}) = E_q e^{-ik_qx}$ and $p_q^{NL}(\mathbf{r}) = P_q^{NL}e^{-iqk_1x}$ being the slowly-varying-in-space envelopes of the field and the polarization, and $\Delta k_q = k_q - qk_1$ being the phase mismatch between the polarization and the harmonic field. We have implicitly assumed a homogeneous medium but this is in general false, particularly for a gas jet, which has a roughly cylindrical shape. We can overcome this problem by substituting the phase $kx$ by the optical path integral $\int_{-\infty}^{x} k(x')dx'$. In the previous equation we have to change $\Delta k_q x$ by $\langle \Delta k_q x\rangle = \int_{-\infty}^{x} \Delta k_q(x')dx'$. Assuming a cylindrical symmetry around the propagation axis, the number of photons emitted in each mode per unit of time is

$$\Upsilon_q = \frac{c}{4\hbar q\omega_0} \int r'|e_q(r')|^2 dr'. \tag{1.104}$$

This study can be extended to long pulses (as compared with the optical cycle), then considering the envelopes varying also slowly in time, $e_q(\mathbf{r}',t')$. In this case,

the total number of photons is $N_q = \int \Upsilon_q(t')dt'$, where the integral has to be calculated along the pulse duration.

To solve equation (1.103), we need to know the non-linear response of the medium . This response is given by the product of the dipole momentum and the atomic density, $p_q^{NL}(x,r) = N(x)d_q(x,r)$. In general, this cannot be solved analytically, but in the case of very weak fields we can use a perturbative approach. We shall then write the response of the medium as $P_q = N\chi^{(q)}e_1^q/2^{q-1}$. Considering an incident field with a Gaussian profile, as is usual in experiments, we shall have

$$e_1 = \frac{be_0}{b+2ix}\exp\left(-\frac{k_1 r^2}{b+2ix}\right), \tag{1.105}$$

with $b$ the so-called confocal parameter, which is related to the width of the focal spot by the expression $b = w_0^2/k_1$; $e_0$ is the maximum amplitude of the field. Calculation of the number of photons emitted yields the result

$$N_q = \frac{\pi^2 b^3}{4\hbar}\tau_q N_0^2 |\chi^{(q)}(e_0/2)^q|^2 |F_q|^2. \tag{1.106}$$

In the previous expression, $N_0$ is the maximum value of the atomic density distribution inside the medium, given by $N(x) = N_0\rho(x)$; $\tau_q$ is the integral of the $q$th power of the temporal shape of the laser intensity (which thus depends on the time envelope of the pulse), and $F_q$ is the so-called phase matching factor, defined as

$$F_q = \int_{-\infty}^{\infty} e^{-i[\langle \Delta k_q x\rangle + \phi^{(foc)}]}(1+4x^2/b^2)^{1-q/2}2\rho(x)dx/b. \tag{1.107}$$

$\phi^{(foc)} = (q-1)\arctan(2x/b)$ is the Guoy phase shift for a Gaussian beam [71], which is the $\pi$ shift suffered by the beam in the focal spot. Close to the focal region, the phase shift can be approximated by $\phi^{(foc)} \simeq \Delta k_q^{(foc)} x = 2(q-1)/b\ x$. If we consider the ideal case of a medium with a rectangular profile and width $L$ and a collimated beam ($b \gg L$), the phase matching factor takes the form

$$F_q = \frac{2L}{b}\frac{\sin([\Delta k_q + \Delta k_q^{(foc)}]L/2)}{[\Delta k_q + \Delta k_q^{(foc)}]L/2}. \tag{1.108}$$

We see that the phase mismatch increases with the harmonic order and with the decrease in the beam waist, both factors lowering the visibility of the harmonics, specially the high order ones. It is useful to introduce two different lengths in order to clarify our analysis. The first one is the amplification length, $L_{amp}$, given by the size of the envelope of $P_q$ (the area in which the amplitude of $P_q$ is concentrated), which does not always coincide with the whole width of the medium, $L$; the second one is the coherence length $L_{coh}$, defined as the space along which there is a constructive interference between the harmonics and the fundamental field. It is usually defined as $L_{coh} = \pi/\Delta k$. $\Delta k$ has two contributions. One comes from chromatic dispersion and the other from the focusing phase and there will therefore be two corresponding coherence lengths, $L_{coh}^{disp} = \pi/\Delta k$ and $L_{coh}^{foc} \simeq \pi b/2(q-1)$. The total coherence length will be the harmonic mean of both. In order to have a good propagation,the ideal situation would be that the effects due to dispersion and focusing should cancel each other out, which would yield an infinite coherence length. In fact, we only need the coherence length to be as long as the amplification length because no harmonics are generated beyond $L_{amp}$. However, if $L_{coh} < L_{amp}$, the output signal is oscillatory-like. To obtain the desired cancellation of effects, $\Delta k^{disp}$ must be negative because the other contribution is always positive and increases with the harmonic order. In the case of rare gases, the value of $\Delta k^{disp}$ depends on the working range of frequencies: if the frequency is below the first resonance, the refractive index increases slightly with the frequency (normal dispersion) and $\Delta k^{disp}$ would be positive and small, the phase mismatch therefore being solely due to the focusing geometry. If the frequency is higher and we enter the resonance range, dispersion can take high values; positive if it is normal, or negative if it is anomalous. In the latter case, dispersion and focusing effects can cancel for some harmonics. If the frequency is higher than the ionization potential, the existence of ionized electrons plays a decisive role, as we shall see.

Notwithstanding the previous considerations, high order harmonics and the plateau structure are clearly visible in experiments. It is thus evident that a perturbative approach does not work properly for weak fields. Indeed, if one calculates the phase mismatch from the polarization created by the dipole momenta obtained in single atom simulations numerically, one sees that the phase mismatch is not so important and is less dependent on the harmonic order [68]. This is no longer true when the free electron density is high.

### 1.6.2 Phase mismatch effects in ionized media

When the frequency or the intensity of the field are high enough to yield a noticeable ionization, we can no longer neglect the effect of free electrons in the propagation of harmonics. Equation (1.103) can be extended taking into account the absorption due to the free electrons, allowing $\Delta k_q$ to have an imaginary part. We can then replace $\Delta k_q x$ by $\langle \Delta k_q x \rangle = \int_{-\infty}^{x} (\Delta k_q(x') - i\kappa_q(x'))dx'$. A simpler approach can be made if the electron density is not very high. In this case, we can neglect collisions among electrons and use the well-known expression for the refractive index [72]

$$n_{el}(\omega) = \sqrt{1 - \left(\frac{\omega_p}{\omega}\right)^2}, \tag{1.109}$$

$\omega_p = (4\pi N q^2/m)^{1/2}$ being the plasma frequency, which reduces to $\omega_p = (4\pi N_e)^{1/2}$ for electrons in atomic units. For rare gases, the plasma frequency is always much lower than the visible frequencies (if the wavelength of the laser is 1 $\mu$m, the electron density must be greater than $10^{21}$ cm$^{-3}$ to equalize the plasma and field frequencies, but the densities are orders of magnitude lower in the experiments). We can then approximate $n_{el} \simeq 1 - \omega_p^2/2\omega^2$, which yields an additional phase mismatch

$$\Delta k_q^{el} = \frac{\omega_p^2(q^2-1)}{2qc\omega_0}. \tag{1.110}$$

This new contribution is always positive and varies linearly with $q$ for high order harmonics. To have an idea of the magnitude of the phase mismatch caused by free electrons, we can compare it with the focusing contribution. It can be seen that for a beam with wavelength of 1 $\mu$m and confocal parameter $b = 10$ mm, the density above which the effect of free electrons is more important than the focusing one is $N_e \sim 7 \times 10^{14}$ cm$^{-3}$, a thousand times lower than the density which is typically found in experiments with noble gases with pressures of 15 Torr. Hence, the effect of free electrons is the most important one in real cases and elicits important phase mismatches.

Another effect strongly linked to the previous one is beam defocusing. Since the field intensity is higher near its center, there are more ionized electrons in this area, and hence its local refractive index is lower than the one in the external part. Therefore, the field "prefers" to propagate through the external part and ring patterns are observed in the experimental harmonic fields. When the field is very intense, the opposite occurs because the ponderomotive force is so high that the electrons move away, filamentation appearing.

Let us now recall the harmonics generated by free electrons. The effects of phase mismatches are especially dramatic in this case because the emitted radiation is usually weak. These effects can be estimated by simply calculating the radiation field of a set of electrons in an intense electric field. These calculations give as a result that electron densities of the order of $10^{17}$ cm$^{-3}$ are sufficient to permit constructive interference of only four or five harmonics, whose intensities scale as the square of the free electron density, whilst the higher ones are practically invisible due to phase mismatch effects [73]. Fortunately, when density increases, collective effects become important and there are other mechanisms able to generate much more intense harmonics.

## 1.7 Harmonic generation in plasmas

A plasma is simply a gas of ionized particles. This gas is composed by electrons and ions which, having a very different charge-mass ratio, behave in a different way when moved by external and internal electromagnetic fields. The usual approach in the study of plasmas is to treat electrons and ions as two fluids and split the system dynamics into two parts whose spatial and temporal scales are different [74]. When studying the interaction of plasmas with ultrashort pulses, a good approximation is to assume that the ions move very little during the interaction time and that they can be considered as fixed charges. The plasma can be then understood as a gas of electrons subject to a static ionic potential and an external field. We shall gain insight into these aspects when we explain the numerical simulation of plasmas in chapter 3.

We already know that the propagation of an electromagnetic field in a gas of electrons depends on the plasma frequency, or equivalently, on its density. The critical density is the one for which the plasma frequency is equal to the field frequency, $N_c = m\omega_0^2/4\pi q^2$. If we look at equation (1.109), we see that if the density is below the critical value, the field can propagate inside the medium, which is then called an underdense plasma. By contrast, when the density exceeds the critical value, the field is completely absorbed in a very short space and the medium is opaque for radiation with that frequency. This is the case of overdense plasmas.

Study of the interaction between plasmas and intense electromagnetic fields has been of great importance in recent years because of its interest in such different disciplines as astrophysics, accelerated particle physics or inertial confinement fusion [75].

One could think that the harmonics generated in plasmas would be similar to those created by free electrons (section 1.5). For two reasons, this is not true:

propagation effects and collective forces make the electron dynamics completely different. The simplest model is to consider that the effect of the rest of the charges on a single electron is equivalent to a restoring force. Therefore, the evolution equation takes the form

$$\frac{d\mathbf{p}}{dt} = -e\Big(\mathbf{E} + \frac{\mathbf{v}}{c} \times \mathbf{B}\Big) - \omega_{p0}^2 \mathbf{r}, \tag{1.111}$$

This new force completely changes the motion of the electron and hence the emitted radiation [76]. The most evident consequence is that the drift velocity vanishes due to the restoring force.

In the case of an underdense plasma, the most convenient method to study the harmonics is to use a hydrodynamical description of the medium, which resembles a fluid. Such study is out of the scope of this work but has been addressed in detail in several references [64, 77]. The harmonics are observed to be generated by two mechanisms: the effect of the nonlinear relativistic motion of the electrons analyzed in section 1.5 and the collective oscillations of the electron density. Unfortunately, both effects cancel in the lowest order and hence the generated harmonics are rather weak. The final result, when defocusing effects and chromatic dispersion are taken into account, is that the total power radiated in low harmonics has a dependence of the type

$$P_{2M+1} \propto \Big(\frac{\omega_{p0}}{\omega_0}\Big)^{4M} \frac{a_0^{4M}}{\gamma_0^{6M}} P_0, \tag{1.112}$$

$P_0$ being the incident field power and $a_0$, $\gamma_0$ the parameters defined in section 1.5. The power decreases rapidly with the order because the plasma is underdense. The maximum value is obtained when $a_0 = 2$, and it diminishes beyond that intensity. Thus, it is useless to raise the laser intensity very much because the generation of harmonics will not be more efficient. Moreover, we have to take into account the problems deriving from the phase mismatch effects explained above. It is therefore not surprising that there is no exact evidence of harmonic generation in underdense plasmas. The solution, as we shall see, is overdense plasmas.

An overdense plasma is characterized by a plasma frequency greater than the field frequency, which prevents the propagation of the field inside the medium and causes its nearly total reflection. Unlike the underdense case, there is a considerable body of experimental evidence of high order harmonic generation in overdense plasmas. In the seventies, up to the eleventh harmonic was observed in experiments with $CO_2$ laser pulses with a duration of 2 ns [78]. The first revolution was an experiment by Carman *et al.* in 1980. Those authors irradiated plastic and metallic foils with a $CO_2$ laser with an intensity higher than $10^{15}$ W/cm$^2$, creating a plasma which emitted harmonics up to the 46th order. These harmonics did not have rapidly decreasing intensities but did display some kind of plateau structure [79, 80]. The observed harmonics were odd and even, and less intense half-harmonic frequencies were also detected. These experiments immediately drew the attention of many scientists because of their potential as an efficient mechanism to generate high frequency coherent radiation. The earliest theoretical models explained the experimental results reasonably well and a value was found for the cutoff frequency up to which harmonics could be generated, given by

$$\omega_{co} = \sqrt{\frac{N}{N_c}}\omega_0. \tag{1.113}$$

From the previous expression, it is clear that the frequency limit is driven by the maximum electron density and the laser wavelength (by means of $N_c$). However, a recent experiment performed by Norreys *et al.* [81] has thrown doubt on the previous results and the cutoff law. They used a neodymium laser with 5 ps pulses and an intensity of $10^{19}$ W/cm$^2$ impinged onto plastic foil, observing harmonics beyond the 70th order with efficiencies greater than $10^{-6}$, i.e., they obtained megawatts of radiation in wavelengths of around 15 nm. If expression (1.113) were correct, the electron density in the medium should have been 17 times higher than the typical density of the target in the solid state, which is difficult to believe. At the same time, more complex theoretical studies have been carried out,

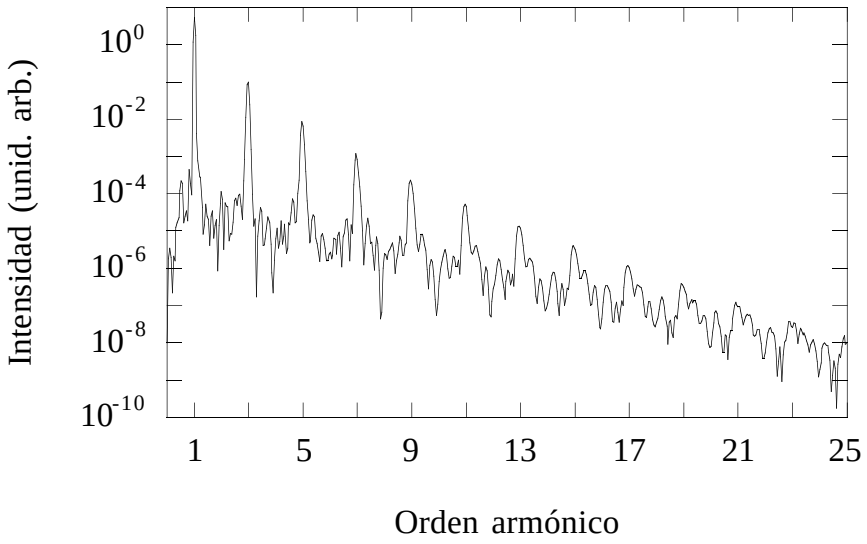


Figure 1.11: Spectrum of the reflected field when a pulse with a duration of 20 optical cycles and maximum amplitude $E_0 = 5$ a.u. impinges perpendicularly onto a homogeneous cold plasma whose density is four times the critical one.

many of them with the help of the so-called "particle-in-cell" numerical simulations. These have shed light on the generating mechanisms of these harmonics and have reproduced the experimental results quite well [82, 83, 84, 85, 86]. Figure 1.11 shows a typical spectrum corresponding to the interaction between an intense pulse and an overdense plasma.

There are several processes able to generate high frequency radiation in overdense plasmas but we shall not explain all of them here. Most of them are more effective when the laser impinges obliquely onto the target surface and the direction of polarization is in the incidence plane ($p$ polarization). This is because the coupling of the field and the plasma oscillations, which are longitudinal, is more intense in that case. Under normal incidence conditions, this coupling takes place by means of the $\mathbf{v} \times \mathbf{B}$ term of the Lorentz force, which is of second order except in the ultrarelativistic case. Despite this, we shall restrict ourselves to this par-

ticular case since our interest lies in studying the effects of ionization, which in principle do not depend on the geometry of the interaction. Let us therefore explain how harmonics are generated by the above-mentioned mechanism, forgetting about others such as resonant absorption, parametric instabilities or transversal inhomogeneities (see, for instance, [64] and references therein).

We have said that the electrons in a dense plasma are subject not only to the external field but also to the collective forces which prevent their free motion in the plasma and which in a first approximation are harmonic-like and depend on the plasma frequency. These forces reduce the drift motion in the field propagation direction and hence a more selective radiation both in frequencies and in directions is obtained. We also have to take into account that the field is reflected in a very short space, especially for high densities. The interaction takes place in a very thin layer which oscillates as a mirror with twice the frequency of the incident pulse (let us recall the eight-shaped figure with double frequency in the longitudinal direction). An example of the oscillations of the surface electrons is offered in figure 1.12, in which collective motion is clearly depicted. These surface oscillations generate the whole secondary radiation, which is mainly reflected since it cannot propagate inside the medium (except for very thin foils, as we shall show).

A simple approach to explain how harmonics are generated is the so-called *oscillating mirror* model [85, 86]. This assumes a well defined boundary surface between the vacuum and plasma which moves around the initial surface of the medium, given by the position of the boundary ions, as shown in figure 1.12. The simplest version of this model [86] solves the equation of motion for the electrons (1.111). For a field which is linearly polarized in the $y$ direction and propagates along the $x$ axis, perpendicularly to the boundary surface, the equations take the form

$$\frac{dp_y}{dt} = -eE_y\left(t-\frac{x}{c}\right)+e\frac{v_x}{c}B_z\left(t-\frac{x}{c}\right), \tag{1.114}$$

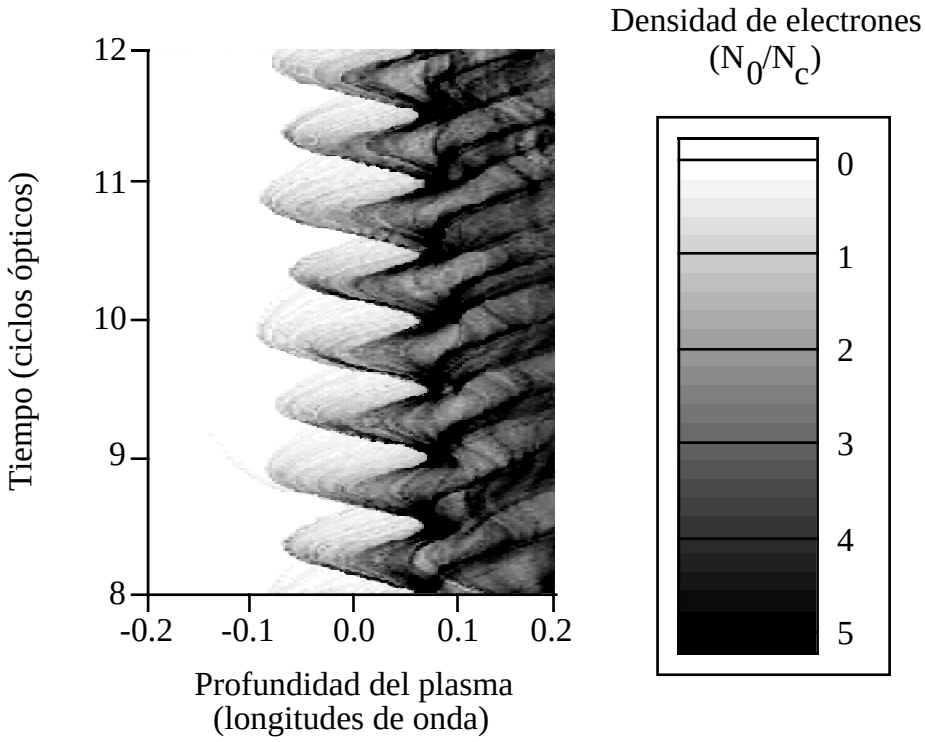


Figure 1.12: Evolution of the free electron density at the surface of an overdense plasma impinged by an intense electromagnetic field.

$$\frac{dp_x}{dt} = -e\frac{v_y}{c}B_z\left(t-\frac{x}{c}\right) - \omega_p^2 x, \tag{1.115}$$

$$\frac{dx}{dt} = v_x, \tag{1.116}$$

where the plasma frequency is assumed to be constant inside the medium. When the plasma is highly overdense, it makes sense to think that the boundary surface behaves like a perfect mirror in which the total field vanishes, and hence

$$E_R\left(t+\frac{x(t)}{c}\right) + \frac{1-\beta_x}{1+\beta_x}E_0\sin\left[\omega_0\left(\frac{t-x(t)}{c}\right)\right] = 0, \tag{1.117}$$

$E_R$ being the reflected field and assuming an incident field with constant amplitude and frequency $\omega_0$. The relativistic factor $(1-\beta_x)/(1+\beta_x)$ comes from performing a Lorentz transformation to the laboratory frame from the rest frame, on which we should impose the continuity of the field [87].

Solving equations (1.114)-(1.117) we obtain a reflected field with high harmonics due to the $\mathbf{v}\times\mathbf{B}$ term in the equations of motion and also due to the retardation effect in equation (1.117), which plays a fundamental role. In a first approximation, we only obtain odd harmonics in our case (normal incidence and linearly polarized field). The study can be extended to different geometries, obtaining different selection rules: in oblique incidence and polarization perpendicular to the incidence plane ($s$ polarization), odd $s$-polarized and even $p$-polarized harmonics appear. The latter are less intense and vanish at normal incidence. If the field impinges obliquely but is $p$-polarized, even and odd harmonics are obtained with the same polarization as the incident field. In the case of circularly polarized pulses, weak harmonics can be generated in any polarization but only at oblique incidence. Under normal incidence conditions, no harmonics are generated because the amplitude of the field is always constant [85, 86].

We have therefore seen that the collective oscillations of the surface of an overdense plasma with a sharp density profile subject to an intense laser pulse, in addition to other relativistic effects such as retardation, can generate high harmonics.

In fact they are one of the most promising sources of coherent high frequency intense radiation. In this section, we have not considered the effect of ionization because we have assumed a preformed plasma. Later on, we shall see that things change in the case of medium intensity fields, which need several optical cycles to ionize the target.

# Chapter 2

# Harmonic generation in an open two-level system

In this chapter we shall attempt to explain the effect of a time-dependent ionization rate and the role of bound-bound transitions on the harmonics generated by atoms in the tunnelling ionization regime. With this aim, we shall introduce an atomic model consisting of two bound levels whose population can be ionized (in this sense we call it *open*) and rescattered with the core. We have chosen this model because it is the simplest one which includes both bound-bound (one) and bound-continuum (two) transitions. In spite of its simplicity, it can provide some useful information.

## 2.1 Harmonic generation in two-level systems

Two-level systems have been widely used as a model for the interaction between electromagnetic fields and matter [88]. It is clear that to reduce the dynamics of a quantum system to the evolution of only two of its levels is a simplification that can only be justified if the field intensity is low and its frequency is close to a resonance. However, such a model can also yield information beyond its theoretical range of validity.

Let us recall the evolution equations of a two-level system under the effect of an

external field in the dipole approximation. We start with the Schrödinger equation (we are using atomic units again)

$$i\frac{\partial}{\partial t}|\psi\rangle = (H_0 + H_{int})|\psi\rangle. \tag{2.1}$$

The atomic Hamiltonian $H_0$ includes the kinetic energy term and the electrostatic Coulomb potential, whereas the interaction Hamiltonian in the dipole approximation is $H_{int} = -E(t)x$, where we are assuming a linearly polarized field in the $x$ direction. We further assume that the wavefunction is a linear combination of two eigenstates of the atomic Hamiltonian

$$|\psi\rangle = a_0(t)|0\rangle + a_1(t)|1\rangle. \tag{2.2}$$

If we place our energy origin at ground level, the atomic Hamiltonian acts over both eigenstates as

$$\begin{aligned} H_0|0\rangle &= 0|0\rangle, \\ H_0|1\rangle &= \omega_T|1\rangle, \end{aligned} \tag{2.3}$$

where $\omega_T$ is the transition frequency, i.e., the difference between the energy levels of both states. Now we project (2.1) on both states to obtain the evolution equations of the system

$$\frac{da_0(t)}{dt} = -iE(t)d_{01}a_1(t), \tag{2.4}$$

$$\frac{da_1(t)}{dt} = -iE(t)d_{01}a_0(t) - i\omega_T a_1(t), \tag{2.5}$$

where $d_{01} = \langle 1|x|0\rangle$, which can be assumed to be real and we have used the fact that, due to the symmetry of the potential, $\langle 0|x|0\rangle = \langle 1|x|1\rangle = 0$. The time-dependent dipole moment will be $d(t) = d_{01}[a_0^*(t)a_1(t) + a_0(t)a_1^*(t)]$ and we use its second derivative to calculate the spectrum. The population of the levels are simply $P_i(t) = |a_i(t)|^2$. Equations (2.4) and (2.5) are nonlinear because of the

time-dependent field and they cannot be solved analytically for a sinusoidal field. This nonlinearity is able to generate frequencies other than the incident and the transition frequencies.

Henceforth, we shall assume that our two-level system resembles the first two states of the hydrogen atom coupled via an electric dipole transition, i.e., the ground state $1s$ and the excited state $2p_x$. The transition frequency in this case is $\omega_T = 0.375$ a.u. and the dipole moment is $d_{01} = 0.745$ a.u. [89]. We shall also choose the initial state to be the ground level. The effect of choosing the excited level or a linear combination of both (ground and excited) as the initial state is an enhancement of the couplings between the transition frequency and the laser frequency, which results in more intense hyper-Raman lines (combinations of the transition and field frequencies) in the observed spectrum [90]. When ionization is taken into account, there is an additional effect consisting of the appearance of two harmonic spectra with different intensities shifted by the transition frequency [91, 92]. The field will always have the form $E(t) = E_0 S(t) \sin(\omega_0 t)$, with an envelope $S(t)$ with a trapezoid shape, two ramp cycles and the rest of constant amplitude. Here, we shall not address the effect of non-monochromatic fields, which has been widely studied in the literature, especially the particular case of two-colour pulses. Interested readers can obtain more information in [7], for instance. To solve the evolution equations (2.4) and (2.5) numerically, we use a fourth-order Runge-Kutta algorithm with a sufficiently small timestep [93].

Figure 2.1 shows the evolution of the populations of both states and the dipole moment when our two-level system is subject to a pulse with a frequency of $\omega_0 = 0.04$ a.u. and an amplitude of $E_0 = 0.06$ a.u., parameters corresponding to the tunnelling ionization regime for the hydrogen atom. We note small oscillations in the populations, the excited one always being less than 2 percent of the total. The dipole moment also seems to oscillate harmonically with the laser frequency.

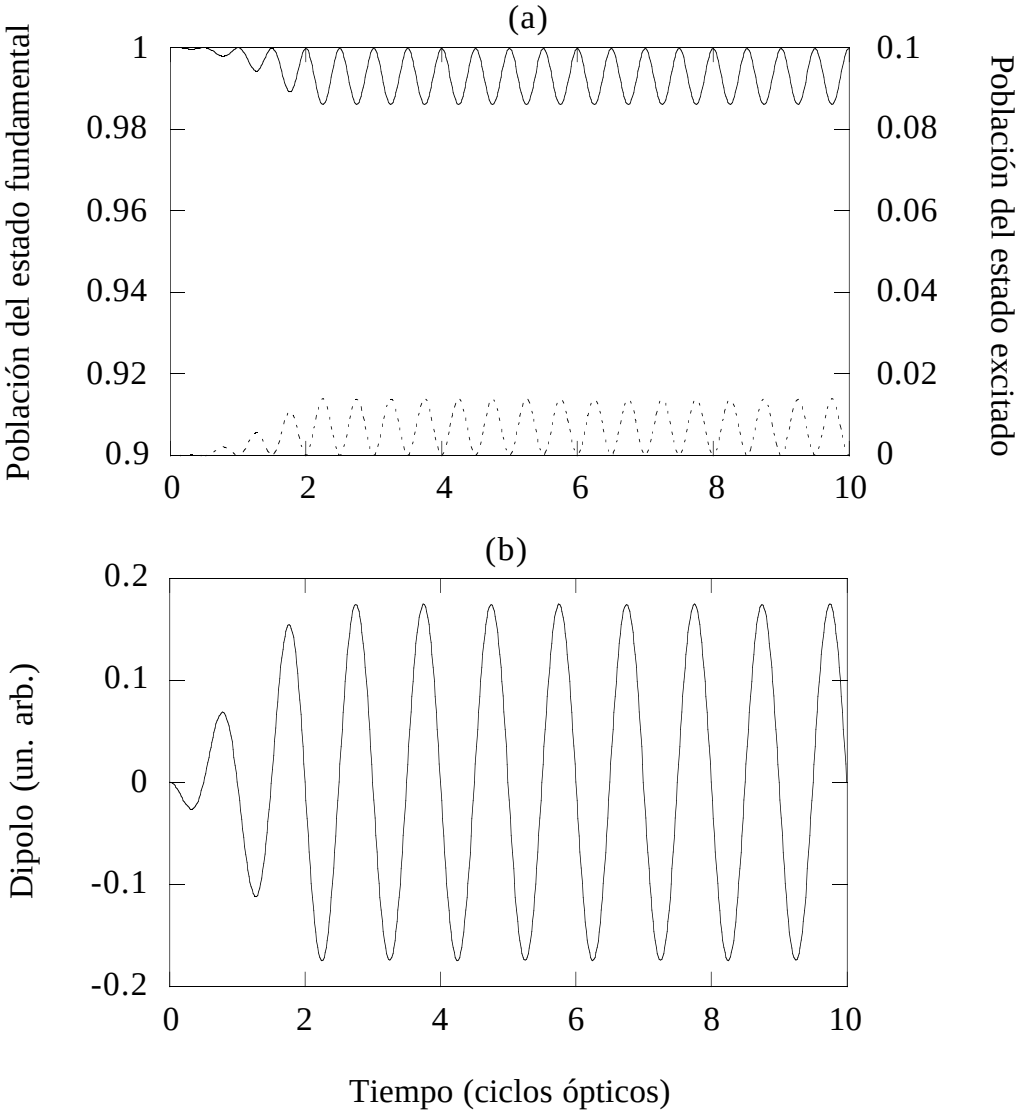


Figure 2.1: Evolution of the population of the ground (solid line) and excited (dotted line) states when the incident pulse has a frequency of $\omega_0 = 0.04$ a.u., an amplitude of $E_0 = 0.06$ a.u., and a duration of 10 optical cycles, two of them of linear ramp turn-on (a). Plot (b) represents the corresponding dipole moment.

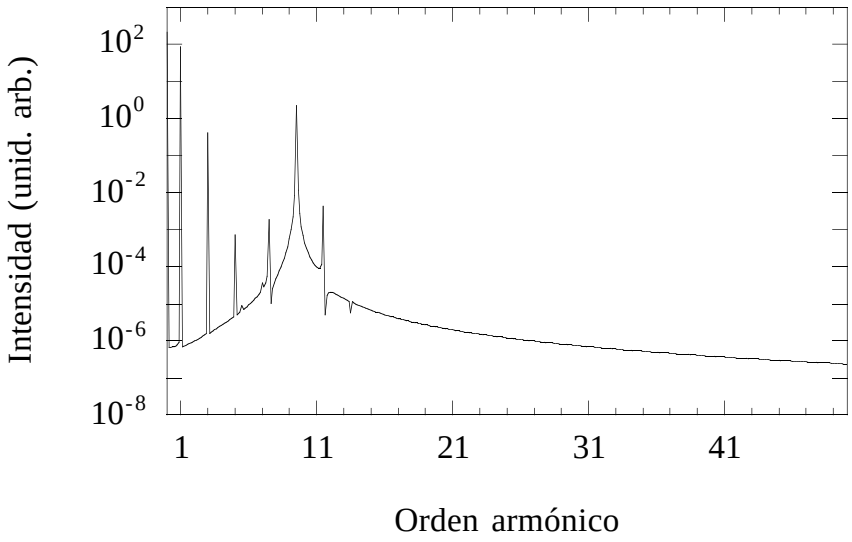


Figure 2.2: Spectrum corresponding to the dipole acceleration for the same parameters as in figure 2.1.

If we Fourier transform the dipole acceleration (neglecting the two ramp cycles), we obtain what is depicted in figure 2.2. We see that the fundamental frequency is obviously the most intense one and that there are peaks corresponding to the third and fifth harmonics and the transition frequency, in this case $\omega_T \simeq 9.4\omega_0$, also appears clearly surrounded by two satellite peaks at $\omega_T - \omega_0$ and $\omega_T + \omega_0$. This is not a very stimulating spectrum, but it is well-known that a two-level system can generate a harmonic spectrum with features similar to those of a real atom, i.e., a plateau with harmonics of roughly the same frequency and a sharp cut-off frequency [36]. Figures 2.3 and 2.4 show what happens when the field amplitude is raised up to $E_0 = 0.5$ a.u. First, both populations oscillate with greater amplitude, more than a fourth of the total population reaching the excited level and smaller oscillations with a higher frequency appear. In correspondence, the dipole moment oscillates strongly in an anharmonic way. The result is clear in the spectrum, which consists of intense peaks up to the 30th order with a plateau and a decreasing zone

as from roughly the 21st harmonic. There are in addition other frequencies that are combinations of the field and the transition frequencies.

An expression for the cut-off frequency can be obtained in a rigorous way [89, 94] but it can be also obtained with a simple adiabatic approach [89, 90, 95]. In the case of small field frequencies, smaller than the transition and the Rabi ( $\Omega_R = d_{01}E_0$) ones, as is the case, one can envisage that the transitions take place not between the non-perturbed states but between the instantaneous dressed states, whose energies are calculated from the eigenvalues of the Hamiltonian

$$H = \begin{pmatrix} 0 & d_{01}E(t) \\ d_{01}E(t) & \omega_T \end{pmatrix}, \tag{2.6}$$

and prove to be

$$\lambda_{\pm} = \frac{\omega_T}{2} \pm \frac{1}{2}\sqrt{\omega_T^2 + 4d_{01}^2 E(t)^2}. \tag{2.7}$$

Thus, the effective transition frequency varies among the minimum and maximum of the energy difference between the dressed states, $\lambda_+ - \lambda_- = \sqrt{\omega_T^2 + 4\left(E(t)d\right)^2}$, which give the values of the beginning, $\omega_T$, and the cutoff, $\omega_{co} = \sqrt{\omega_T^2 + 4\Omega_R^2}$, of the plateau. In this case, the cutoff frequency takes a value of $\omega_{co} \simeq 20.8\omega_0$, which fits in quite well with the result in figure 2.4. The appearance of this kind of spectrum in such a simple system has led some people to speculate that the plateau structure observed in experiments could be related to bound-bound transitions. However, it is obvious that when the field amplitude is half an atomic unit we can no longer represent the hydrogen atom by a simple two-level system. In particular, we cannot forget the effects of ionization since in a real case hardly any bound population would remain after a couple of cycles. Let us see, then, what happens when we introduce ionization into our model.

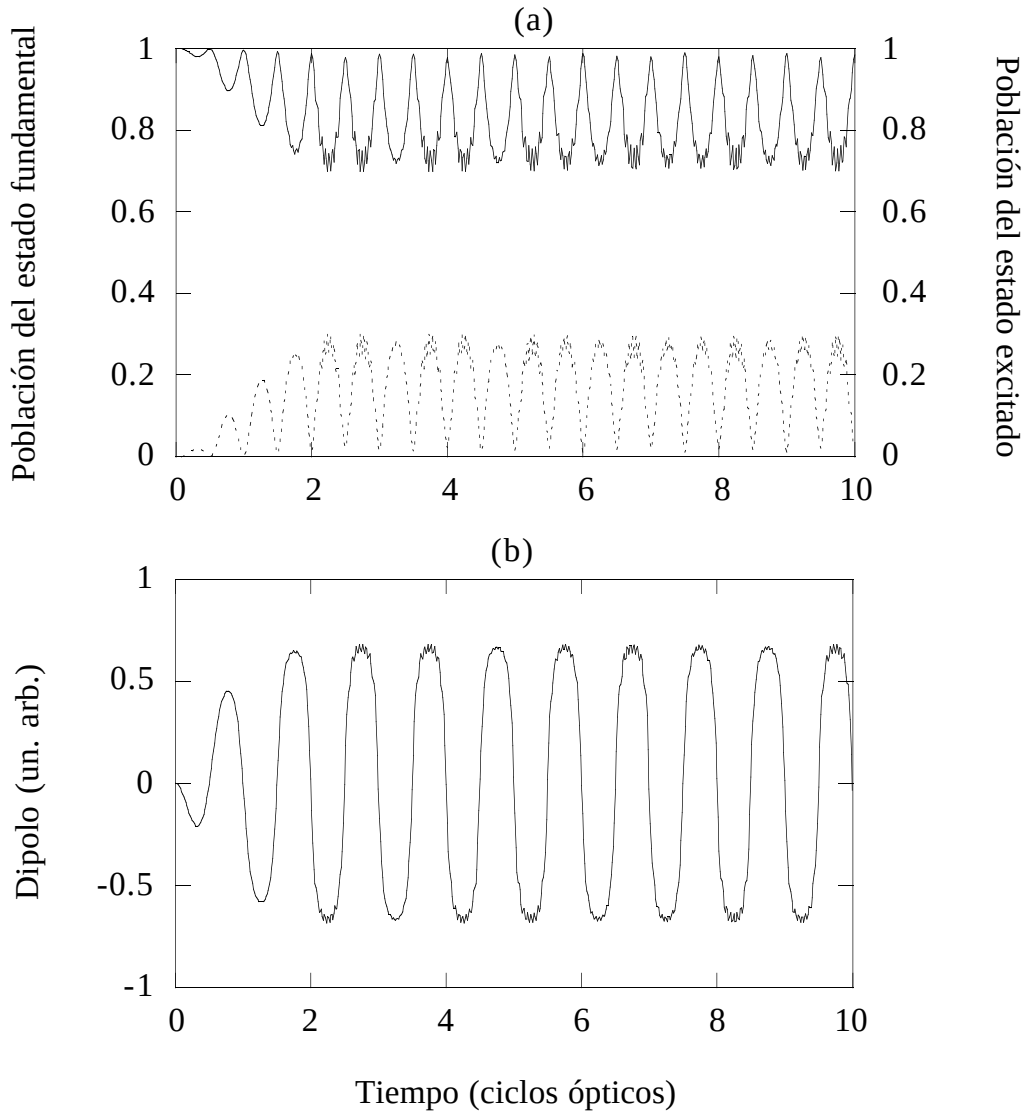


Figure 2.3: The same as in figure 2.1 but with a field amplitude of $E_0 = 0.5$ a.u.

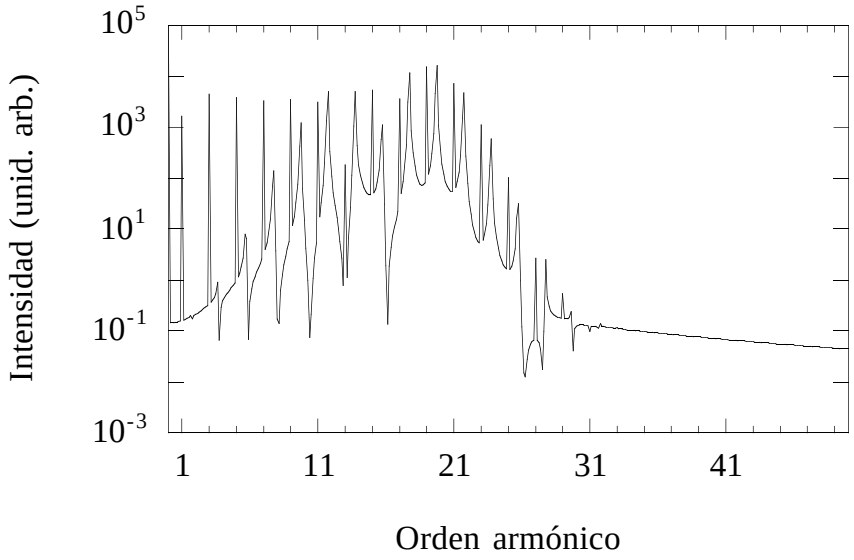


Figure 2.4: Spectrum corresponding to the parameters of figure 2.3.

## 2.2 Effect of time-dependent ionization on the harmonics generated by bound-bound transitions [95]

The effect of ionization on a closed system such as a two-level atom is the loss of both population and coherence. The simplest way to include it in our equations is by means of an ionization rate that will describe the amplitude decay in each level. We shall then have an open two-level system, as seen in figure 2.5, whose equations of motion are

$$\frac{da_0(t)}{dt} = -iE(t)d_{01}a_1(t) - \frac{\gamma_0(t)}{2}a_0(t), \tag{2.8}$$

$$\frac{da_1(t)}{dt} = -iE(t)d_{01}a_0(t) - \Big[\frac{\gamma_1(t)}{2} + i\omega_T\Big]a_1(t). \tag{2.9}$$

The ionization rates are obtained from equation (1.15) considering the $1s$ and

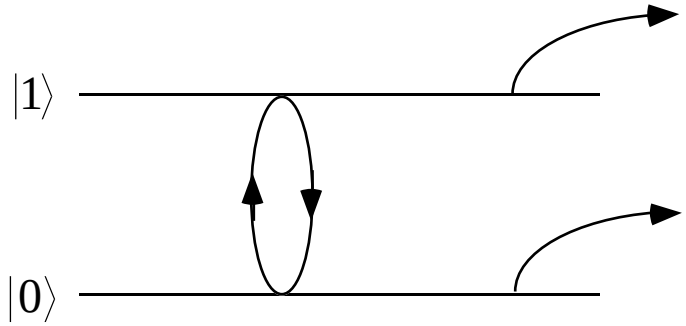


Figure 2.5: Scheme of the open two-level system. Arrows represent the population transfer.

$2p$ states

$$\gamma_0(t) = 4E_0^{-2}|E(t)|\exp\left(-\frac{2}{3|E(t)|}\right), \tag{2.10}$$

$$\gamma_1(t) = 2^{-7}E_0^{-4}|E(t)|\exp\left(-\frac{1}{12|E(t)|}\right). \tag{2.11}$$

Both rates strongly, though indirectly, depend on time through the electric field, as we see in figure 2.6. The ionization has two maxima, corresponding to the extremes of the field, and vanishes when the field changes its sign. When the field amplitude is $E_0 = 0.06$ a.u., the ionization rate in the excited state is four orders of magnitude greater than the ground state and hence is the most important one. Solving equations (2.8) and (2.9) for our usual parameters ($E_0 = 0.06$ a.u., $\omega_0 = 0.04$ a.u.), we obtain a spectrum which differs considerably from that of the two-level system, as we see in figure 2.7. The mere inclusion of a time-dependent ionization causes the generation of high harmonics (here up to the 50th order) with higher intensities than the few peaks of the closed two-level system. The most intense peaks are those close to the transition frequency of the two levels.

We can better understand what happens by taking a look at the temporal evolution of the populations and the dipole moment, depicted in figure 2.8. The ground state population decreases almost monotonically, despite small Rabi-like oscillations which are not visible in the figure, whereas the excited one varies

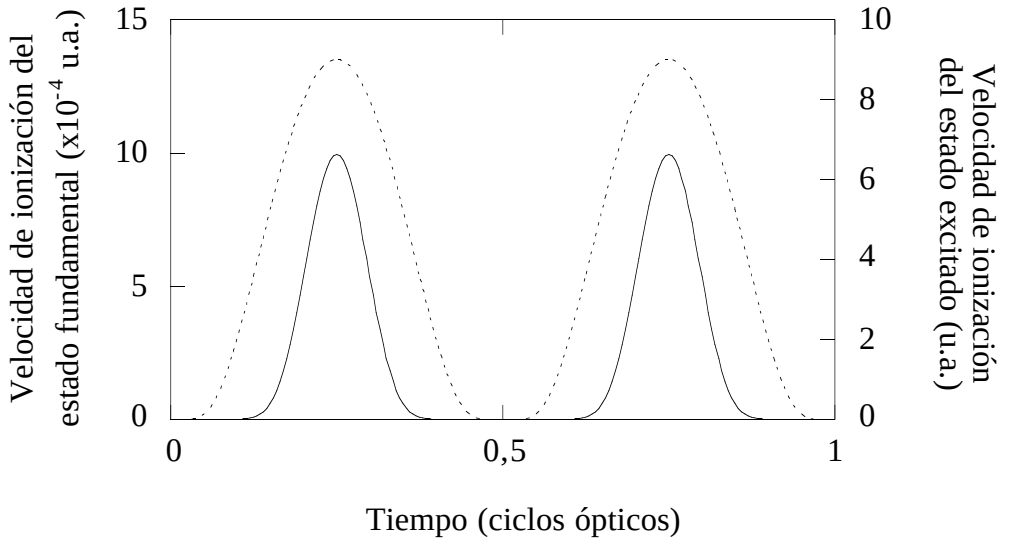


Figure 2.6: Ionization rates along an optical cycle for a sinusoidal field with an amplitude of $E_0 = 0.06$ a.u. The solid line represents the ground state rate and the dotted line the excited state rate. Notice the difference in the scales.

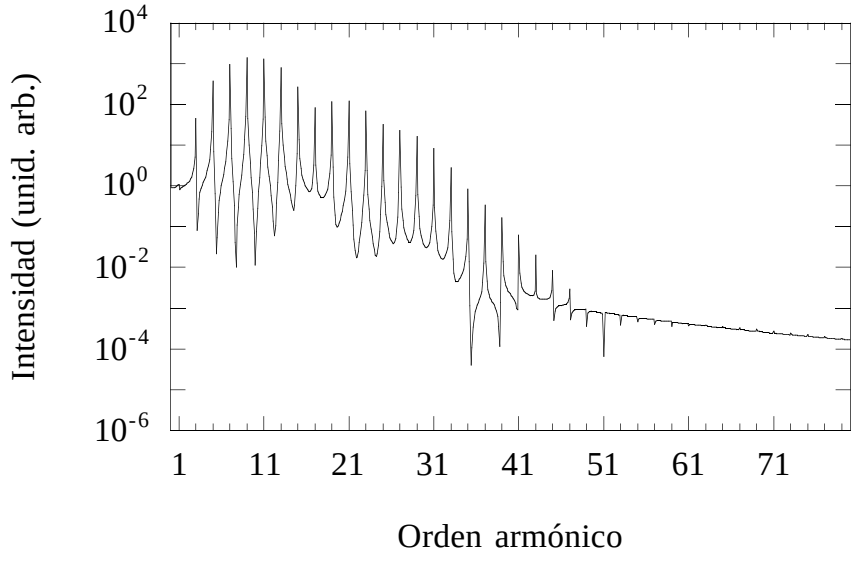


Figure 2.7: Spectrum corresponding to the solution of equations (2.8) and (2.9) for an external field with the same parameters as in figure 2.2.

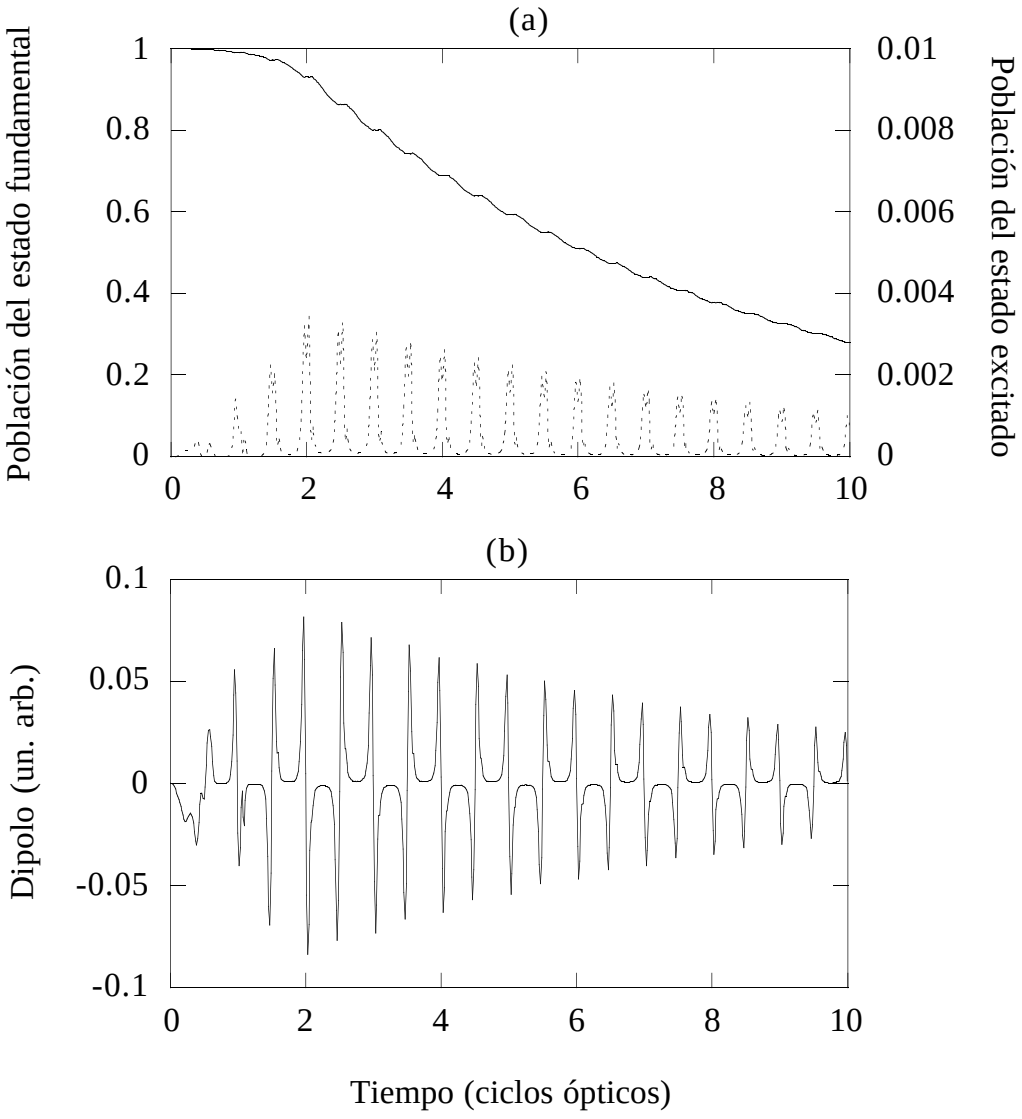


Figure 2.8: The same as in figure 2.1 but introducing time-dependent ionization in both levels.

sharply, never being greater than $4 \times 10^{-3}$. These sharp variations have their maxima when the field goes to zero. The effect of these oscillations on the dipole moment can be observed in plot 2.8b, which clearly explains the generation of high harmonics. The oscillations in the population of the excited state are due to the following mechanism: the external field excites a small part of the population from the first to the second state, which undergoes a rapid depletion because of the high ionization rate. When the field is zero, the ionization rate vanishes and part of the population can survive in the excited level exactly at that instant, although it ionizes as soon as the field amplitude increases slightly. The excited level therefore acts as an intermediate state for the ground state population to be ionized. In fact, the population directly ionized from the excited state is much smaller than the population ionized from the excited one, as seen in figure 2.9. The much greater population at ground level cannot cancel its minimal ionization rate. Actually, we could neglect ionization from the ground level by making $\gamma_0(t) = 0$ and the spectrum obtained would be the same (for the parameters we are using, of course).

High harmonics could be interpreted from the above-mentioned adiabatic point of view. The addition of ionization rates is equivalent to a dynamical broadening of the energy levels by an imaginary term. This term is huge when the field is maximum or minimum in the case of the excited level and therefore the instantaneous energies of the dressed states are broadened beyond the transition frequency, which yields very high harmonics.

Before going further, we wish to remark that the generation of high harmonics does not depend on the exact form of the ionization rates; instead, it exists whenever these rates depend on time. One could argue that the form of $\gamma_1(t)$ given by expression (2.11) is not valid because for most of the time the excited level is in the barrier suppression regime for the field amplitude we are using. We can use

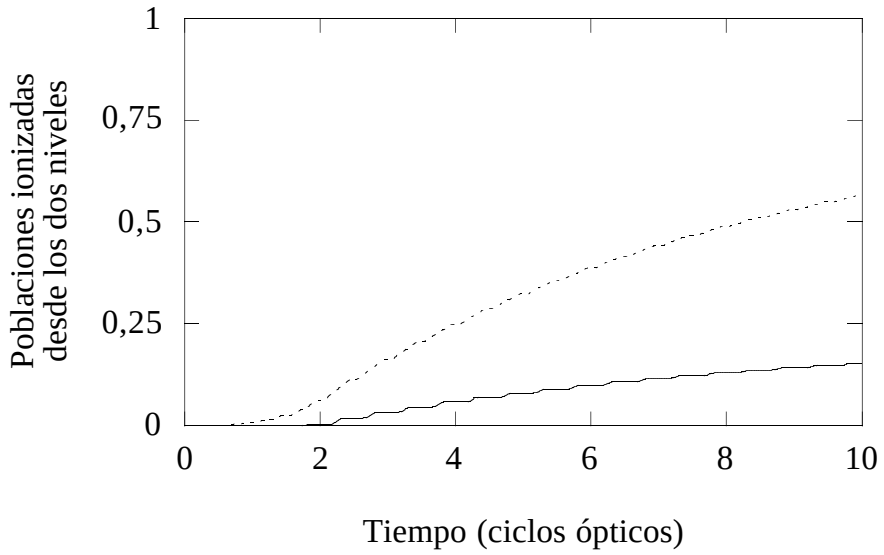


Figure 2.9: Ionized populations from ground (solid line) and excited (dotted line) levels in the case of figure 2.8.

a semiclassical approach and assimilate the ionization with the flux of population that goes over the barrier, whose velocity is the linear momentum of the released electrons, which is given by the difference in energy between the excited level and the top of the barrier, $p = \sqrt{2|V_{ef} + \omega_1|}$. The maximum of the potential barrier $-1/x - E(t)x$ is $V_{ef} = -2\sqrt{|E|}$ and $\omega_1 = -\epsilon_2 = 0.125$ a.u. When the field amplitude is below the classical critical value $E_1^{(cr)} = 0.0039$, the excited state lies below the barrier and we can neglect ionization. Thus, the ionization rate would take the form [95]

$$\gamma_1^{(sc)}(t) = \sqrt{4|E(t)|^{1/2} - 2\omega_1}\ \Theta(|E(t)| > E_1^{(cr)}). \tag{2.12}$$

This expression gives us an ionization rate whose maximum is smaller than the one in (2.11), but it has the disadvantage that it has no derivative at $E_1^{(cr)}$. This affects the harmonic spectrum obtained with it, as observed in figure 2.10. Again, we have high order harmonics and in this case the intensities do not decrease but

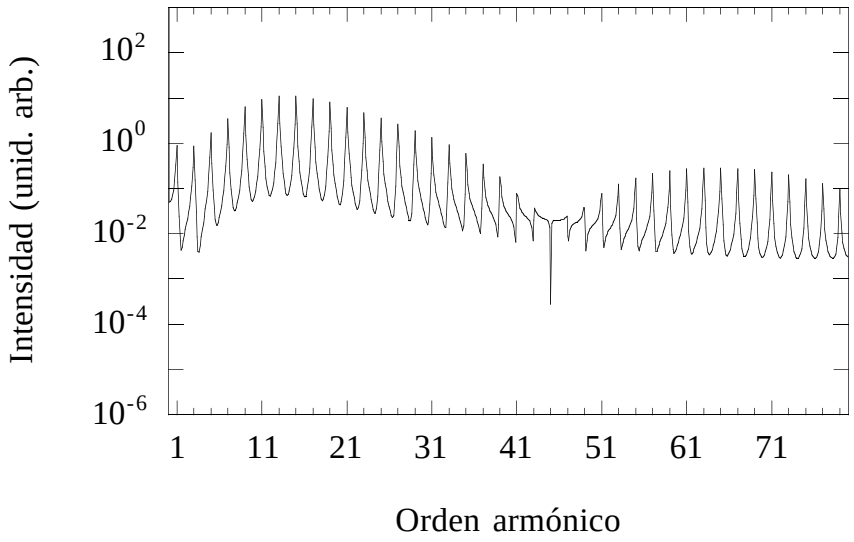


Figure 2.10: Spectrum obtained with expression (2.12) for the ionization from the excited level when the field has the same parameters as in figure 2.7.

remain more or less the same up to very high frequencies, with no cutoff. A further example is depicted in figure 2.11, where a simple dependence $\gamma_1(t) \propto |E(t)|^2$ has been chosen and there are fewer harmonics, although they also exist.

We can then deduce that it is a general trend that a rapidly varying-in-time ionization generates high harmonics in a two-level system, regardless of the exact form of the ionization rate. This is an alternative mechanism to the transitions between bound and free states which are responsible, as we explained in section 1.4, for the plateau and cutoff frequency in the tunnelling regime spectra. These transitions should be taken into account in any realistic model.

## 2.3 Harmonic generation with two-level systems including ionization and recombination [96]

In order to recover the plateau of harmonics and the cutoff frequency, we have to take into account the transitions between high energy continuum states and bound

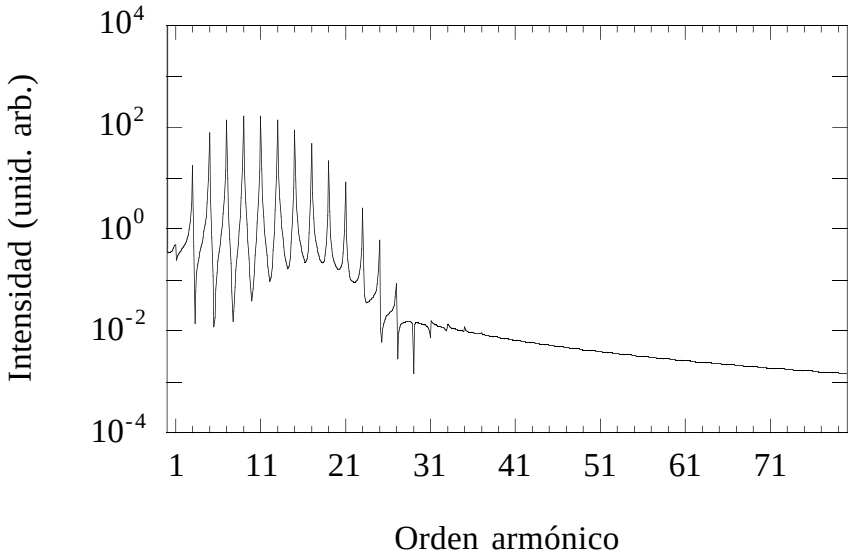


Figure 2.11: Spectrum obtained with an ionization rate for the excited level proportional to $|E(t)|^2$ for the same field parameters as in figure 2.7.

states. We shall do this by refining our two-level system such that it includes recombination, at the same time trying to keep the model simple to be able to interpret its results. We shall assume that the ionized population goes to the continuum and there evolves as a classical particle but keeping a quantum trace; namely, a phase which permits a coherent recombination when it comes back to the core position. Let us now explain the model step by step [96].

Following our equations (2.8) and (2.9), the population ionized from the $|j\rangle$ level (ground or excited) during a timestep $\Delta t$ is

$$\frac{\Delta P_j^{ion}}{\Delta t} = \gamma_j(t)|a_j(t)|^2. \tag{2.13}$$

This population generates a wavepacket at each instant of time whose amplitude is $[\Delta P_j^{ion}]^{1/2}$ with an appropriate phase factor. This phase can be found if we admit that in the tunnelling regime everything evolves adiabatically, and hence it is the same phase as that of the leaving level except for a sign due to the interaction

with the field which changes the parity of the state. Explicitly, the amplitude of the wavepacket ionized from $|j\rangle$ between $t_0$ and $t_0 + \Delta t$ is

$$a_j^{ion}(t_0; t_0) = [\Delta P_j^{ion}]^{1/2} \frac{a_j(t_0)}{|a_j(t_0)|} \frac{E(t_0)}{|E(t_0)|}. \tag{2.14}$$

This wavepacket evolves as a classical particle subject to the external field according to equations (1.64)-(1.66). Here we neglect the effect of the atomic potential on the continuum wavepacket, as well as the spatial dependence of the field, the magnetic field and the rest of the relativistic effects. We can justify these assumptions since the field intensity in the tunnelling regime is low, the excursion of the ionized particle will be much shorter than the laser wavelength and its velocity will be much smaller than $c$. We then continue within the range of validity of the dipole approximation. From equation (1.72), we obtain the change of phase of the particle in the continuum, given by the classical action

$$\Phi(t_0, t) = \int_{t_0}^{t} dt' \Big\{ \frac{\dot{x}(t')^2}{2} + I_j \Big\}. \tag{2.15}$$

Following on with our adiabatic point of view, we assume that the potential energy of the state does not change during the ionization process and hence the potential energy term in equation (2.15) is $I_0 = 0$ for the ground state and $I_1 = \omega_T$ for the excited one. This will affect the cutoff frequency in the spectrum, as we shall see below. Thus, the evolution of each wavepacket ionized at $t_0$ will be

$$a_j^{ion}(t_0; t) = a_j^{ion}(t_0; t_0) e^{-i\Phi(t_0, t)}. \tag{2.16}$$

As we already know, some of these particle-wavepackets will return to the ion position and some of them will not. We can forget about the latter ones since they will not contribute to harmonic generation and we shall only take into account those which return and only the first time they do so. The following recollisions do not change the cutoff frequency of the harmonics and they only slightly affect the intensities of the plateau harmonics [97, 98]. We assume that when the particles

return, they interact with the bound states as an additional pseudolevel. The evolution equations take the form

$$\frac{\mathrm{d}a_0(t)}{\mathrm{d}t} = -\frac{\gamma_0(t)}{2}a_0(t) - iE(t)[d_{01}a_1(t) + d_{0c}a_0^{cont}(t)], \tag{2.17}$$

$$\frac{\mathrm{d}a_1(t)}{\mathrm{d}t} = -\Big(\frac{\gamma_1(t)}{2} + i\omega_T\Big)a_1(t) - iE(t)[d_{01}a_0(t) + d_{1c}a_1^{cont}(t)], \tag{2.18}$$

where the amplitude of the states in the continuum which rescatter with the core is

$$a_j^{cont}(t) = \int_0^t a_j^{ion}(t_0;t)\delta(x(t_0;t))dx(t_0;t). \tag{2.19}$$

The Dirac delta distribution means that we only consider the recombination of the ionized states when their classical trajectory, $x(t)$, crosses the coordinate origin. The dipole matrix elements between a free continuum state and the bound ones can be computed taking the continuum state as a plane wave [23, 51] and take the form

$$d_{0c}(v) = i\frac{2^{7/2}\alpha^{5/4}}{\pi}\frac{v}{(v^2+\alpha)^3}, \tag{2.20}$$

$$d_{1c}(v) = \frac{2^7\alpha^{7/4}}{\pi}\frac{v^2}{(4v^2+\alpha)^3(v^2+\epsilon_1)}, \tag{2.21}$$

where $\alpha$ is twice the ionization potential and $\epsilon_1$ is the energy of the excited level.

The assumption that recombination only takes place at the instant of time when the ionized particle is at the origin leads to an underestimation of the transition probability $d_{jc}(v)\Delta t$, since the numerical timestep $\Delta t$ is much smaller than the actual interaction time, especially if we take into account the broadening of the wavefunction during its excursion in the continuum. To avoid this, we correct the recombination term, multiplying $d_{jc}(v)$ by $T_i/\Delta t$, where $T_i = l_{int}/v$ is the interaction time, which is proportional to the interaction length (typically the atom size) and inversely proportional to the particle's velocity. For the sake of simplicity, we shall use constant dipole moments $d_{jc} = d_{jc}(v_{prom})$, where $v_{prom} = 0.665E_0/\omega_0$

is the mean velocity of the particles when they first rescatter with the core, which has been computed numerically. In any case, the choice of the expression for the dipole moment does not qualitatively affect our results.

If we solve equations (2.17) and (2.18) for our usual parameters, we obtain the spectrum depicted in figure 2.12. Note that the first harmonics are similar to the ones in figure 2.7, in which no recombination was included. The novelty of the spectrum is the existence of higher harmonics with a notorious plateau structure up to a cutoff frequency close to the 55th harmonic, followed by a sharp decrease. This spectrum resembles the one obtained for a real hydrogen atom in the tunnelling ionization regime. The position of the cut-off frequency is slightly different from that obtained in the real hydrogen: $\omega_T + 3.17U_p$ instead of $I_p + 3.17U_p$. This results from keeping the potential energy of the tunneled electron fixed during the ionization and excursion, implying that the maximum energy of the electrons ionized from the upper level at the instant of the rescattering with the core is precisely $\omega_T + 3.17U_p$. We know that this can be corrected since the electrons leave the ion not at $x = 0$, but at a different position, and also because the recollision does not take place exactly at $x = 0$ due to the broadening of the wavepacket. Taking these aspects into account, the cut-off position would be more diffuse. In any case, for the parameters we are using, the difference between $I_p$ and $\omega_T$ is only two or three harmonics; i.e., almost negligible.

We can separate the effects of time-dependent ionization and coherent recombination as in figure 2.13, in which we have depicted the spectrum obtained from solving equations (2.17) and (2.18) using time-independent averaged ionization rates (see section 1.2), which in our case are $\gamma_0^{pr} = 4(3/\pi E_0)^{1/2}\exp(-2/3E_0)$, $\gamma_1^{pr} = 2^{-11/2}(3/\pi)^{1/2}E_0^{-5/2}\exp(-1/12E_0)$. Comparing this spectrum with the previous one, we notice that the lower order harmonics are much less intense, while the the higher ones remain roughly the same. It is then clear that the exact form of the

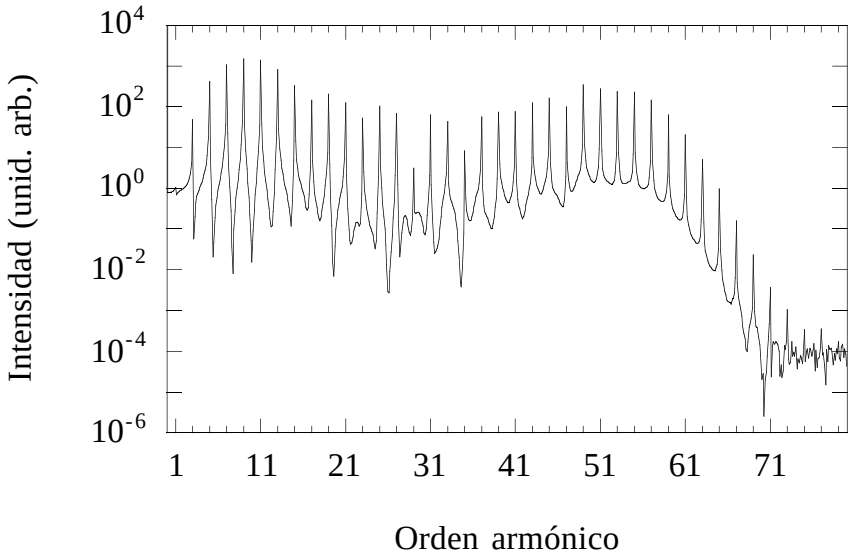


Figure 2.12: Spectrum corresponding to the solution of equations (2.17) and (2.18) for an external field with the same parameters as in figure 2.2.

ionization rates is only important for the intensities of the lower order harmonics.

We can also observe, as in previous cases, the time evolution of populations and the dipole moment, depicted in figure 2.14. At first sight, they are quite similar to the case when only ionization was considered (figure 2.8). As regards the populations, the difference with the previous case is minimal, the final population of the ground level being slightly greater, due to the returning electrons, and the excited population being almost the same. Regarding the dipole moment, the difference is seen in small oscillations when the dipole has a low value, which can be appreciated in detail in figure 2.15. These small oscillations are responsible for the generation of higher order harmonics; those corresponding to the plateau and the cut-off area.

The fact that the population returning to the bound states from the continuum is so small suggests an alternative interpretation of the physics involved in our model. Harmonics have been usually attributed to transitions from the continuum

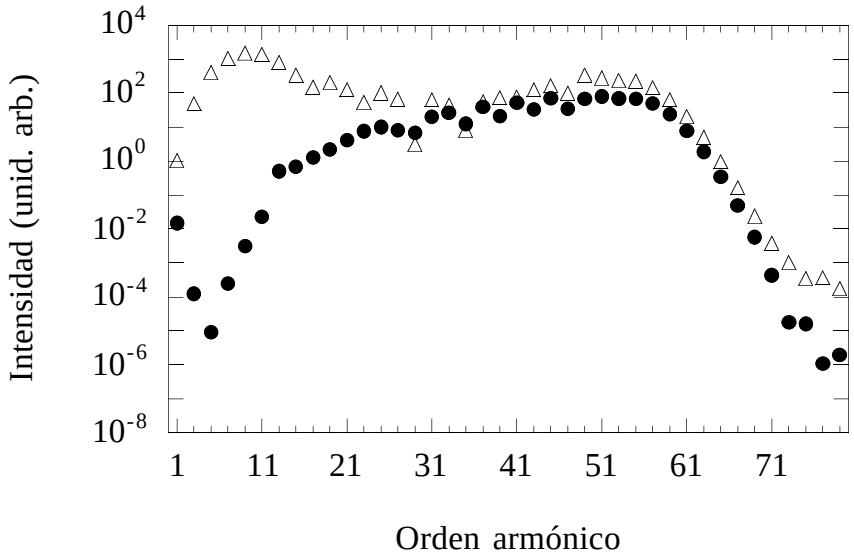


Figure 2.13: Harmonic intensities obtained with time-independent averaged ionization rates (black dots) and time-dependent ones (open triangles).

to bound states, neglecting the transitions between bound states. We believe that the role of these transitions is important because the values of dipole moments corresponding to transitions between bound states are orders of magnitude higher than those belonging to transitions between bound-free states [23]. Moreover, the ionized population spreads over all the free states and the fraction of population in the relevant states, those with high kinetic energies which generate high harmonics, is very small. We can analyze this in further detail. The total dipole moment in our system consists of two different parts, $d(t) = d_{b-b} + d_{b-c}$, where the contributions of the bound-bound the bound-free transitions are, respectively

$$d_{b-b} = d_{01}(a_0 a_1^* + a_0^* a_1), \tag{2.22}$$

$$d_{b-c} = d_{0c}(a_0 a_0^{cont*} + a_0^* a_0^{cont}) + d_{1c}(a_1 a_1^{cont*} + a_1^* a_1^{cont}). \tag{2.23}$$

In figure 2.16 we observe the spectrum generated by each of these contributions. The bound-bound one is in this case four orders of magnitude higher than in the

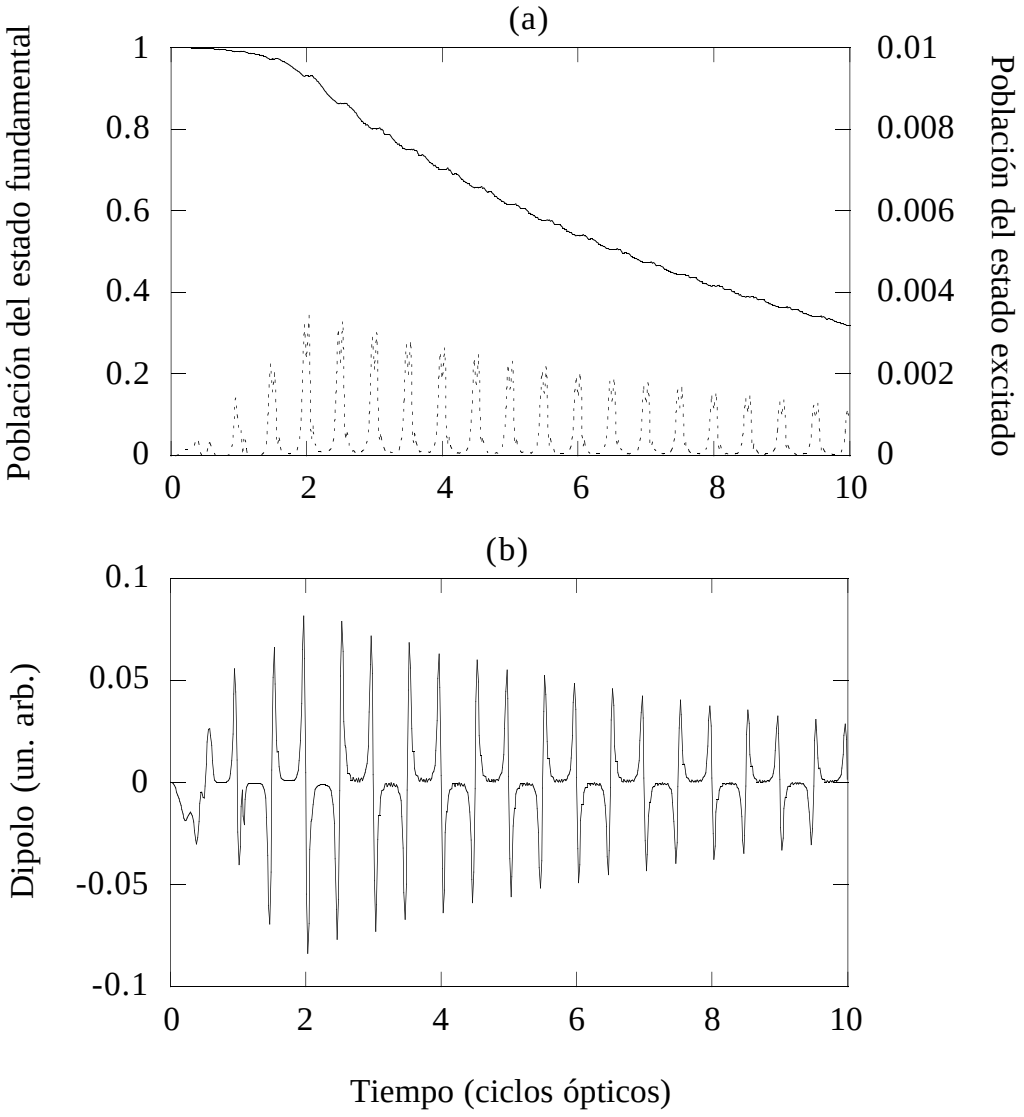


Figure 2.14: Time evolution of populations (a) and the dipole moment (b) when both ionization and recombination are included in our model. The field parameters are $E_0 = 0.06$ a.u. and $\omega_0 = 0.04$ a.u.

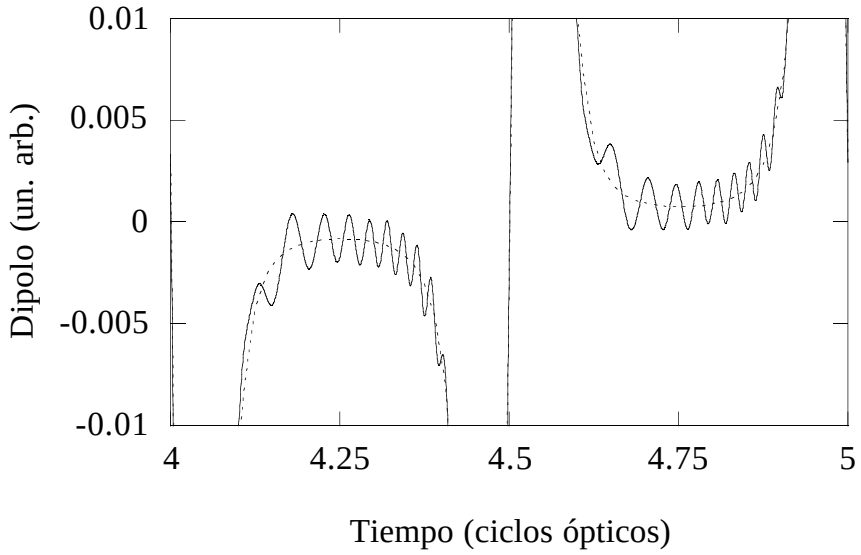


Figure 2.15: Detail of figure 2.14b. The dotted line represents the dipole moment when recombination is not taken into account.

case of the plateau harmonics, its importance being quite clear.

In our opinion, the mechanism by which harmonics are generated is the following: the coupling between bound states and high energy free states induces fast oscillations in the bound states amplitudes. As a consequence, the dipole moment between them oscillates with those high frequencies, generating the harmonic spectrum. The bound-bound transition then acts like a resonator or amplifier of the small oscillations due to the coherent recombination. Of course, the spectrum of free-bound transitions includes those high order components but its contribution is noticeably smaller. In a real atom, even free-free transitions, which are forbidden in our simple model, generate a spectrum with the same characteristics known to us [99], but also in this case the dipole matrix elements between free states are smaller and hence their contribution to the spectrum is also small. Only if the pulse is much longer than the time needed to fully ionize the atom will the free-free contribution become dominant in the harmonic generation process.

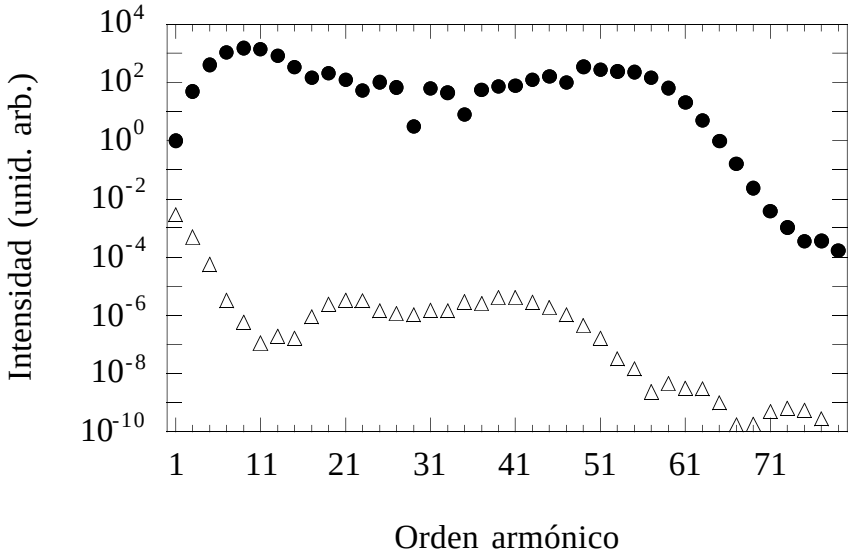


Figure 2.16: Intensities of the harmonics generated by the bound-bound transition (black dots) and bound-free transition (open triangles) contributions to the dipole acceleration for the same parameters as in the previous figure.

We can offer a further basis to this idea from the calculations made with short-range potentials with a limited number of bound states. Becker *et al.* have studied the dynamics of a system with a regularized delta-function potential [100], obtaining spectra which are qualitatively similar to the hydrogen spectrum but several orders of magnitude less intense. Krause *et al.* [42] compared hydrogen spectra with those obtained with a Yukawa-like potential, $V(r) = -Ze^{-\alpha r}/r$, which allows one to change the number of bound states simply by changing the $Z$ and $\alpha$ parameters. In figure 2.17, we see a comparison of the harmonic spectrum of hydrogen and those obtained with the Yukawa-like potential with one ($Z = 1.93$ a.u., $\alpha = 1$ a.u.), two ($Z = 1.16$ a.u., $\alpha = 0.17$ a.u.) and four ($Z = 1.05$ a.u., $\alpha = 0.05$ a.u.) bound states and the same ground state energy. When only one bound state exists, the harmonics are very weak, whereas when there are four the similarity with the hydrogen spectrum is considerable. This is due not only to the

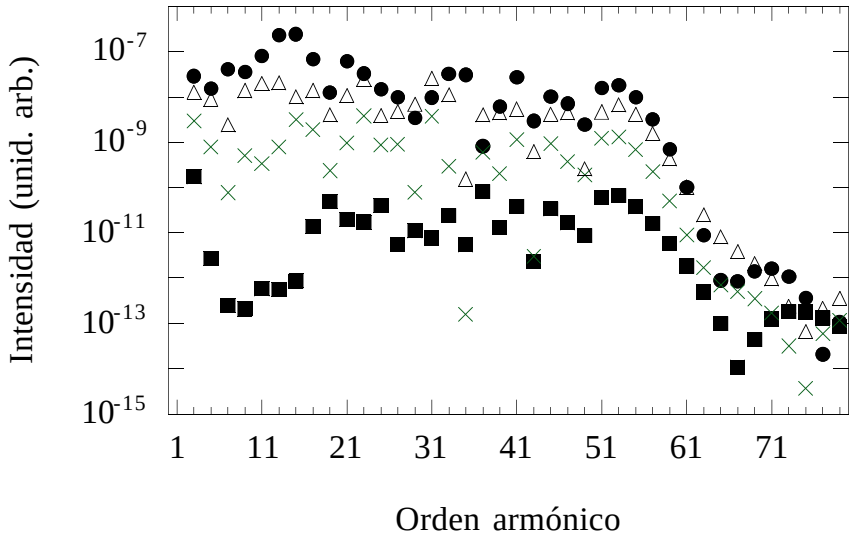


Figure 2.17: Intensity of the harmonics generated by a Coulomb potential (black dots) and a Yukawa-like potential with one (black squares), two (crosses) and four (open triangles) bound states and the same ionization potential. The field parameters are $E_0 = 0.06$, $\omega_0 = 0.04$.

existence of resonances that enhance the efficiency of ionization but also to the amplification of the dipole oscillations among the above bound states.

To check the validity of our model we can compare our results with the solution of the one-dimensional Schrödinger equations described in section 1.4.3. We believe this is the best benchmark of our model, which is also one-dimensional. In this case, we choose the parameters of the potential $Z = 1$ a.u. and $a_0 = 1.412$ a.u., which yield the energy of the fundamental state $I_p = 0.5$ a.u. The first excited state has a different energy from three-dimensional hydrogen and we have to change the parameters in our model to $\omega_T = 0.267$ a.u., $d_{01} = 1.297$ a.u. Figure 2.18 shows the comparison between the results of our model and those given by the one-dimensional Schrödinger equation. Not only the cut-off position, with a shift due to the potential energy difference $I_p - \omega_T$, but also the intensities of the intermediate harmonics are similar. In fact, the most remarkable difference appears in the first harmonic intensity, which is much higher in the hydrogen calculation than in ours. This is due to the fact that our dipole acceleration does not include the motion of the free wavepackets outside the core, which has the field frequency and which is of course included in the 1D hydrogen equation results. One last fact supporting the importance of bound-bound transitions is that the contributions to the dipole acceleration of the first bound-bound transition are much greater than that corresponding to the transitions between these first two bound states and the continuum state with momentum $k = \sqrt{6U_p}$ in the one-dimensional hydrogen, which is roughly the one which gives the cut-off frequency, as we observe in figure 2.19. The first contribution has the same order of magnitude as the total radiation, whereas the bound-continuum contribution is several orders of magnitude weaker.

In sum, we can say that the role of bound-bound transitions in harmonic generation in the tunnelling ionization regime is more important than usually assumed. Likewise, the fact that the ionization process is not uniform but strongly time-

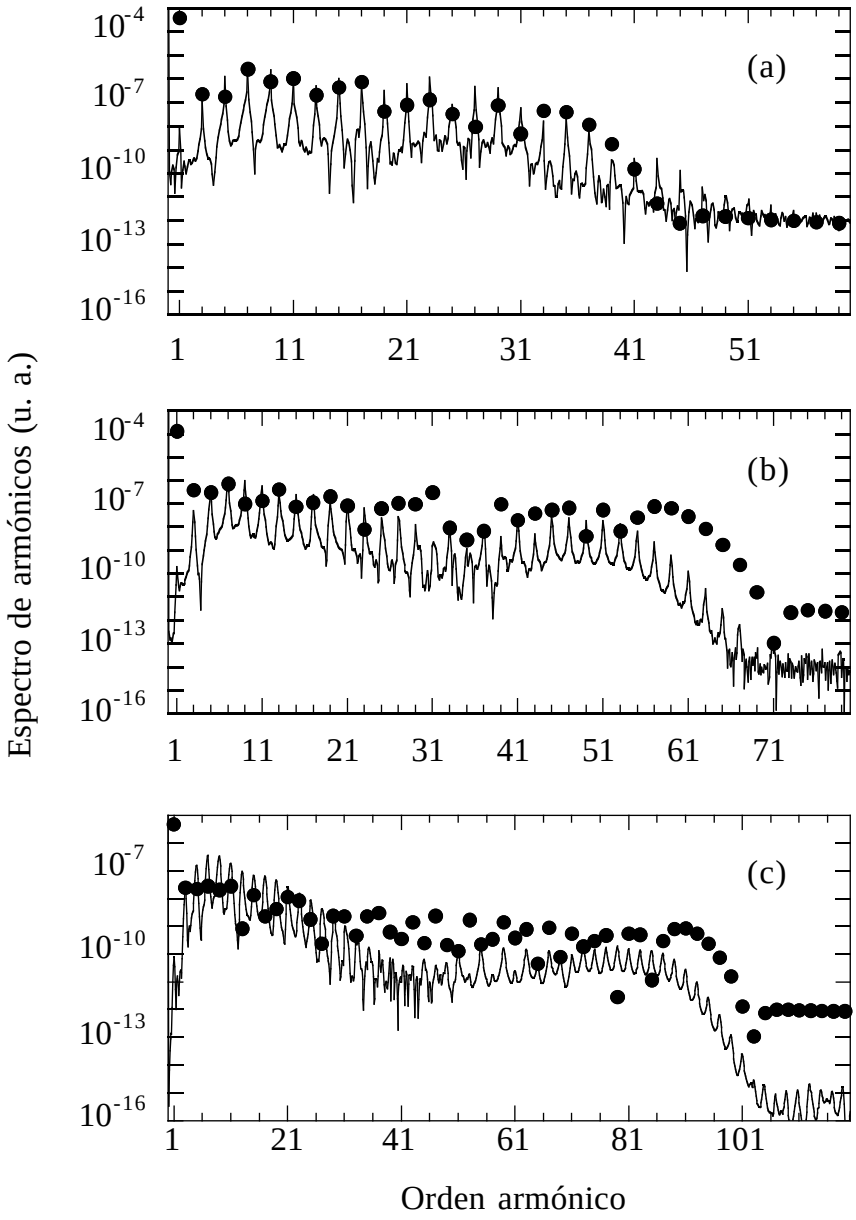


Figure 2.18: Comparison of the intensity of the harmonics given by our model (full curve) and the one-dimensional Schrödinger equation (black dots) for parameters $\omega_0 = 0.04$ a.u. and $E_0 = 0.04$ a.u. (a ), $E_0 = 0.06$ a.u. (b) and $E_0 = 0.08$ a.u. (c).

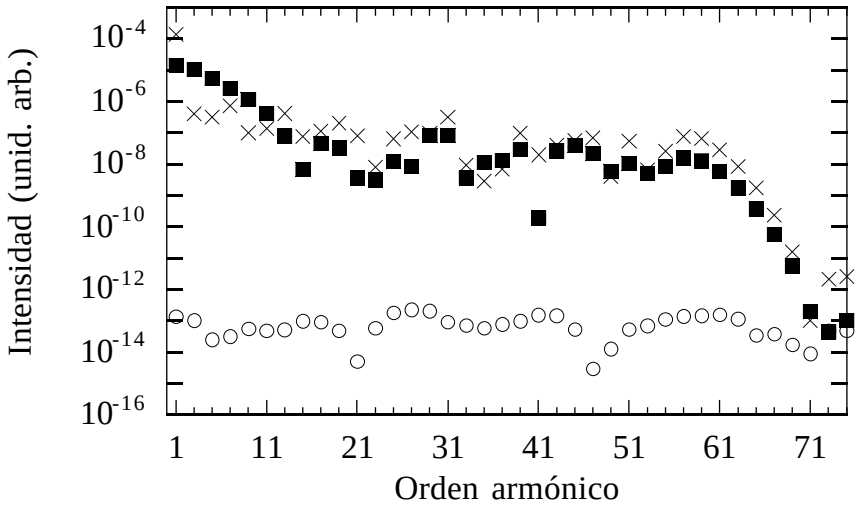


Figure 2.19: Harmonics generated by the one-dimensional Schrödinger equation for $E_0 = 0.06$ a.u. and $\omega_0 = 0.04$ a.u. Crosses represent the total harmonic yield, black squares the contribution from the dipole between the ground and first excited level and open circles the contribution from the dipole between the first two bound states and a continuum level with momentum $k = \sqrt{6U_p}$.

dependent along an optical cycle is an additional mechanism which can generate harmonics and which is specially relevant in the intensities of the lower harmonics. The open two-level model introduced by us provides a fair amount of information about these two aspects, but we wish to remark that in no way is it a universal model; rather, it can only be used in the tunnelling regime, since it does not take into account multiphoton or barrier suppression transitions when the field is more intense, nor the effect of other bound levels. In spite of these limitations, it is qualitatively acceptable and gives reasonable results when compared with the one-dimensional Schrödinger equation.

# Chapter 3

# Numerical simulation of the interaction between plasmas and laser pulses

The aim of this chapter is to explain the models and algorithms we have used to simulate the interaction between an ionizing medium and an intense electromagnetic field. We shall use two different models. One of them is a so-called "particle-in-cell" (PIC) code, widely used in a broad variety of problems in plasma physics, and the other is a much simpler model that has the advantage of permitting us to adequately study the generation and propagation of harmonics during the ionization of a not very dense medium with a relatively weak field.

## 3.1 Plasma simulation via particle codes

There are two possible approaches in the field of plasma simulations. One is the description of the plasma as a fluid, completely disregarding the particular features of its components. In this case, one has to solve the magnetohydrodynamic equations of the plasma, which differ depending on the problem in question. The other possibility is the kinetic description, which takes into account more detailed models of the plasma, including the interactions among particles through the electromag-

netic field. This second approach includes the solution of the kinetic equations of the plasma in the phase space (Vlasov or Fokker-Planck [74]) and the simulation of single particles, following the evolution of a set of particles interacting among themselves and with the external fields. Each of these descriptions has its own advantages and disadvantages. Magnetohydrodynamical codes have proved useful in large scale problems dealing with experimental devices but they lack sufficient detail to explain the basic physical phenomena when the energy distribution of the particles is very different from a Maxwellian one (for instance, a cold plasma generated by photoionization). In this case, the description with particles is necessary. The same happens when the trajectories of the single electrons cross, i.e. when collisions become important. This is why we shall first use use a particle description, which conserves almost all the physics of real problems at the expense of extending the calculations.

Here we shall summarize the main characteristics of a particle code, without discussing all the details. The description will become more detailed with regard to the particular model we have chosen. The literature contains many references to the particle simulation of plasmas, which in recent years has become one of the most important disciplines in the field of plasma physics. We refer the interested reader to the works [74, 101, 102], which were used by us, for further information. A recent report about simulations in plasma physics can be found, for instance, in [103].

The idea of describing a plasma by means of the motion of its particles may seem completely absurd if we take into account the number of particles usually existing in experiments (we can think in terms of more than $10^{20}$ particles in one $cm^3$) and recall that we have to solve the equations of motion for each particle, as well as Maxwell equations to find the fields generated by them and the external ones. With currently available computers, it is impossible to simulate the motion of more than

$10^8$ particles along a few optical cycles within a reasonable amount of time. So what are these particle codes, so widely used and so commonly accepted by the scientific community? The explanation is that code "particles" are not real particles but macroparticles or charge clouds with finite dimensions, which include many point particles and move as a whole. This trick of grouping the charge in large particles seems at first sight unjustified, mainly because it implies a loss of information about particle-particle collisions (very harmful in numerical simulations due to the Coulomb potential singularity), which are frequent in the case of high densities. However, several reasons permit us to justify, to a certain extent, this approach. In the case of a hot plasma, whose particles have an initial velocity distribution with a thermal energy, there is a characteristic length, $\lambda_D = \sqrt{kT/4\pi e^2 N_0}$, called the Debye length, which defines the radius inside which particle-particle effects are more important and outside which collective effects become crucial. If we are only interested in the effects with a scale greater than $\lambda_D$, we can disregard collisions among particles because they will be screened by collective forces. The second argument is that it is not possible, numerically, to consider point particles since we are constricted by our space-time grid. Hence, we can benefit from this and choose our particles' width as greater than the Debye length, reducing in this case the collisional cross section to a much smaller value than in the zero-radius case. For cold plasmas, the Debye length would be null and the microscopic field would not be screened. However, we can go further into the land of quantum physics and consider that electrons are not point particles but wavepackets, which not only move but broaden when subjected to electromagnetic fields, so that collisions among point particles will never occur whereas they will among charge clouds. In our case, the grid size will typically be ten or twenty atomic units and the particle size will be the same or similar. The time needed by a free Gaussian packet to pass from a width of one atomic unit (that of the electron inside the atom) to ten atomic

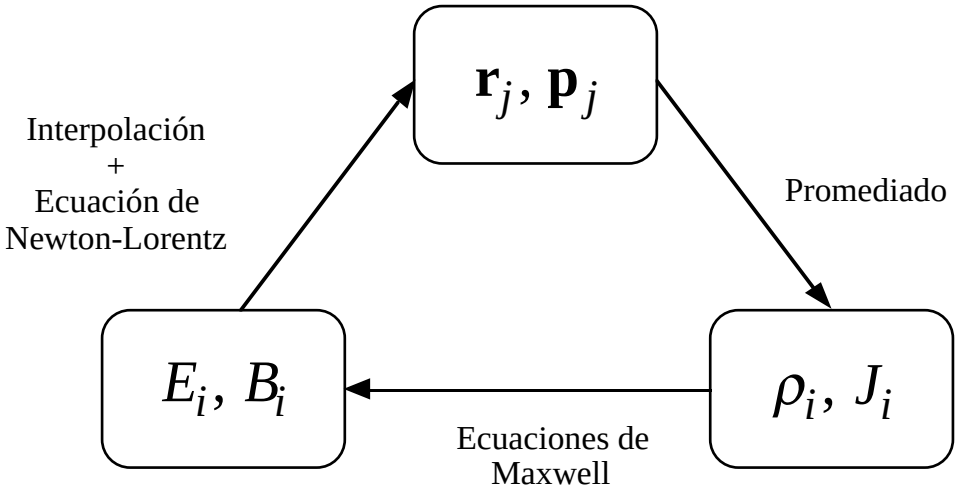


Figure 3.1: Basic cycle in a particle code.

units is roughly twenty atomic units, a tenth of an optical cycle for the frequencies we are dealing with and hence to treat such a packet as a macroparticle is not so absurd. All these justifications are obviously partial and one can always fall back on the authority argument, which in this case says that particle simulations have given very good results that can be checked experimentally. Such simulations are widely accepted nowadays and important problems only arise when the plasmas are highly overdense, with electron densities orders of magnitude higher than in solids, which make binary collisions crucial in the system dynamics.

In a code particle we have the following variables:

- The position $\mathbf{r}_j$ and momentum $\mathbf{p}_j$ of each particle.

- The charge $\rho_i$ and current $\mathbf{J}_i$ densities in the spatial grid points.

- The electromagnetic fields $\mathbf{E}_i$, $\mathbf{B}_i$ in the spatial grid points which must be interpolated in each particle's position to find the force which acts on it and moves it.

Hence, the code consists of the iteration of a cycle such as that shown in figure 3.1. Variations appear when one goes to the specific solution of each step. In our case, we shall use a one-dimensional in space, two-dimensional in velocity (1D2V)

code. Let us explain this. If a plane wave normally impinges onto a thin homogeneous slab, we can assume that all the spatial variations will occur in the direction of propagation of the field because there is symmetry in the transversal plane and all the particles in the medium move in the same way. In a real experiment, we shall have a more or less focused beam, but if the slab width is much smaller than the beam width, which can be achieved with very thin slabs (there are experiments with foils measuring only tens of nanometre in thickness), and if the laser is intense and only slightly focused (at present, it is possible to obtain intensities of $10^{18}$ W/cm$^2$, which are higher than the ones we use, focused on sections of tenths of mm$^2$), we can carry out the plane wave approximation without making any important mistakes. Hence, we lose typically transversal effects such as self-focusing, channel formation, etc., which occur when the intensities are higher than those we are interested in. The geometry of our simulations is depicted in figure 3.2, in which the electric field is polarized along the $y$ direction. The motion of the charges take place in the $XY$ plane and there is no $v_z$ velocity component. Due to the symmetry, the particles are assumed to be slabs with width $a$ and infinite transversal dimensions, i.e., they are charge sheets instead of particles. In this and next section, we again use Gaussian units, which are more appropriate than atomic ones.

Let us start with the solution of the equations of motion of the particles. We shall use a *leapfrog* method, which consists in finding positions and momenta in alternate instants of time. If we have the equations of motion

$$\frac{d\mathbf{p}}{dt} = q\left[\mathbf{E} + \frac{1}{c}\mathbf{v} \times \mathbf{B}\right], \tag{3.1}$$

$$\frac{d\mathbf{r}}{dt} = \mathbf{v}. \tag{3.2}$$

with $\mathbf{p} = m\gamma\mathbf{v}$, we assume we know the momenta at instant $t - \Delta t/2$ and the positions and forces at $t$, and hence the momenta are advanced to $t + \Delta t/2$ and

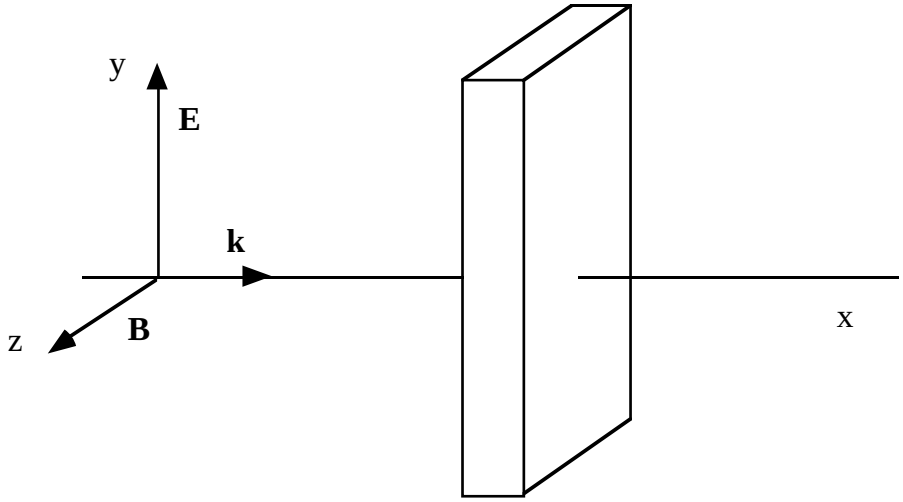


Figure 3.2: Scheme of the interaction geometry

the positions to $t + \Delta t$. There are several possible algorithms of the *leapfrog* type. We shall use one by Boris, which is fast and can be reversed in time [101]. If we set $\mathbf{u} = \gamma \mathbf{v}$, with $\gamma^2 = 1 + u^2/c^2$, the finite difference equation for each momentum that needs to be solved is

$$\frac{\mathbf{u}^{n+1/2} - \mathbf{u}^{n-1/2}}{\Delta t} = \frac{q}{m}\left[\mathbf{E}^n + \frac{1}{c}\frac{\mathbf{u}^{n+1/2} + \mathbf{u}^{n-1/2}}{2\gamma^n} \times \mathbf{B}^n\right]. \tag{3.3}$$

The easiest way to solve this equation is to separate the force corresponding to the electric field and the magnetic one. This can be achieved by defining two intermediate momenta $\mathbf{u}^+$ and $\mathbf{u}^-$ as

$$\mathbf{u}^- = \mathbf{u}^{n-1/2} + \frac{q\mathbf{E}^n \Delta t}{2m}, \tag{3.4}$$

$$\mathbf{u}^+ = \mathbf{u}^{n+1/2} - \frac{q\mathbf{E}^n \Delta t}{2m}. \tag{3.5}$$

$$\tag{3.6}$$

Using (3.4) and (3.5) in (3.3), we arrive at

$$\frac{\mathbf{u}^+ - \mathbf{u}^-}{\Delta t} = \frac{q}{2mc\gamma^n}(\mathbf{u}^+ + \mathbf{u}^-) \times \mathbf{B}^n. \tag{3.7}$$

It can be seen that $(\gamma^n)^2 = 1 + (u^-/c)^2 = 1 + (u^+/c)^2$ to second order in $\Delta t$. Equation (3.7) is only a rotation of $\mathbf{u}$ around the axis defined by $\mathbf{B}$ an angle $\theta = -2\arctan(qB\Delta t/2mc\gamma)$, which can be solved in two steps

$$\mathbf{u}' = \mathbf{u}^- + \mathbf{u}^- \times \mathbf{t}, \tag{3.8}$$

$$\mathbf{u}^+ = \mathbf{u}^- + \mathbf{u}' \times \mathbf{s}, \tag{3.9}$$

with $\mathbf{t} = q\Delta t\mathbf{B}/2mc\gamma^n$, $\mathbf{s} = 2\mathbf{t}/(1+t^2)$. Once we know $\mathbf{u}^{n+1/2}$, the positions are advanced as

$$\mathbf{r}^{n+1} = \mathbf{r}^n + \mathbf{v}^{n+1/2}\Delta t = \mathbf{r}^n + \frac{\mathbf{u}^{n+1/2}\Delta t}{\gamma^{n+1/2}}, \tag{3.10}$$

with $\gamma^{n+1/2} = \sqrt{1 + (u^{n+1/2}/c)^2}$. In this way we integrate the equations of motion in a fast and effective manner. In our case, we have only to advance $v_x$, $v_y$ and $x$. Let us now explain now how to calculate the charge and current densities from the positions and velocities of the particles.

In all our simulations, we shall keep the ions fixed since they are much heavier than the electrons and they hardly move during our short pulses. We have checked our results including the motion of the ions and they remain basically unchanged for our parameters. The positive charge density will then be constant and can be calculated at the beginning (in the case of a preionized plasma) in a way that cancels the initial negative charge density, which will be uniform along the slab width. Hence, only the negative charge density will be calculated at each timestep. We use a linear interpolation method. Let us consider that our charge sheets have the same length as the space grid, $\Delta x$, and that they are uniformly charged. We then distribute their charge between the two closest grid points, as is depicted in figure 3.3. If a particle is placed between the points $i$ and $i+1$, exactly at $(i+r)\Delta x$, the charge assigned to point $i$ will be $q_i = q(1-r)$ and the charge assigned to point $i+1$, $q_{i+1} = qr$. This kind of interpolation is what gives the name of these simulations: "particle-in-cell" (PIC). The effect of interpolation is

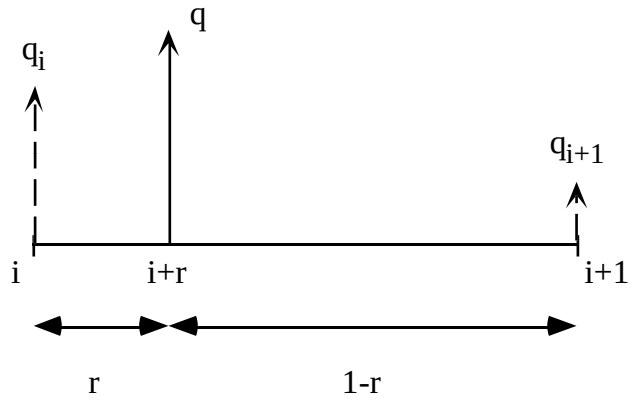


Figure 3.3: Scheme of the charge interpolation of a $\Delta x$ long particle.

to smooth the binary interactions among particles and to reduce the noise in the results.

Once we have assigned the charge of each particle to the grid points, the charge density is calculated simply by summing up the whole charge at each point and dividing it by the spatial step. In this way we need only one loop over the particles to have the charge density at each grid point. Regarding the current density, the mechanism is the same but we have to multiply each charge by the corresponding velocity. An identical linear interpolation is also used to calculate the fields in the positions of the particles after solving the Maxwell equations. The most conflictive point is to solve the Maxwell equations, especially when the intensity is high and relativistic effects become important. We shall study this aspect in the next section.

## 3.2 Solution of Maxwell equations. Relativistic correction in PIC codes [104]

When solving the Maxwell equations, it is usual to start directly from the equations for the electric and magnetic fields

$$\nabla \times \mathbf{E} = -\frac{1}{c}\frac{\partial}{\partial t}\mathbf{B}, \tag{3.11}$$

$$\nabla \times \mathbf{B} = \frac{1}{c}\frac{\partial}{\partial t}\mathbf{E} + \frac{4\pi}{c}\mathbf{J}, \tag{3.12}$$

$$\nabla \cdot \mathbf{E} = 4\pi\rho, \tag{3.13}$$

$$\nabla \cdot \mathbf{B} = 0. \tag{3.14}$$

The solutions of Faraday's and Ampère's laws are very simple in our 1D2V approximation; the one regarding the inexistence of magnetic monopoles is trivial and Coulomb's law becomes an algebraic equation in the k-space [101]. The problem is precisely equation (3.13), which is an instantaneous non-local equation, i.e., the longitudinal field in one point depends on the charge density in its surroundings at the same instant of time. Obviously, this happens because the solution of the Maxwell equations includes both retarded and advanced terms. The latter have no clear physical meaning and can lead us to some mistakes in the relativistic case, when retardation becomes important. This is why we prefer to solve the wave equations for the potentials (1.17) and (1.18) and choose the retarded solutions, which in the case of continuum charge and current densities in the Lorentz gauge can be written as [105]

$$\phi(\mathbf{r},t) = \int \left.\frac{\rho(\mathbf{r}',t')}{|\mathbf{r}-\mathbf{r}'|}\right|_{t'} d\mathbf{r}', \tag{3.15}$$

$$\mathbf{A}(\mathbf{r},t) = \frac{1}{c}\int \left.\frac{\mathbf{J}(\mathbf{r}',t')}{|\mathbf{r}-\mathbf{r}'|}\right|_{t'} d\mathbf{r}', \tag{3.16}$$

where $t' = t - |\mathbf{r}-\mathbf{r}'|/c$. Similarly to the single particle case (1.24), the charge density of a discrete set of point charges is

$$\begin{aligned}\rho(\mathbf{r},t) &= \int d\mathbf{r} \sum_m q_m \delta[\mathbf{r} - \mathbf{r}_m(t)] \\ &= \int d\mathbf{r} \sum_m q_m \delta\Big[\mathbf{r} - \mathbf{r}_m(0) - \int_0^t d\tau \mathbf{v}_n(\tau)\Big].\end{aligned} \tag{3.17}$$

The common approach in plasma particle calculations is to compute the charge density from equation (3.17) discretized in the spatial grid

$$\rho(\mathbf{r}_i,t) = \frac{1}{\Delta V} \sum_{\substack{m \\ x_m^\alpha = x_i^\alpha}} q_m. \tag{3.18}$$

$\Delta V$ is the volume element of the spatial grid; $i$ labels the spatial cell in the grid, and the summatory is restricted to those particles whose position $\mathbf{r}_m$ at instant $t'$ is within the cell located at $\mathbf{r}_i$, i.e. $x_m^\alpha = x_i^\alpha$, in 4-vector notation. Once the charge density has been calculated in this way, one is tempted to substitute it in (3.15) and calculate the scalar potential as

$$\phi(\mathbf{r}_i, t) = \sum_j \frac{\rho(\mathbf{r}'_j, t - |\mathbf{r}_i - \mathbf{r}'_j|/c)}{|\mathbf{r}_i - \mathbf{r}'_j|} \Delta V, \tag{3.19}$$

which is clearly wrong since for a single particle it reduces to the retarded Coulomb potential

$$\phi(\mathbf{r}_i, t) = \frac{q}{|\mathbf{r}_i - \mathbf{r}'(t')|}, \tag{3.20}$$

and we know that the right expression is given by the Liénard-Wiechert potential (1.28), in which the velocity of the particle is included. The reason for the misleading equation (3.19) is that we have implicitly taken as unity the spatial integral of the retarded delta function in (3.17), whilst in fact

$$\int \delta[\mathbf{r}' - \mathbf{r}_m(t')] d\mathbf{r}' = \int \left. \frac{1}{1 - \beta_m \cdot n} \right|_{t'(\mathbf{u})} \delta(\mathbf{u}) d\mathbf{u} \neq 1. \tag{3.21}$$

Calculation of the fields generated by the charges in a particle code should introduce retardation at two different levels. First, one has to use the charge densities calculated at previous times and, second, the velocity denominators characteristic of the Liénard-Wiechert correction must be taken into account. One way of performing both steps simultaneously is to compute the potential associated with each charge and to calculate the total potential as the superposition of these single-particle potentials,

$$\phi(\mathbf{r}, t) = \sum_m \phi_m(\mathbf{r}, t) = \sum_m \frac{1}{1 - \mathbf{v}_m(t'_m) \cdot \mathbf{n}_m(t'_m)/c} \frac{q_m}{|\mathbf{r} - \mathbf{r}_m(t'_m)|}. \tag{3.22}$$

Although this is a correct way of calculating the whole potential, it lacks one of the best advantages of PIC algorithms, which is the possibility of calculating

the charge and current densities associated with a set of charges and using them to compute the corresponding fields. Hence, we only need a loop of size $\mathcal{N}_p$, where $\mathcal{N}_p$ is the total number of particles, to have the densities in the whole grid and another loop of size $\mathcal{N}_g$, where $\mathcal{N}_g$ is the number of points of the spatial grid, to solve the Maxwell equations in each point. By contrast, using equation (3.22) we shall need a loop over all the particles to compute the potential in a single grid point with coordinate $\mathbf{r}$. This would require a double loop of size $\mathcal{N}_p \times \mathcal{N}_g$ to solve the potential in the whole grid. If we did this, the computation time would be unreasonably long. Fortunately, we can overcome this problem with the help of a series of approximations.

The assumption of fixed ions simplifies our calculations because the ionic potential, $\phi_i(\mathbf{r})$, remains constant in time, although the method can easily be extended to mobile ions. The total charge density is then $\rho(\mathbf{r},t) = P(\mathbf{r}) - N(\mathbf{r},t)$, $P$ being the positive charge density and $N$ the negative one. The latter will generate a scalar potential $\phi_e(\mathbf{r},t)$ and a vector potential $\mathbf{A}(\mathbf{r},t)$ (the fixed ions do not contribute to the vector potential). First, let us factorize the summation of equation (3.22) into a set of partial summations of particles which share the same volume element at the same time ($x_m^\alpha = x'^\alpha$). The charge of the particles being the same, as is usual in simulations with preformed plasmas but not when ionization is present and each particle has a different charge, we have

$$\phi_e(\mathbf{r},t) = -\int d\mathbf{r}' \frac{N(\mathbf{r}',t')}{|\mathbf{r}-\mathbf{r}_m|} \frac{1}{\mathcal{N}(\mathbf{r}',t')} \sum_{\substack{m \\ x_m^\alpha = x'^\alpha}} \frac{1}{1 - \mathbf{v}_m(t')\cdot\mathbf{n}/c}, \tag{3.23}$$

where $\mathcal{N}(\mathbf{r},t)$ is the number of particles sharing the same volume element at time $t$. Defining the averaged velocity of the electrons in each volume element as

$$\mathbf{v}(\mathbf{r}',t') = \frac{1}{\mathcal{N}(\mathbf{r}',t')} \sum_{\substack{m \\ x_m^\alpha = x'^\alpha}} \mathbf{v}_m(t'), \tag{3.24}$$

we have $\mathbf{v}_m(t') = \mathbf{v}(\mathbf{r},t') + \Delta\mathbf{v}_m(t')$. The velocity term in the denominator in equation (3.23) may be expressed as a Taylor series in the velocity fluctuations,

$\Delta\mathbf{v}_m(t')/c$

$$\frac{1}{1-\mathbf{v}_m(t')\cdot\mathbf{n}/c} \simeq \frac{1}{1-\mathbf{v}(t')\cdot\mathbf{n}/c} \times \left\{1+\frac{\Delta\mathbf{v}_m(t')\cdot\mathbf{n}/c}{1-\mathbf{v}(t')\cdot\mathbf{n}/c}+\left[\frac{\Delta\mathbf{v}_m(t')\cdot\mathbf{n}/c}{1-\mathbf{v}(t')\cdot\mathbf{n}/c}\right]^2+\cdots\right\} \quad (3.25)$$

Performing the summation in equation (3.23), the first term of the Taylor series amounts to $\mathcal{N}(\mathbf{r}',t')$ and the second one vanishes because of the definition of $\Delta\mathbf{v}_m(t')$. The third one contains the following sum,

$$\sum_{\substack{m\\ x_m^\alpha=x'^\alpha}} \left(\Delta\mathbf{v}_m(t')\cdot\mathbf{n}\right)^2 = \frac{1}{2}\sum_{\substack{m\\ x_m^\alpha=x'^\alpha}} \Delta v_m^2(t') = \frac{3\mathcal{N}(\mathbf{r}',t')}{2m}k_BT(\mathbf{r}',t'), \quad (3.26)$$

where we have assumed an isotropic distribution of the velocity fluctuations and we have introduced a local time-dependent non-relativistic temperature $T(\mathbf{r},t)$ [106]. $k_B$ is the Boltzmann constant. Keeping the series expansion at second order, the potential approximation suitable for our particle-in-cell calculations is

$$\phi_e(\mathbf{r},t) \simeq -\int \frac{1}{|\mathbf{r}-\mathbf{r}'|}\frac{N(\mathbf{r}',t')}{1-\mathbf{v}(t')\cdot\mathbf{n}/c}\left\{1+\frac{3k_BT(\mathbf{r}',t')/2mc^2}{\left[1-\mathbf{v}(t')\cdot\mathbf{n}/c\right]^2}\right\}d\mathbf{r}'. \quad (3.27)$$

In principle, this truncated expression is only valid if $|\Delta\mathbf{v}(t)| < c - v(t)$. This is ensured for particles faster than average by the relativistic dynamics itself. The velocity distribution in the relativistic regime is, however, strongly asymmetric and particles with velocities well below the mean value may exist. Although these particles do not fulfill the truncation condition, their contribution to the integral is not essential, since their velocity-dependent denominator is large. Regarding the vector potential, we can write this as

$$\mathbf{A}(\mathbf{r},t) = -\int d\mathbf{r}'\frac{N(\mathbf{r}',t')}{c|\mathbf{r}-\mathbf{r}_m|}\frac{1}{\mathcal{N}(\mathbf{r}',t')}\sum_{\substack{m\\ x_m^\alpha=x'^\alpha}}\frac{\mathbf{v}(t')+\Delta\mathbf{v}_m(t')}{1-[\mathbf{v}(t')+\Delta\mathbf{v}_m(t')]\cdot\mathbf{n}/c}. \quad (3.28)$$

If we define the current density as

$$\mathbf{J}(\mathbf{r},t) = \sum_{\substack{m\\ x_m^\alpha=x'^\alpha}} q_m\mathbf{v}_m(t')\delta(\mathbf{r}-\mathbf{r}')$$

$$= \sum_{\substack{m \\ x_m^\alpha = x'^\alpha}} q_m \delta(\mathbf{r}-\mathbf{r}')[\mathbf{v}(t') + \Delta\mathbf{v}_m(t')] = -\mathbf{v}(\mathbf{r},t)N(\mathbf{r},t), \quad (3.29)$$

then the first term in the sum of equation (3.28) leads to a mean-velocity contribution to the vector potential of

$$\mathbf{A}_v(\mathbf{r},t) \simeq \int \frac{1}{c|\mathbf{r}-\mathbf{r}'|} \frac{\mathbf{J}(\mathbf{r}',t')}{1-\mathbf{v}(t')\cdot\mathbf{n}/c} \left\{ 1 + \frac{3k_B T(\mathbf{r}',t')/2mc^2}{[1-\mathbf{v}(t')\cdot\mathbf{n}(t')/c]^2} \right\} d\mathbf{r}'. \quad (3.30)$$

The second term of the summatory can be evaluated as

$$\sum_{\substack{m \\ x_m^\alpha = x'^\alpha}} \frac{\Delta\mathbf{v}_m(t')}{1-[\mathbf{v}(t')+\Delta\mathbf{v}_m(t')]\cdot\mathbf{n}/c} \simeq \sum_{m x_m^\alpha = x'^\alpha} \frac{\Delta\mathbf{v}_m(t')\,(\Delta\mathbf{v}_m(t')\cdot\mathbf{n})}{[1-\mathbf{v}(t')\cdot\mathbf{n}/c]^2}, \quad (3.31)$$

and, for an isotropic distribution of the velocity fluctuations, we might find

$$\mathbf{A}_{\Delta v}(\mathbf{r},t) \simeq -\int \frac{1}{|\mathbf{r}-\mathbf{r}'|} \frac{N(\mathbf{r}',t')\mathbf{n}}{[1-\mathbf{v}(t')\cdot\mathbf{n}(t')/c]^2} \frac{3}{2} \frac{k_B T(\mathbf{r}',t')}{mc^2}. \quad (3.32)$$

The complete vector potential is therefore $\mathbf{A}(\mathbf{r},t) = \mathbf{A}_v(\mathbf{r},t) + \mathbf{A}_{\Delta v}(\mathbf{r},t)$. These expressions are useful for three-dimensional calculations with relativistic plasmas, either cold or hot, whenever the approximations we have used are valid. But we are interested in a much simpler case: a cold plasma and a one-dimensional medium. The first condition simplifies the expressions by making $T(\mathbf{r},t) = 0$. In particular, the term $\mathbf{A}_{\Delta v}(\mathbf{r},t)$ vanishes. Regarding the second one, let us try to find adequate expressions for the one-dimensional potentials.

For a cold plasma, we can write equation (3.27) in cylindrical coordinates $(\rho,\varphi,x)$ (see figure 3.4) as

$$\phi_e(x,t) \simeq -\int dx' \int\int \rho d\rho d\varphi \frac{N^2(x',t')}{R}$$
$$\times \left[ N(x',t') + J_x(x',t')\tfrac{x-x'}{Rc} + J_y(x',t')\tfrac{\rho\cos\varphi}{Rc} + J_z(x',t')\tfrac{\rho\sin\varphi}{Rc} \right]^{-1}, \quad (3.33)$$

where, as always, $R = |\mathbf{r}-\mathbf{r}'|$ and we have used equation (3.29) and $\mathbf{n} = (\mathbf{r}-\mathbf{r}')/R$. Since $R = c(t-t')$, and keeping $x'$ constant, we have $RdR = \rho d\rho$, and hence

$$\phi_e(x,t) \simeq -c^2 \int dx' \int_{-\infty}^{t-|x-x'|/c} dt' \int_0^{2\pi} d\varphi N^2(x',t')$$
$$\times \left\{ cN(x',t') + J_x(x',t')\zeta + [J_y(x',t')\cos\varphi + J_z(x',t')\sin\varphi]\sqrt{1-\zeta^2} \right\}^{-1} \quad (3.34)$$

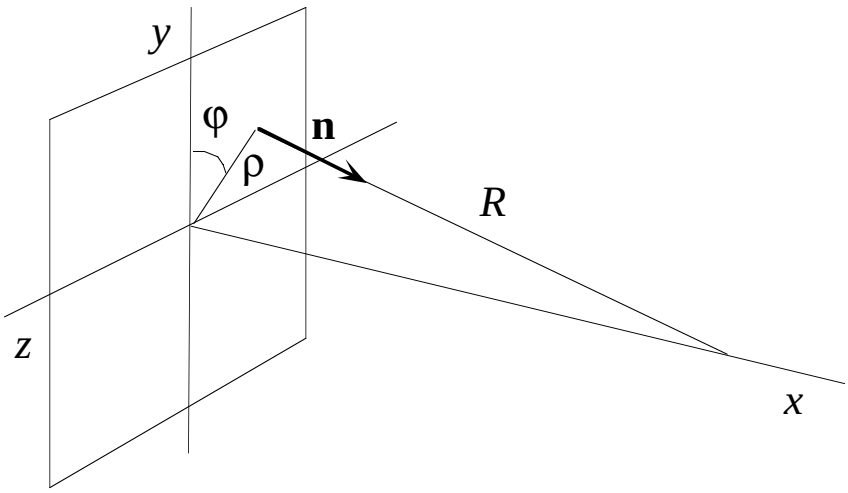


Figure 3.4: Geometry of the one-dimensional problem in cylindrical coordinates.

with $\zeta = (x - x')/[c(t - t')]$. The integral over the angle $\varphi$ can be easily calculated, giving the final expression for the scalar potential as

$$\phi_e(x,t) \simeq -2\pi c^2 \int dx' \int_{-\infty}^{t-|x-x'|/c} dt' N^2(x',t') \times \left\{ [cN(x',t') + J_x(x',t')\zeta]^2 - [J_y^2(x',t') + J_z^2(x',t')]\,[1-\zeta^2] \right\}^{-1/2}. \quad (3.35)$$

In a similar way one can obtain the expression for the vector potential, which takes the form

$$\mathbf{A}(x,t) \simeq -2\pi c \int dx' \int_{-\infty}^{t-|x-x'|/c} dt' N(x',t')\mathbf{J}(x',t') \times \left\{ [cN(x',t') + J_x(x',t')\zeta]^2 - [J_y^2(x',t') + J_z^2(x',t')]\,[1-\zeta^2] \right\}^{-1/2}. \quad (3.36)$$

We notice that the scalar potential as well as each component of the vector potential can be written as

$$\Lambda(x,t) \simeq \int dx' \mathcal{F}_\Lambda(x', x, t - |x - x'|/c) \quad (3.37)$$

where $\mathcal{F}_\Lambda(x', x, t - |x - x'|/c)$ is the corresponding integral in time. It is clear that despite our one-dimensional approximation, integration of the potentials has a two-dimensional complexity since it depends on two variables, $x$ and $x'$. This bidimensionality reflects the anisotropy of the electric field induced by the relativistic

velocity. There are, however, situations which allow a one-dimensional reduction of equations (3.35) and (3.36). Let us consider the case of a thin plasma slab whose radiation we wish to observe at a considerable distance from it. In this situation, $R >> |x - x'|$ for most of the region where the integral $\mathcal{F}_\Lambda(x', x, t - |x - x'|/c)$ extends. We can therefore approximate (3.35) as

$$\phi_e(x,t) \simeq -2\pi \int dx' \int_{-\infty}^{t-|x-x'|/c} \frac{c^2 N^2(x',t')dt'}{\left\{c^2 N^2(x',t') - [J_y^2(x',t') + J_z^2(x',t')]\right\}^{1/2}}, \quad (3.38)$$

and the components of the potential vector can also be approximated similarly. Also, for the case we are interested in, the external electric field is transversal and it is expected that the charges will mainly move in the transversal plane, and hence $|J_y^2(x',t') + J_z^2(x',t')| > |J_x^2(x',t')|$, thus ensuring the correctness of the approximation. We have therefore reduced the problem to finding the solution of four equations of the type:

$$\Lambda(x,t) = \int dx' \mathcal{F}_\Lambda\left(x', t - \frac{|x-x'|}{c}\right), \quad (3.39)$$

which are easily solved numerically. In order to do this, we split the integrals into two contributions, one propagating rightward and the other leftward. If the spatial grid extends along the interval $[0, L]$, each integral is computed as $\Lambda(x,t) = \Lambda^+(x,t) + \Lambda^-(x,t)$, where

$$\Lambda^+(x,t) = \int_0^x dx' \mathcal{F}_\Lambda\left(x', t - \frac{|x-x'|}{c}\right), \quad (3.40)$$

$$\Lambda^-(x,t) = \int_x^L dx' \mathcal{F}_\Lambda\left(x', t + \frac{|x-x'|}{c}\right). \quad (3.41)$$

Choosing the spatial and temporal steps such that $\Delta x = c\Delta t$, we have

$$\Lambda^+(x+\Delta x, t+\Delta t) = \Lambda^+(x,t) + \int_x^{x+\Delta x} dx' \mathcal{F}_\Lambda\left(x', t - \frac{|x-x'|}{c}\right). \quad (3.42)$$

Calculation of the integral between $x$ and $x + \Delta x$, at second order, is

$$\int_x^{x+\Delta x} dx' \mathcal{F}_\Lambda\left(x', t - \frac{|x-x'|}{c}\right) \simeq \frac{\Delta x}{2}[\mathcal{F}_\Lambda(x,t) + \mathcal{F}_\Lambda(x+\Delta x, t+\Delta t)], \quad (3.43)$$

and the same holds for the part propagating from right to left

$$\Lambda^-(x-\Delta x, t+\Delta t) = \Lambda^-(x,t) + \int_{x-\Delta x}^{x} dx' \mathcal{F}_\Lambda\left(x', t + \frac{|x-x'|}{c}\right), \tag{3.44}$$

and the integral is solved as

$$\int_{x-\Delta x}^{x} dx' \mathcal{F}_\Lambda\left(x', t + \frac{|x-x'|}{c}\right) \simeq \frac{\Delta x}{2}[\mathcal{F}_\Lambda(x,t) + \mathcal{F}_\Lambda(x-\Delta x, t+\Delta t)]. \tag{3.45}$$

The boundary conditions are $\Lambda^+(0,t) = 0$, $\Lambda^-(L,t) = 0$. $\mathcal{F}_\Lambda(x,t)$ is always an integral of the type

$$\mathcal{F}_\Lambda(x,t) = \int_{t_0}^{t} dt' g_\Lambda(x,t'), \tag{3.46}$$

where $t_0$ is the initial time and $g_\Lambda(x,t)$ is a function of the charge and current densities. We can propagate the integral simply as

$$\mathcal{F}_\Lambda(x,t+\Delta t) = \mathcal{F}_\Lambda(x,t) + \Delta t \; g_\Lambda\left(x, t + \frac{\Delta t}{2}\right). \tag{3.47}$$

With the *leapfrog* method, we know the velocities and therefore the current density at half-integer time instants and we can use them in $g_\Lambda(x, t+\Delta t/2)$. For the charge density, we take $N(x, t+\Delta t/2) = 1/2[N(x,t) + N(x,t+\Delta t)]$. Thus, we calculate the potentials in a simple and fast way. To calculate the fields, we use equations (1.20) and (1.21), which, for our geometry, reduce to

$$E_x = -\frac{\partial}{\partial x}\phi - \frac{1}{c}\frac{\partial}{\partial t}A_x, \tag{3.48}$$

$$E_y = -\frac{1}{c}\frac{\partial}{\partial t}A_y + E_{0y}, \tag{3.49}$$

$$B_z = \frac{\partial}{\partial x}A_y + B_{0z}, \tag{3.50}$$

where $E_{0y}$, $B_{0z}$ are the electric and magnetic components of the incident field, which take the form $E_{0y}(x,t) = B_{0z}(x,t) = E_0 S(\eta)\sin(\eta)$, with $\eta = \omega_0 t - k_0 x$ and $S$ an envelope which, from now on and unless otherwise specified, has the shape of a sine squared function. Equations (3.48)-(3.50) are solved by transforming the derivatives into finite differences at first order.

We shall now estimate the importance of the relativistic corrections we have to include in the code to see in which range of parameters they must be taken into account. To this end, we have performed simulations of a pulse with a frequency of $\omega_0 = 0.05$ a.u. (or wavelength roughly $\lambda_0 \simeq 0.9\ \mu$m) and a duration of twenty cycles impinging a slab of a preformed plasma of width $0.1\lambda_0$ (to keep the approximation made in equation (3.38) valid) and density 1.65 times the critical value. We have solved the potentials with the Liénard-Wiechert correction (equation (3.38) and the same for the vector potential) and without it, using the retarded Coulomb potentials, which is equivalent to assuming $v/c << 1$ and hence $J/c << N$, i.e., we use the expressions

$$\phi_e(x,t) \simeq -2\pi c \int dx' \int_{-\infty}^{t-|x-x'|/c} N(x',t')dt', \tag{3.51}$$

$$\mathbf{A}(x,t) \simeq 2\pi \int dx' \int_{-\infty}^{t-|x-x'|/c} \mathbf{J}(x',t')dt'. \tag{3.52}$$

The contribution of the positive charges is always

$$\phi_p(x,t) \simeq 2\pi c \int dx' \int_{-\infty}^{t-|x-x'|/c} P(x',t')dt'. \tag{3.53}$$

Figure 3.5 shows the harmonic spectra of the field transmitted through the slab (a) and reflected by it (b) when the field amplitude is moderate (1 a.u.). We see that the difference when the Liénard-Wiechert correction is included (dotted line) and when it is neglected (solid line) is minimal, although the transmitted harmonics are slightly more intense, the contrary of the reflected ones. The profiles of the reflected and transmitted fields have not been depicted because they seem identical. We can conclude that for the non-relativistic regime, which these parameters correspond, the Liénard-Wiechert correction is not important and can be neglected.

Increasing the field amplitude by one order of magnitude, up to $E_0 = 10$ a.u., which means an increase in intensity by a factor of 100 ($I_0 \approx 4 \times 10^{18}$ a.u.), dramatically changes the results, as seen in figure 3.6. In this case, the increase in the

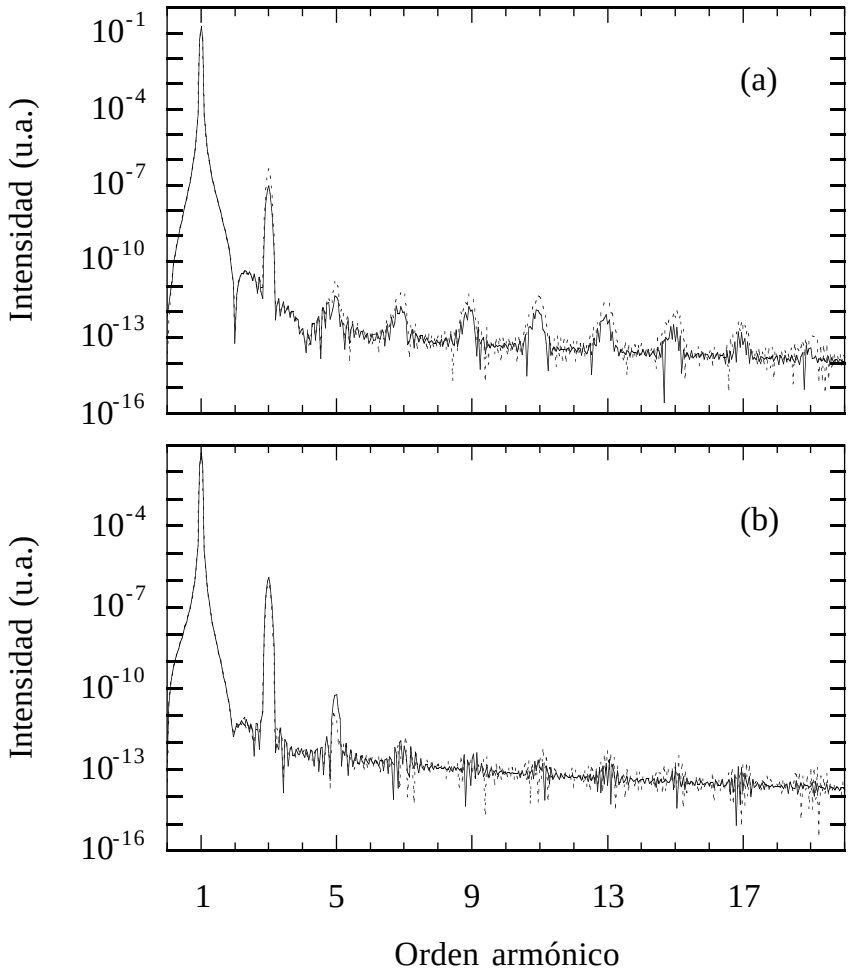


Figure 3.5: Harmonic spectrum of the transmitted (a) and reflected (b) fields in a thin slab when we make a calculation with (dotted line) and without (solid line) the Liénard-Wiechert correction. The incident pulse has a frequency of $\omega_0 = 0.05$ a.u., a duration of twenty cycles, and an amplitude $E_0 = 1$ a.u.

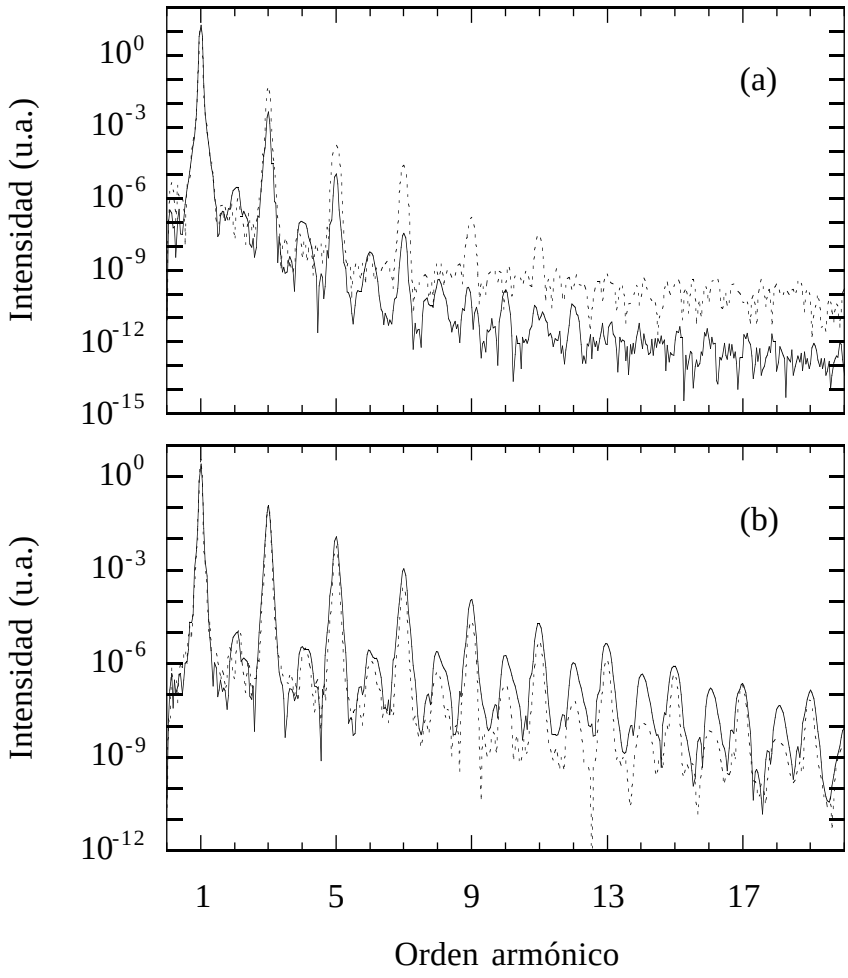


Figure 3.6: The same as in figure 3.5 but with a field amplitude of $E_0 = 10$ a.u.

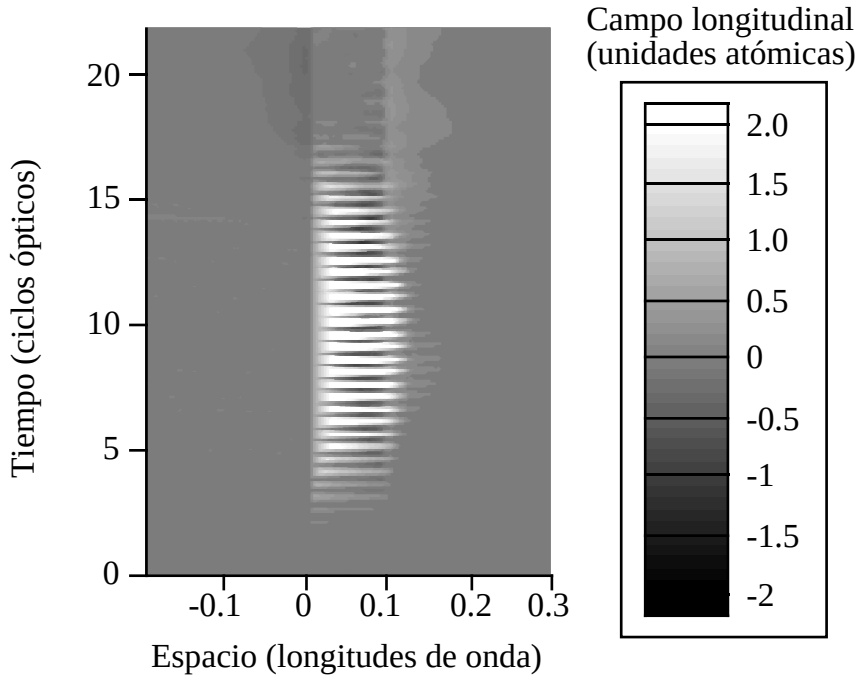


Figure 3.7: Evolution in space (horizontal axis) and time (vertical axis) of the longitudinal electric field $E_x$ for an incident pulse with maximum amplitude $E_0 =$ 10 a.u. when the Liénard-Wiechert correction is not included in the computation of the potentials.

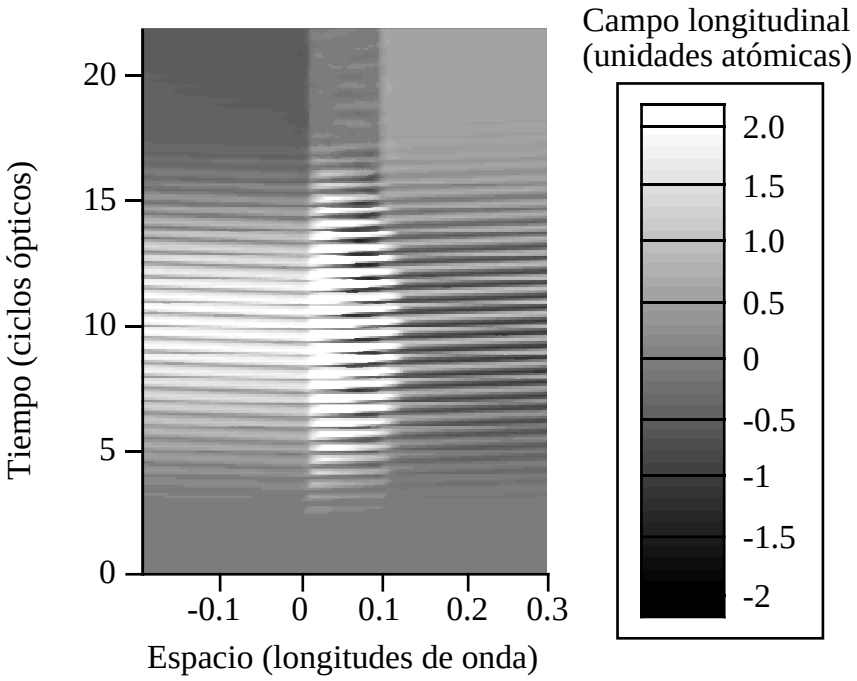


Figure 3.8: The same as in figure 3.7 but introducing Liénard-Wiechert correction.

transmitted harmonic intensities when the Liénard-Wiechert correction is included is several orders of magnitude, whilst the reflected ones are less intense. To gain insight into what is happening, we observe figures 3.7 and 3.8. The first depicts the evolution of the longitudinal $E_x$ field in space (horizontal axis) and time (vertical axis) during the previous simulations using the retarded Coulomb potentials. We observe the oscillations of the field near the pulse maximum. These oscillations are restricted to the slab space (between $x = 0$ and $x = 0.1\lambda_0$) and are generated by the motion of the electrons due to the $\mathbf{v} \times \mathbf{B}$ term of the Lorentz force, the same mechanism that generates harmonics, as we already know. When the external field decreases, the oscillations are damped and the longitudinal field diminishes. Figure 3.8 represents the same field when the Liénard-Wiechert correction is taken into account. Now, the oscillations of the longitudinal field are much more intense due to the breaking of the symmetry of the Coulomb potential. Let us recall that

the field generated by a moving relativistic charge had two contributions (equation (1.30), the velocity or near field, which depends on the distance to the observation point as $R^{-2}$, and the acceleration or far field, which decreases as $R^{-1}$. The latter is the radiation field because of its longer range and because it is commonly detected. However, in our case the velocity field is more interesting because in a thin slab the near field dominates the electromagnetic interactions. This field, for a single particle, can be written in terms of its instantaneous position and the non-retarded time in the laboratory frame as [31]

$$\mathbf{E}(\mathbf{r},t) = \frac{q\mathbf{n}}{\gamma^2 R^2[1-\beta^2\sin^2\psi]^{3/2}}, \tag{3.54}$$

where $\psi = \arccos(\mathbf{n}\cdot\mathbf{v})$. This field is strongly anisotropic because the effective charged observed in the direction orthogonal to the charge's displacement is much larger than the charge at rest. In our calculations, particles mainly move in the direction parallel to the field polarization, i.e. along the $y$ axis. As they quiver, their effective charge observed in the $x$ direction fluctuates from the rest charge to higher values. When the effective charge is greater than the rest charge, the ions, which are fixed (or at least move much slower than electrons) and have a constant effective charge, cannot compensate the excess of negative charge and hence the longitudinal field increases due to this transitory non-neutrality. The result is an enhancement of plasma oscillations, which is reflected in the scattered radiation. It should also be noted that since the plasma neutrality is lost, a residual longitudinal field may be detected at some distance from the target.

We have observed, therefore, that the Liénard-Wiechert correction may be important for very intense fields, but for fields whose amplitude is close to the atomic unit or smaller, its influence is weak. That, and also in order to simplify the computations, is why we shall neglect the Liénard-Wiechert correction and all our simulations will be made with the retarded Coulomb potentials.

## 3.3 Ionization in a PIC code

So far we have not mentioned ionization, which is the key point in our work. To include it in a particle code, we have to introduce an additional step in the loop in figure 3.1 in which the ionization is calculated and the corresponding particles included. We do this immediately after calculating the fields from the Maxwell equations and before moving the particles. We start with an initial configuration in which every point in the spatial grid inside the slab is assigned a bound charge, $Q_0$, and a corresponding density $N_b(x,0) = N_0 = Q_0/\Delta x$. Both the positive and the negative free charges are zero (we could also start from a partial ionization state, but this possibility has not been considered here). At each time step, we compute the amount of ionized charge from equation

$$\frac{\partial}{\partial t} N_b(x,t) = -W(x,t) N_b(x,t), \tag{3.55}$$

where $W$ is the ionization rate. We shall then have that the ionized charge density between $t$ and $t + \Delta t$ is $\Delta N_b(x, t + \Delta t) = W(x,t) N_b(x,t) \Delta t$. Once we know the ionized charge, we create a particle with charge $q = \Delta N_b(x, t+\Delta t)\Delta x$ and we place it in the grid point corresponding to position $x$. At the same time, we increase the positive charge density at that point to the same extent that the bound density decreases.

All our work deals with photoionization and we shall assume that the ionization rate is completely determined by the electric field, neglecting the collisional ionization. Collisional ionization may be important in some regimes and when the times considered are long enough. In our case, the main reason for disregarding collisional ionization is that it depends on the collisional cross section and this becomes more important when the ions become heavier. We shall consider hydrogen ions, which are the lightest ones, for which the probability of collisional ionization is very small, as we shall show. We choose hydrogen because of the simplicity of

its ionization rates, which we already know, and also because it is an one-electron atom and there is only one ionization stage, which considerably simplifies the calculations. We shall use as the ionization rate the simple expression (1.3) with a field amplitude depending on time and space, which is the most widely used expression in the literature

$$W(x,t) = \frac{4}{|E(x,t)|} \exp\left(-\frac{2}{3|E(x,t)|}\right), \tag{3.56}$$

where, again, we are using atomic units. The impact ionization rate is given by the expression [107] $W_{col} = N\bar{v}\sigma(\bar{v})$, where $N$ is the electron density, $\bar{v}$ the mean velocity, which satisfies $\bar{v} = |J/N|$, and $\sigma(\bar{v})$ is the collisional cross section, which depends on the velocity of the incident electrons. There is no universal expression for collisional cross sections since they depend on many factors. Generally, interpolations of experimental data fitted by simple curves are used. In particular, use is often made of the expression [108, 109]

$$\sigma(K) = \frac{1}{I_p K}\left[A \ln\left(\frac{K}{I_p}\right) + \sum_{i=1}^{\mathcal{N}} B_i \left(1 - \frac{I_p}{K}\right)^i\right], \tag{3.57}$$

where $K$ is the electron's kinetic energy , $I_p$ is the ionization potential of the atom or the ion, and $A$, $B_i$ are particular constants for each species. For hydrogen, it is sufficient to take four terms in the summatory to obtain a cross section with 93% reliability. The data are: $I_p = 13.6$, $A = 0.1845$, $B_1 = -0.0186$, $B_2 = 0.1231$, $B_3 = -0.1901$ and $B_4 = 0.9527$. $I_p$ is obviously given in electronvolts and the other constants in $10^{-13}\mathrm{eV}^2\mathrm{cm}^2$.

We see the photoionization rate as a function of the field amplitude in figure 3.9a. We shall use the same expression for higher fields, out of its theoretical range of validity, because in those cases total ionization occurs well before the field reaches its maximum value, during the first part of the pulse, as we shall see, and no important errors will be incurred. In figure 3.9b, we see the impact ionization rate in the case of a hydrogen medium with critical density. Even the

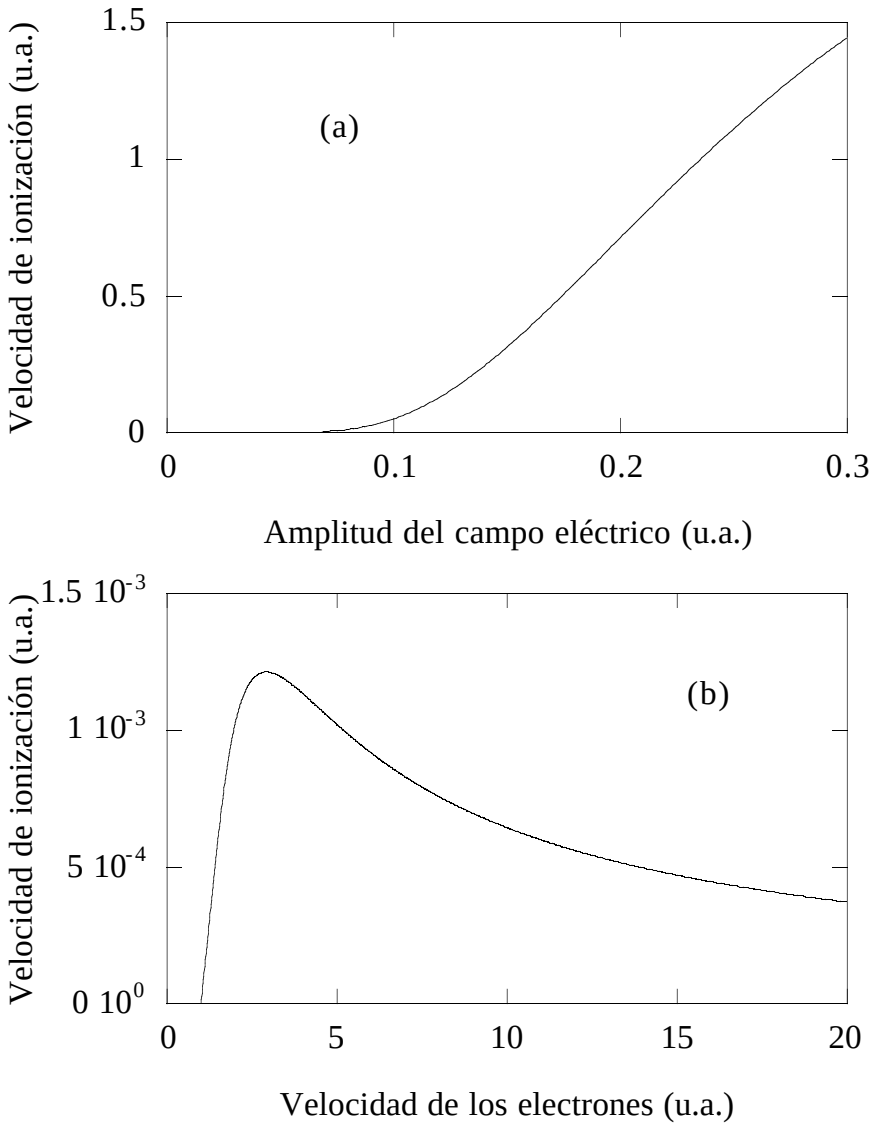


Figure 3.9: Photoionization rate as a function of the field amplitude given by equation 3.56 (a). Collisional ionization rate as a function of the velocity of the incident electron given by expression 3.57 (b).

maximum impact rate, which is close to a velocity of three atomic units, is orders of magnitude lower than the photoionization rate when the field is approximately 0.1 atomic units. If the density were ten times the critical value, the collisional ionization rate would also be irrelevant and this is why we do not consider it in our calculations. We refer interested readers to previous works dealing with the role of collisional ionization in the propagation of electromagnetic fields in ionizing media, which is always less important than the role of photoionization when the ions are small, the densities are not very high and the fields have intensities similar to the ones we are using [107, 110, 111].

We also neglect the possibility of recombination for a simple reason: when densities are high, the loss of coherence due to phase mismatches and interactions among free electrons causes the disappearance of the high harmonics that we have studied in the case of isolated atoms and which are also observed in rare media, i.e. there is no coherent recombination. In addition, the population transfer, whether coherent or incoherent (due to collisions, etc.) from free to bound states is irrelevant when the fields are very intense because the kinetic energy of electrons is very high and the ions cannot capture them. For the same reasons, we neglect the contribution of the bound population to the propagation of the field, which is much less important than the contribution of free electrons, except maybe if there are resonances, which we assume is not the case. When there are no resonances, the effect of the bound population can be associated with a background dielectric permittivity, $\varepsilon$, different from the vacuum one and the solution of the propagation equations is exactly the same except for a normalization of the variables. Hence, we shall assume that the medium is transparent when it is totally non-ionized.

## 3.4 Fixed charge model for the generation of a plasma by a laser

We shall now describe another model, much simpler than the previous one, which will permit us to study the effects of ionization in the non-relativistic and low density case with ease. This model was introduced by Brunel in 1990 [112] and has been widely used, whether in its original form or with some changes, in works dealing with propagation in ionizing media [107, 110, 113, 114, 115, 116]. Once again, we shall only consider the contribution of free electrons to the atomic polarization, disregarding any effect of the atomic potential as well as all relativistic effects (which is only valid for low intensity fields) and the motion of the charges inside the medium (which is only valid for not very high densities). Hence, the problem is one-dimensional since the geometry is still like that shown in figure 3.2 but without a magnetic field. We assume that we have the vacuum in the $x < 0$ semiplane and that an initially transparent ionizing medium extends over the interval $[0, L]$. The wave equation for the electric field, polarized along the $y$ axis, is then quite simple

$$\frac{\partial^2 E}{\partial x^2} - \frac{1}{c^2}\frac{\partial^2 E}{\partial t^2} = \frac{4\pi}{c^2}\frac{\partial J}{\partial t}, \tag{3.58}$$

where the current density is

$$J(t) = -N\bar{v} = -\frac{1}{\Delta V}\sum_{i=1}^{\mathcal{N}(t)} v_i(t). \tag{3.59}$$

As usual, $N$ is the free electron density, $\bar{v}$ the fluid mean velocity, $\mathcal{N}$ the number of free electrons in a volume $\Delta V$ and $v_i$ the velocity of the $i$th electron within this volume. The current at instant $t + \Delta t$ is given by

$$J(t+\Delta t) = -\frac{1}{\Delta V}\sum_{i=1}^{\mathcal{N}(t)} v_i(t+\Delta t) - \frac{1}{\Delta V}\sum_{i=\mathcal{N}(t)+1}^{\mathcal{N}(t+\Delta t)} v_i(t+\Delta t). \tag{3.60}$$

The second summatory on the right hand side of expression (3.60) stands for the electrons which have been ionized in the interval $[t, t + \Delta t]$, since we neglect

the motion of the electrons from one cell to another (that is why this is a *fixed charges* model). If we restrict ourselves to the tunnelling ionization regime, we can approximate the velocity of the ionized electrons to zero, and hence that contribution vanishes. Thus, subtracting (3.59) from (3.60), dividing by $\Delta t$ and passing to the continuum limit, the evolution equation for the current density is

$$\frac{\partial J}{\partial t} = -\frac{1}{\Delta V}\sum_{i=1}^{\mathcal{N}(t)}\frac{dv_i}{dt}. \tag{3.61}$$

All the electrons in the same cell have the same equation of motion, $\dot{v}_i = -E$, and therefore, the evolution equation for $J$ becomes

$$\frac{\partial J}{\partial t} = NE = \frac{\omega_{p0}^2}{4\pi}nE, \tag{3.62}$$

where $\omega_{p0} = \sqrt{4\pi N_0}$ is the maximum plasma frequency when the whole population is ionized and $n = N/N_0$ is the normalized free electron density or ionization degree, whose evolution is given by

$$\frac{\partial n}{\partial t} = W(1-n), \tag{3.63}$$

where $W(x,t)$ is the ionization rate given by expression (3.56). We have used the fact that the bound population is $N_b = N_0 - N$ since the charges do not move. Equations (3.58), (3.62) and (3.63) give the complete evolution of our model, in which only the effect of ionization is included in the propagation of the field, which is therefore separated from all other effects occurring in a real plasma and which are included, more or less precisely, in particle codes.

We can write (3.58) in its integral form

$$E(x,t) = E_i(x,t) - \frac{2\pi}{c}\int_0^L dx' J\left(x', t - \frac{|x-x'|}{c}\right), \tag{3.64}$$

where $E_i(x,t)$ is the incident field. We clearly see that the total field is the sum of the incident one and the reaction field induced by $J$. The reflected field is simply $E_r(t) = E(0,t) - E_i(0,t)$. The numerical solution of equations (3.62) and

(3.63) will be performed using a fourth-order Runge-Kutta method and (3.64) will be solved by splitting the integral into leftward propagating and rightward propagating parts, as was explained in section 3.2. In this way, we can reduce the spatial grid and accelerate the calculations.

# Chapter 4

# Propagation of harmonics in laser-generated plasmas

Once we have set forth all our theoretical and numerical tools, let us study how harmonics are generated and propagated during the ionization of a dense medium by an intense laser pulse. We shall begin with harmonic generation and after that we shall comment on certain propagation effects.

## 4.1 Harmonics generated by inhomogeneous ionization [114, 115]

In order to study whether it is possible to generate harmonics during the propagation of a laser pulse through an ionizing medium, let us use the simple model described in section 3.4. If the incident field has the form $E_i(x,t) = 2F_i(x,t)\cos(\omega_0 t - k_0 x)$, with a slowly-varying-in-time-and-space envelope $F_i(x,t)$, we can search for solutions of the equations (3.62), (3.63) and (3.64) as Floquet series

$$E(x,t) = \sum_{q=-\infty}^{\infty} E_{2q+1}(x,t)\exp[-i(2q+1)\omega_0 t], \tag{4.1}$$

$$J(x,t) = \sum_{q=-\infty}^{\infty} j_{2q+1}(x,t)\exp[-i(2q+1)\omega_0 t], \tag{4.2}$$

$$n(x,t) = \sum_{q=-\infty}^{\infty} n_{2q}(x,t)\exp[-i2q\omega_0 t], \tag{4.3}$$

$$W(x,t) = \sum_{q=-\infty}^{\infty} w_{2q}(x,t)\exp[-i2q\omega_0 t]. \tag{4.4}$$

The ionization rate $W$, as well as $N$, have even terms only because they depend on the field intensity. By contrast, $E$ and $J$ only have odd terms. We assume that all harmonic amplitudes are slowly-varying-in-time, but not in space, since a noticeable reflection may appear when the densities are high enough. We shall also assume that: (a) the ionization rate is much lower than the laser frequency, i.e. only a small proportion of the electrons are ionized during an optical cycle; (b) for this reason, the harmonics are weak and we can ignore their effect on the fundamental one, which (c) is the only source of the other harmonics (we neglect the couplings among high harmonics). All these assumptions can be summarized in two conditions: the field is weak enough to provide a slow ionization and the density of the medium is low enough to prevent strong couplings. With these, substituting the series (4.1)-(4.4) in (3.62), (3.63) and (3.64), we obtain the following set of equations [115]

$$\begin{aligned} E_1(x,t) &= E_i(x,t)\exp(ik_0x) \\ &- \frac{1}{2}ik_0\left(\frac{\omega_{p0}}{\omega_0}\right)^2\int_0^\infty dx'\exp(ik_0|x-x'|)n_0E_1\left(x',t-\frac{|x-x'|}{c}\right), \end{aligned} \tag{4.5}$$

$$\frac{\partial n_0}{\partial t} = w_0(1-n_0), \tag{4.6}$$

$$\begin{aligned} E_{2q+1}(x,t) &= \frac{1}{2}ik_{2q+1}\left(\frac{\omega_{p0}}{\omega_{2q+1}}\right)^2\int_0^\infty dx'\exp(ik_0|x-x'|) \\ &\times \left[\frac{w_{2q}}{\omega_{2q}}E_1\left(x',t-\frac{|x-x'|}{c}\right)+\frac{w_{2(q+1)}}{\omega_{2(q+1)}}E_{-1}\left(x',t-\frac{|x-x'|}{c}\right)\right], \end{aligned} \tag{4.7}$$

where $k_r = rk_0$, $\omega_r = r\omega_0$ and $E_{-1} = E_1^*$. From equation (4.7) we see that there will be harmonic generation whenever the ionization rate has high Fourier components; that is, whenever its dependence on time is fast. This is the case of the expression used by us in the tunnelling regime. Moreover, the field will not be uniform during propagation through the medium and, as a consequence, $W$

will vary appreciably in space. This inhomogeneity means that the harmonics are generated only in those places where ionization takes place. Equation (4.7) can be solved in an approximate way when the density of the medium is very low and there is hardly any reflection. In this case, it is also possible to make a Floquet expansion in the spatial coordinate $x$ [112]. We shall not repeat this here since the slowly-varying envelope approximation fails to describe the propagation of the field when densities are close to their critical value and reflection is important, which is precisely the most interesting case for us [115]. Indeed, the temporal dependence of the ionization rate is again an efficient mechanism for the generation of harmonics.

These harmonics were originally expected to be visible during the transmission of a pulse through a low density gas [112, 113] and they were in fact observed experimentally with a $CO_2$ laser inciding on noble gases [117]. However, we already know that during pulse propagation there is a phase mismatch that causes a loss of visibility of the harmonics in a very short space, especially when there are free electrons. We decided to use media with densities close to or higher than the critical one, where the harmonics can be generated in the same way but are reflected instead of being transmitted [114, 115]. The advantage of reflected harmonics is that they will propagate in vacuum and hence phase mismatch effects will be minimal.

In figure 4.1a we observe the reflected field and the degree of ionization at the boundary when a pulse of maximum amplitude $E_0 = 0.08$ a.u., length 15 cycles and frequency $\omega_0 = 0.05$ a.u. (which unless otherwise stated is the one we shall use from now on) impinges on a slab with density $N_0 = N_c$ when it is fully ionized and whose thickness is $20\lambda_0$. We notice the absence of reflection before the peak of the incident pulse arrives at the boundary surface. At that instant, the field amplitude is high enough to ionize the medium, which changes from transparent to having a density equal to the critical one, at least in the area close to the boundary. Hence,

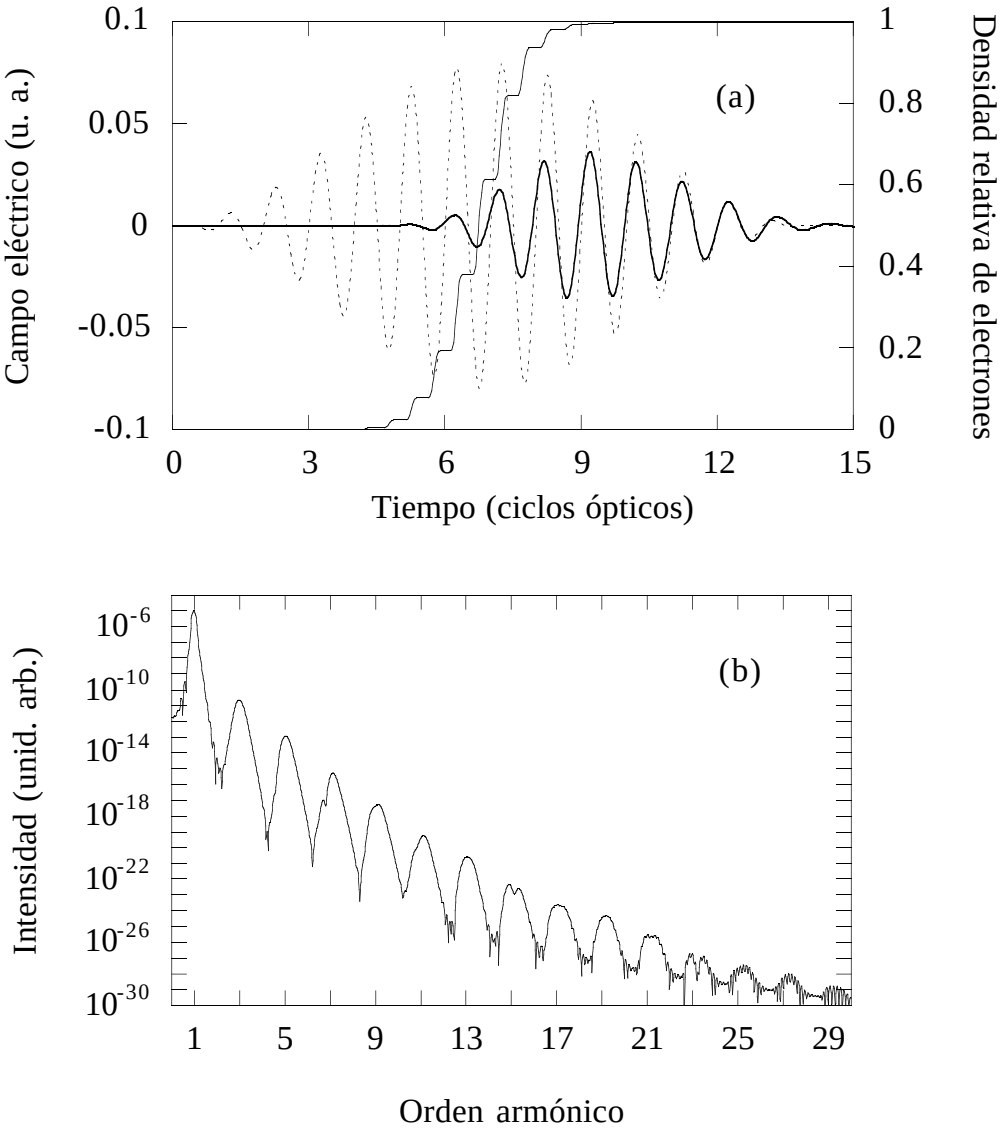


Figure 4.1: (a) Reflected field (thick solid line) when a pulse of frequency $\omega_0 = 0.05$ a.u., length 15 cycles and maximum amplitude $E_0 = 0.08$ a.u. impinges on a medium whose density is equal to the critical one under complete ionization conditions and whose thickness is $20\lambda_0$. The dashed line represents the incident pulse and the thin solid line the free electron density at the boundary. (b) Spectrum corresponding to the reflected field in (a).

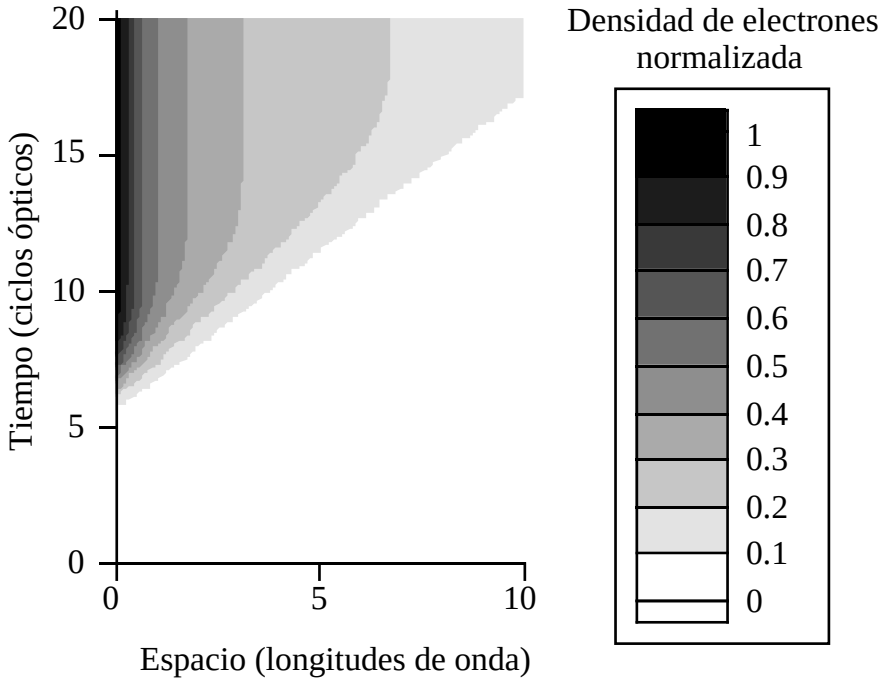


Figure 4.2: Evolution in space and time of the free electron density inside the medium for the case of figure 4.1.

the reflected pulse is less intense and shorter than the incident one. We can also check what we anticipated above: ionization is mainly produced when the electric field is close to its extreme values and therefore the free electron density profile increases stepwise. As a consequence, the reflected field contains harmonics, as we can see in figure 4.1b. These harmonics are not very intense in comparison with the fundamental one, but they are perfectly visible up to a relatively high order. Figure 4.2 depicts the evolution in space and time of the free electron density. We observe the propagation of the ionization front and the stepwise decrease in the stationary plasma density across the medium due to the absorption of the field. In any case, we shall now focus on the reflected field, leaving the effects of propagation for later sections.

In order to obtain a reasonably intense reflected pulse, the medium density should be close to the critical value; otherwise the reflection will be very small. In

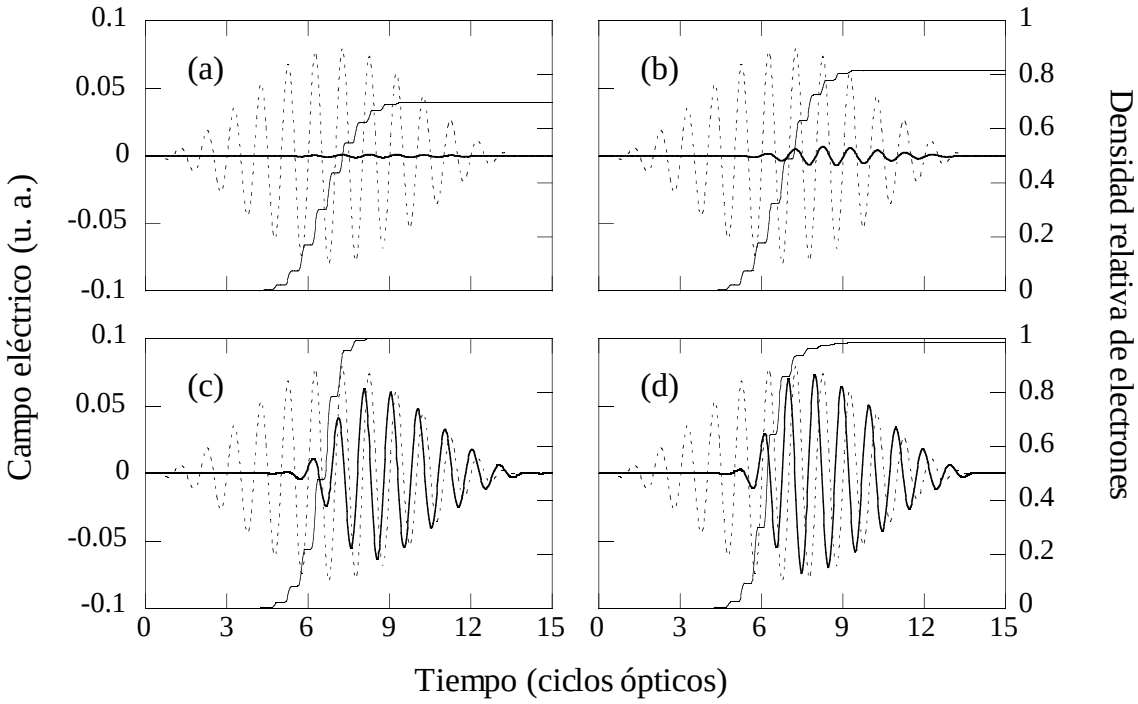


Figure 4.3: Same as figure 4.1a for values of the maximum density $0.1N_c$ (a), $0.4N_c$ (b), $2N_c$ (c) and $5N_c$ (d).

figure 4.3 we see the reflected pulses and density profiles for four different density values; figure 4.4 shows the corresponding spectra. When $N_0 = 0.1N_c$ (a), the reflection is negligible and there is no full ionization, even at the boundary. The reflected harmonics are very weak. When the density is raised up to $N_0 = 0.4N_c$ (b) we obtain a higher reflected field, although the boundary is still not completely ionized. There are more harmonics and these are more intense. For overcritical values, $N_0 = 2N_c$ (c) and $N_0 = 5N_c$ (d), the reflection grows noticeably and the maximum amplitude of the reflected pulse is nearly the same as the incident one, but, as we have already mentioned, the pulse is shorter and asymmetric. This effect could be used to obtain pulses with a sharp turn-on profile. Regarding the harmonics, they are more intense than in the undercritical cases, but their quality is poorer due to phase mismatch effects caused by the fast ionization and the high free electron density near the boundary. Observing 4.1b and 4.4, it may be seen that the best choice to obtain visible harmonics is to have a density equal or slightly lower than the critical one.

The effect of the intensity of the incident pulse is similar to that of the medium density. Figure 4.5 shows the reflected fields, the densities at the boundary, and the spectra for maximum amplitude values $E_0 = 0.06$ and $E_0 = 0.1$ a.u. when the maximum density of the medium is critical. In the case of the weaker field, there is evidently less ionization and the reflected field is therefore lower and has fewer harmonics, although they are clearly visible. The result is quite similar to the one obtained for parameters $E_0 = 0.08$ a.u. and $N_0 = 0.1N_c$. By contrast, when the amplitude is $E_0 = 0.1$ a.u. the ionization is faster and starts before the pulse maximum arrives at the boundary. As a result, the reflected pulse is longer and more intense. The harmonics are also more intense, but also broader. It appears as though the density were higher and the field less intense.

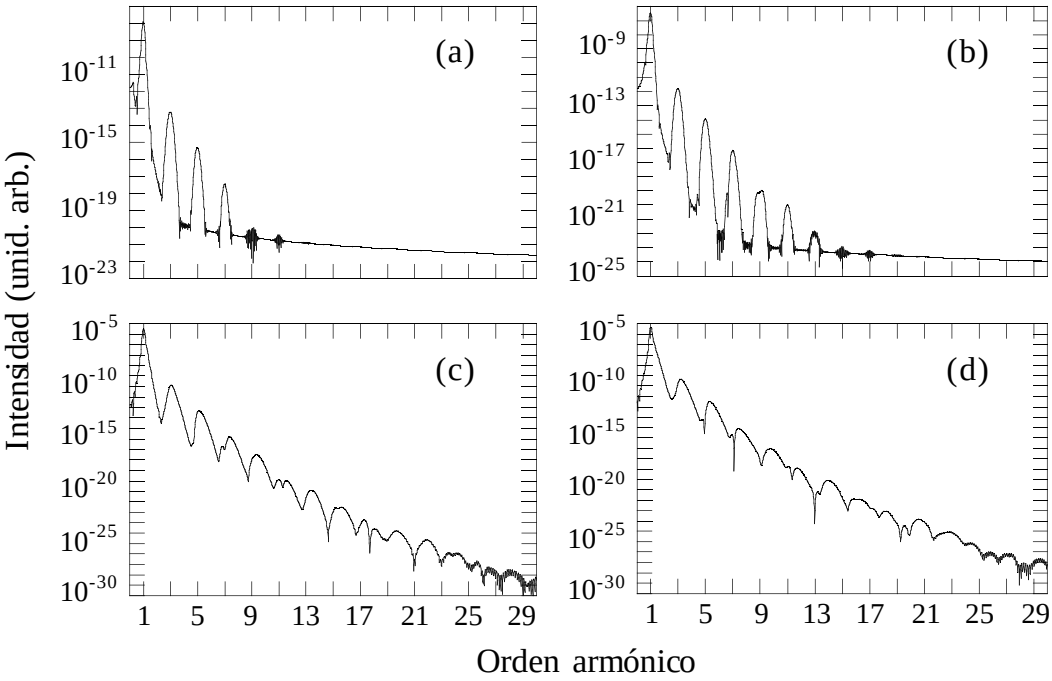


Figure 4.4: Spectra corresponding to the reflected fields in figure 4.3.

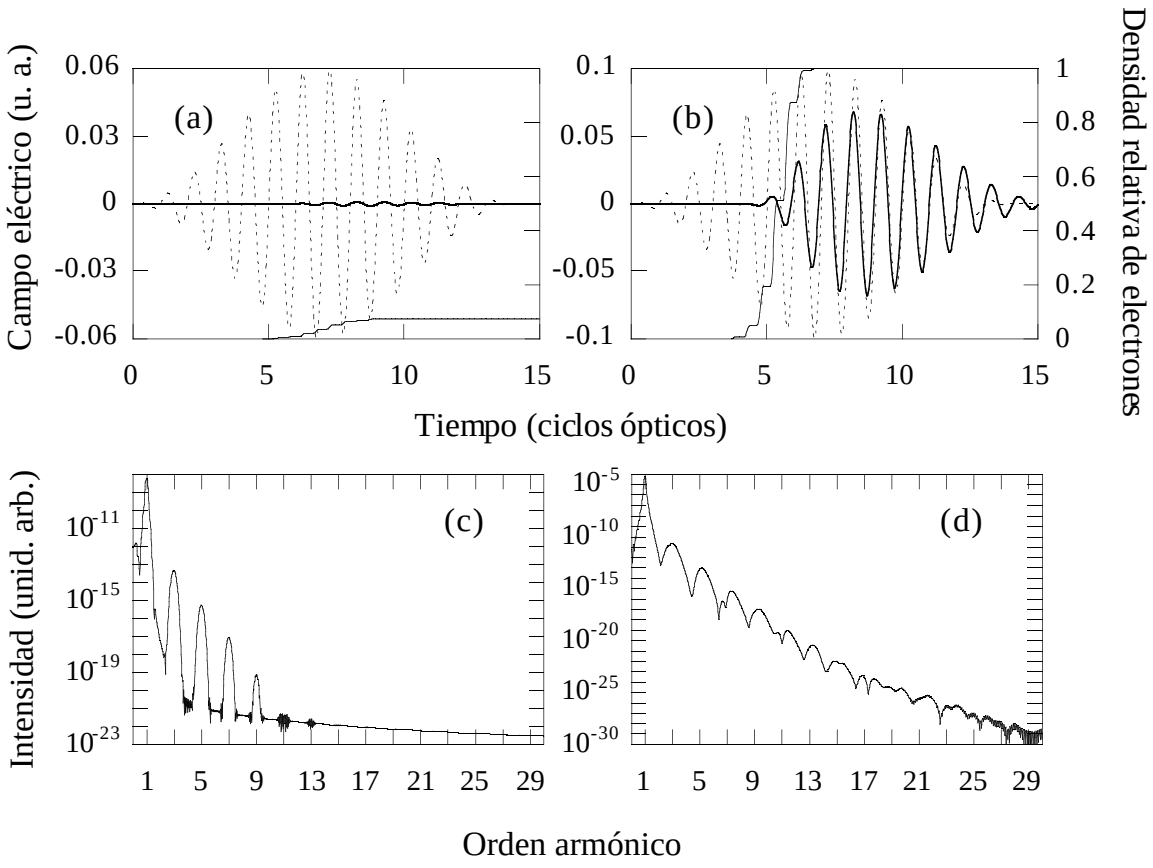


Figure 4.5: Reflected fields and free electron densities at the boundary in the case of a slab whose maximum density takes the critical value when the maximum pulse amplitudes are $E_0 = 0.06$ (a) and 0.1 (b) a.u. (c) and (d) show the corresponding spectra.

## 4.2 Effect of ionization for intense fields [118]

Until now, we have used the fixed-charge model to explain harmonic generation due to time-and-space-dependent ionization. However, it is possible that this simple model, which considers the free electrons as an ideal fluid in which no collective effects are included, may not give very reliable results. We shall now check the validity of this model, comparing its results with those obtained in the particle-in-cell simulations [118].

It can be expected that the fixed charges model will clearly fail for strongly overcritical media because in this case the collective effects are more relevant. Hence, we shall focus on the case of slightly overdense media, which is also the most interesting one regarding harmonic generation, owing to both to ionization and relativistic effects. In addition, we shall now use thin slabs because the harmonics are generated in a short space and enlarging the target only exacerbates the time-consuming calculations. In any case, we shall later see the effects of propagation in thicker slabs when the density and the field intensity are not very high.

We shall consider the parameters related to the slab as fixed. The thickness of the slab will be $0.1\lambda_0$ and its density under full ionization conditions will be $N_0 = 1.69N_c$ ($\omega_{p0} = 1.3\omega_0$). The incident pulse will have a duration of twenty cycles and its maximum amplitude will take three values: $E_0 = 0.1,\ 0.4$ and 4 a.u. In figure 4.6 we show the reflected pulses obtained with both models -PIC and fixed charges- for the three intensities of the incident field. It can be observed that the result is nearly identical for the weakest field and slightly different in the other two cases. We could conclude that the simple model works very well for weak fields and rather well even for strong fields... However, this depends on what we expect of the model. Since we are interested in the harmonics, we have calculated the spectra of these reflected fields, which are shown in figures 4.7, 4.8 and 4.9. All these figures show the results obtained with the PIC code (a), the simple model

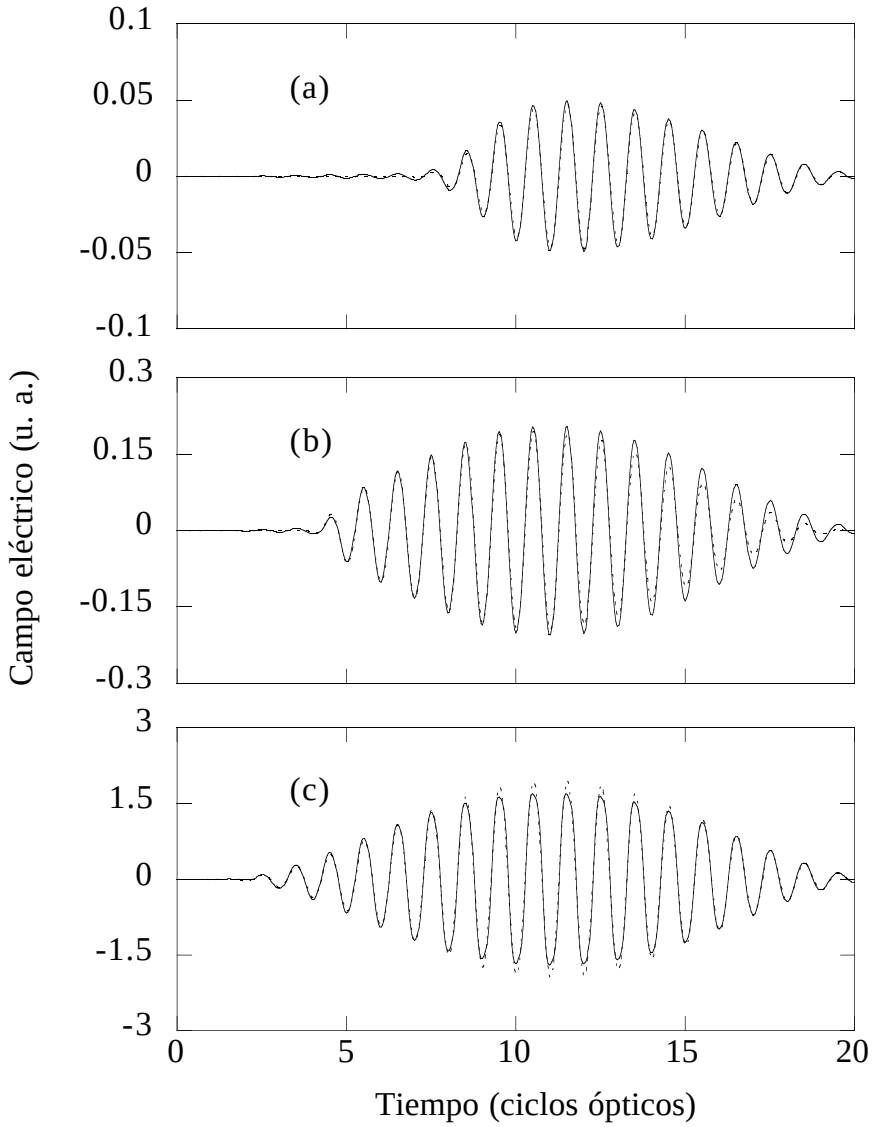


Figure 4.6: Fields reflected on a slab whose thickness and density are, respectively, 0.1 $\lambda_0$ and $N_0 = 1.69\ N_c$ when it is irradiated by a pulse with a length of 20 cycles and a maximum amplitude of $E_0 = 0.1$ (a), 0.4 (b) and 4 (c) a.u. The solid line represents the results obtained with a PIC calculation and the dashed line those from the fixed charge model.

(b) and with a PIC code when we consider that the slab is fully ionized before the interaction with the laser (c).

For a field amplitude of 0.1 a.u. (figure 4.7) we see that the harmonics obtained with both models are almost identical, the only difference being the loss of visibility in the case of the PIC calculation due to the effect of the interaction among particles, which makes the noise level higher. Apart from this, the intensity and shape of the harmonics are exactly the same. By contrast, when we use a preionized slab the result is completely different, with only a small third harmonic peak three orders of magnitude less intense than when we consider ionization. It is now clear that in this case the radiation emitted by the plasma is controlled by the ionization process and that the fixed charge model reproduces the results of the more complex PIC calculation very well. Here, the common approximation in PIC calculations of assuming that the slab is fully preionized is completely wrong.

When the incident field amplitude is raised up to 0.4 a.u. (figure 4.8), the results begin to change. The harmonics produced by ionization are still visible but there is a difference of nearly one order of magnitude in the intensity of the third harmonic between the PIC calculation (a) and the simple model (b). Moreover, this intensity is the same in the case of the preionized slab (c), although in this latter case the peak is clearer because of the absence of phase mismatch effects produced by ionization. In this situation, we can say that the ionization process must be included to perfectly describe the radiation emitted by the medium but that collective effects begin to play the most important role.

Finally, when we reach an amplitude of 4 a.u., the spectra obtained with the ionizing and preionized slab are almost identical, whereas the fixed charge model results are completely different. Hence, this simple model is not at all good for describing the interaction in the case of intense fields, for which the ionization is hardly important and we can disregard its contribution, as has been done in

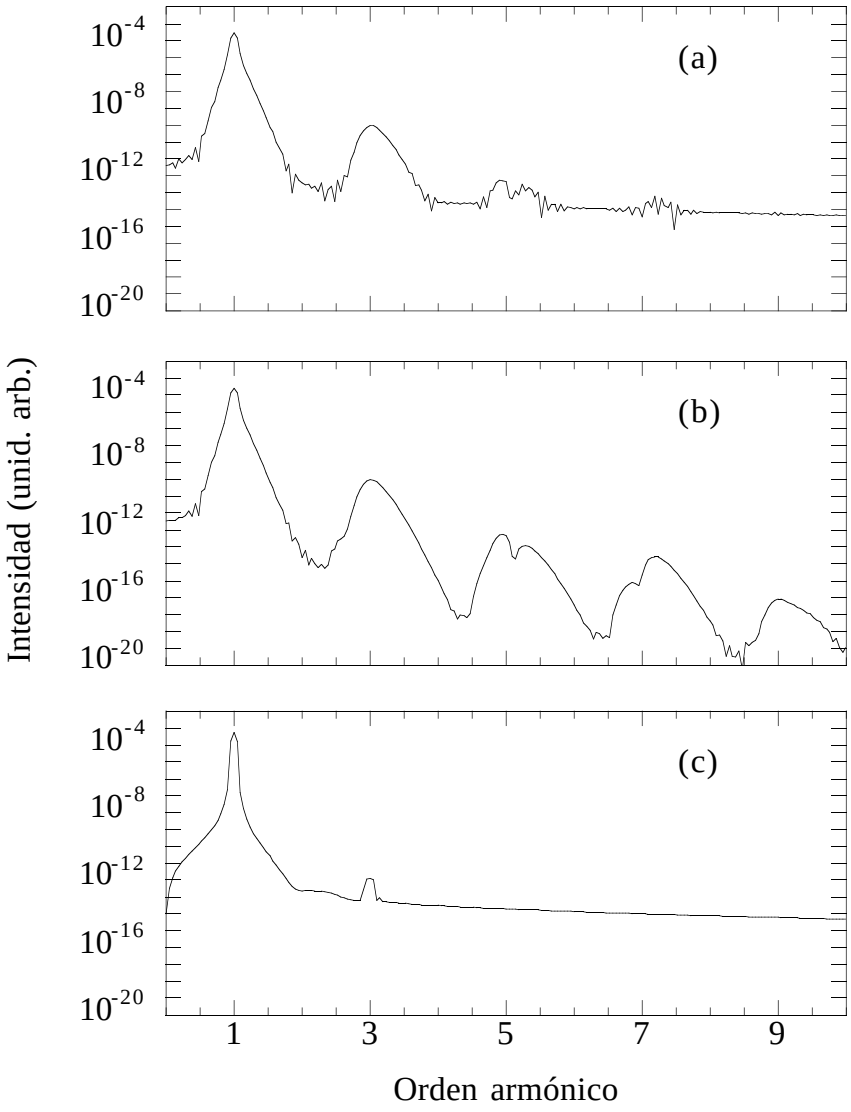


Figure 4.7: Spectra corresponding to the reflected field in 4.6a obtained with the PIC calculation (a), the fixed charge model (b) and a PIC code with a preionized slab.

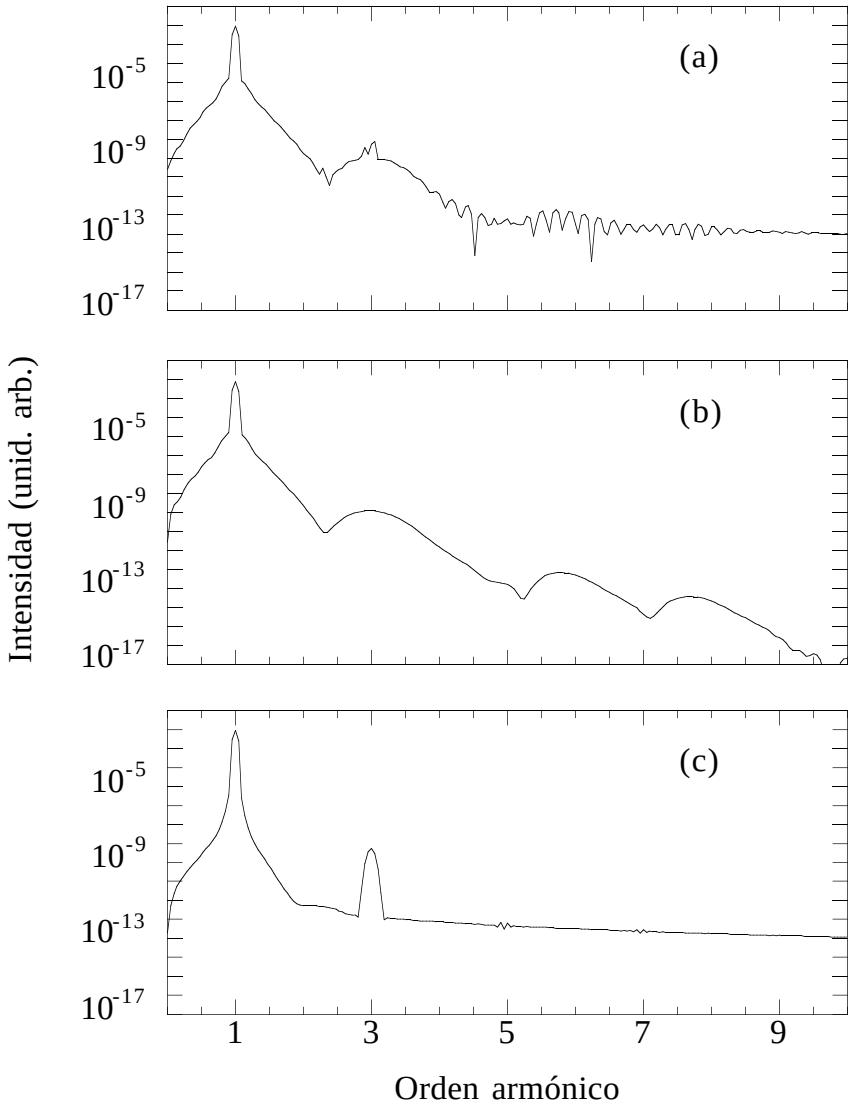


Figure 4.8: The same as figure 4.7 for a field amplitude of 0.4 a.u.

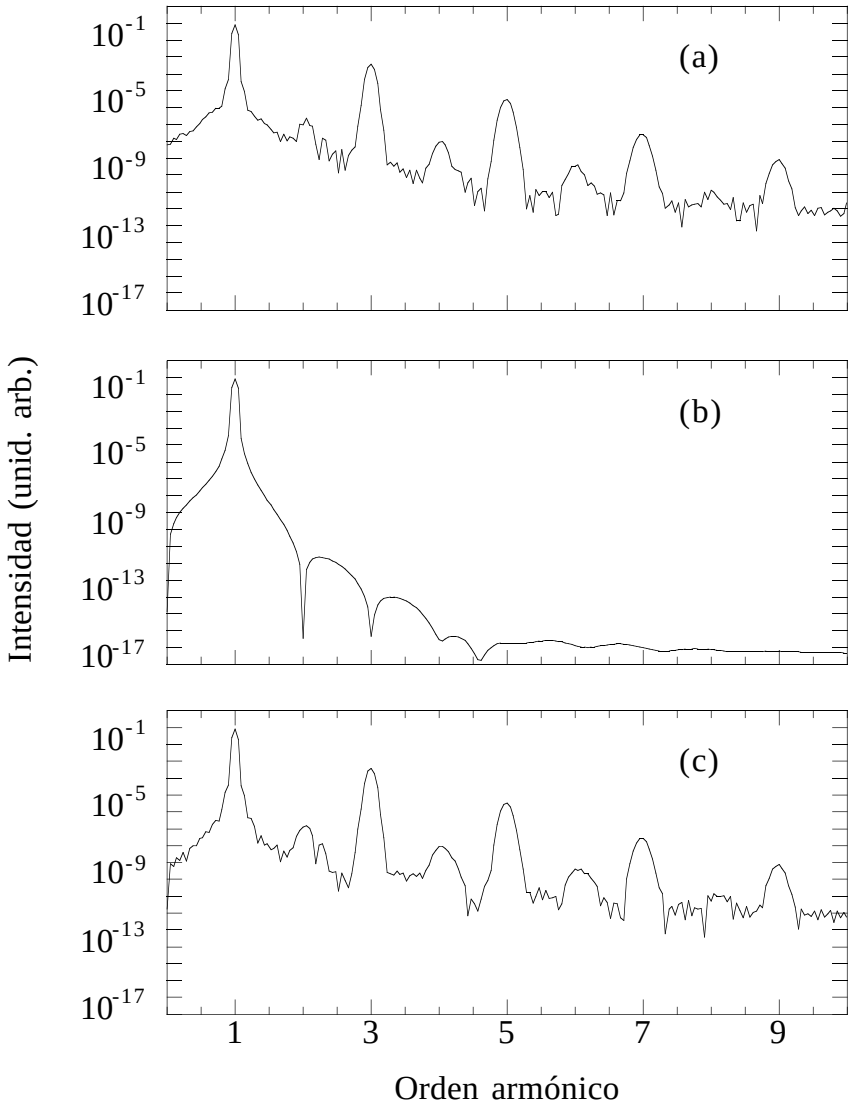


Figure 4.9: The same as figure 4.7 for a field amplitude of 4 a.u.

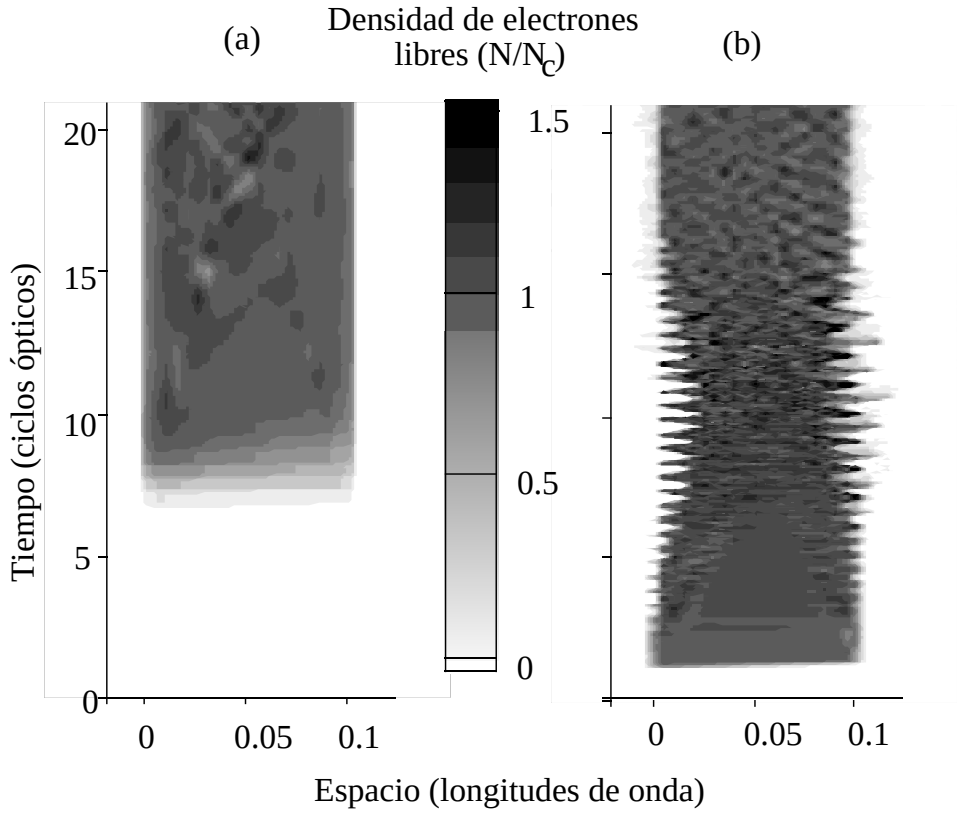


Figure 4.10: Evolution of the free electron density when the incident field has an amplitude of 0.1 (a) and 4 (b) a.u.

previous works [84, 85].

The nature of the harmonics generated in the two limiting cases is very different, as we already know. To state this in even clearer terms, we have represented the evolution in space and time of the free electron energy in both cases. For the weakest field, harmonics are generated during the ionization stage, as we have explained above. It can be observed how the ionization advances stepwise inside the medium once the pulse approaches its maximum. When the ionization is completed, the only mechanism that generates harmonics is the relativistic magnetic

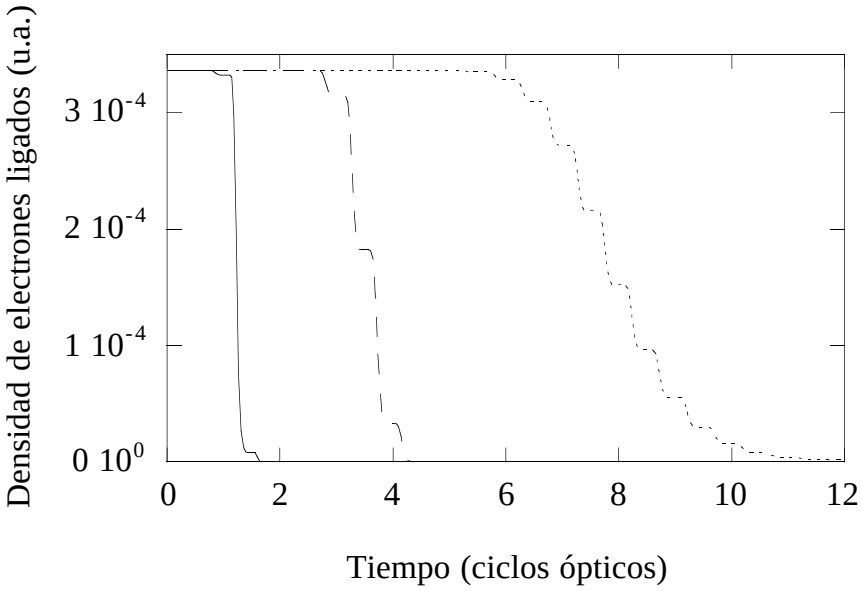


Figure 4.11: Time evolution of the bound electron density in the middle of the slab for incident amplitudes of 0.1 (dotted line), 0.4 (dashed line) and 4 (solid line) a.u.

force, which is very faint for such a weak field. However, when $E_0 = 4$ a.u., the ionization occurs very fast, taking place almost instantaneously in the whole slab after the first cycle of the pulse (when the amplitude of the field is much lower than its maximum and the tunnelling ionization rate can be used) and, as soon as it has occurred, the electrons begin to oscillate like a *moving mirror*. The spatial inhomogeneity of the free electron density inside the medium is also more important.

The importance of each mechanism (ionization and magnetic field) in the total harmonic yield is related to the time required by the medium to become fully ionized. When this time is comparable to the length of the pulse, harmonics will be mainly generated by the ionization process and will have that peculiar broadened shape. By contrast, when this time is very small, the spectrum will consist of sharper peaks generated by the magnetic force. In figure 4.11 we have depicted the evolution of the bound electron density in the middle of the slab for

the three values of the incident pulse amplitude. In the most intense case ($E_0 = 4$ a.u.), the ionization is completed in less than one optical cycle, as stated above, and therefore there are no harmonics due to ionization. In the case of the weakest field ($E_0 = 0.1$ a.u.), the ionization time is approximately four optical cycles, long enough to generate harmonics. In the intermediate case ($E_0 = 0.4$ a.u.), the ionization time is roughly two cycles. It is then clear that in order to obtain harmonics by ionization, the ionization time has to be longer than one cycle. On the other hand, in order to obtain the harmonics through the $\mathbf{v} \times \mathbf{B}$ force, we require that an intense enough field should interact with the electrons over several cycles.

The relative importance of these two regimes will depend on the part of the interaction time during which they are effective. To gain insight into this, in figure 4.12 we have represented the spectrum obtained for the medium amplitude field when a pulse of 40 cycles is considered. The pulse envelope has the same turn-on and turn-off shapes as the 20 cycle envelope, but a central part with twenty cycles of constant amplitude is added. Choice of the same turn-on guarantees that the ionization process is identical in both cases, whilst the addition of the intermediate constant amplitude part means that the time during which the fully ionized medium generates harmonics is longer. We see the increase in the height of the peak corresponding to the third harmonic and a reduction in the broadened peaks corresponding to the ionization process. These observations confirm our previous statement.

We can conclude this section by saying that regarding harmonic generation there are two regimes of ionization, whose difference is given by the relationship between the ionization time and the total length of the pulse. In the case of weak fields, the ionization time is several optical cycles and the harmonics are generated by the time-and-space-dependent ionization. In this case, Brunel's fixed charge

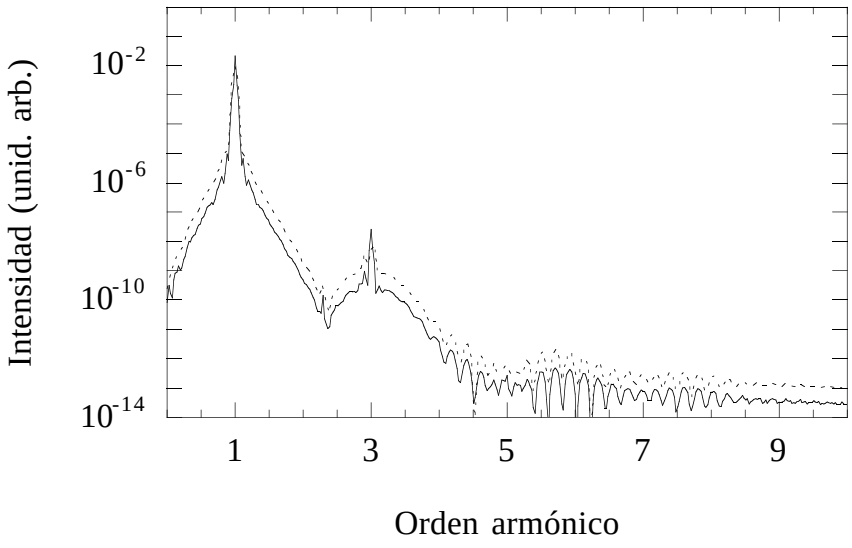


Figure 4.12: Spectrum of the field reflected when the slab is impinged by a pulse of maximum amplitude $E_0 = 0.4$ a.u. and length 40 cycles, ten of turn on, twenty of constant amplitude and ten of turn off (solid line). Dotted line represents the result of figure 4.8, calculated for a twenty cycle long pulse without a constant amplitude part in the center.

model works very well to explain the results. When the field is more intense, however, the ionization time is reduced and higher harmonics are observed due to the magnetic component of the relativistic force acting on the electrons. The role of ionization is then negligible and we can assume that the plasma is preionized before it interacts with the main part of the pulse, which is the one close to its maximum.

## 4.3 Propagation effects

Let us now, somewhat belatedly comment on some of the propagation effects. We shall focus on two chromatic effects such as blueshift and low-frequency filtering and, briefly, on phase mismatch effects in the case of high density media.

### 4.3.1 Wavelength changes. Blueshift

In the harmonics spectra produced by ionization that have been shown up to now, there is one feature common to all of them: the peaks are asymmetric, and always tend towards higher frequencies. In some cases it is also clear that the positions of the maxima do not coincide with the integer harmonic of the incident frequency but rather with a higher value. This effect is known as blueshift and is a direct consequence of the ionization process. Let us explain this frequency shift in simple terms [119, 120].

As the field propagates inside the medium, the latter begins to ionize, varying its refraction index $\eta$ (here we do not use the common notation $n$ in order to avoid confusion with the normalized free electron density). This produces a change in the phase of the field during its propagation through an interval $\delta x$, given by $\phi = k\delta x = k_0\eta\delta x$. The frequency shift will be $\delta\omega = -d\phi/dt = -k_0\partial\eta/\partial t\ \delta x$. The total frequency shift undergone by the field when propagating between $x = 0$ and

$x = L$ will be

$$\Delta\omega = -\frac{\omega_0}{c}\int_0^L dx \frac{\partial\eta(x,t)}{\partial t}. \tag{4.8}$$

This equation is valid only when the change in the refraction index is slow and when the electric field is initially monochromatic, which is not a good approximation for very short pulses whose spectral curve is broad. In the case of not very dense media, we can use the expression for the refraction index given by equation (1.109), expanding the square root as $\eta \simeq 1 - \omega_p^2/2\omega_0^2 = 1 - N/2N_c$. Hence, the frequency shift will be

$$\Delta\omega \simeq \frac{\omega_0}{2cN_c}\int_0^L dx\ W(x,t)(N_0 - N), \tag{4.9}$$

where we have used equation (3.63) for the time derivative of the free electron density. It is clear from (4.9) that there is a frequency shift of positive sign and that this shift will be greater if the ionization is fast and the medium is dense and thick. It is also clear that if we increase the fundamental frequency its harmonics will be shifted too.

In figure 4.13 we can observe how the low harmonics are generated and propagated through a medium with a maximum density of $N_0 = 0.1N_c$ for a pulse with a maximum amplitude of $E_0 = 0.08$ a.u. We observe the continuous broadening of the peaks, which are slowly shifted to higher frequencies. The results were obtained with the fixed charge model.

In fact, this frequency shift is not as simple as it appears to be. The blueshift occurs only in the part of the pulse which ionizes the medium, whilst the rest does not undergo blueshift. Figure 4.14 shows two plots corresponding to two different instants of the propagation of the pulse inside the medium, in this case for a maximum density of $N_0 = 0.4N_c$, for which the propagation effects are more important. A strong phase modulation can be seen. The part close to the maximum, which is the one that ionizes the medium, is compressed and propagates

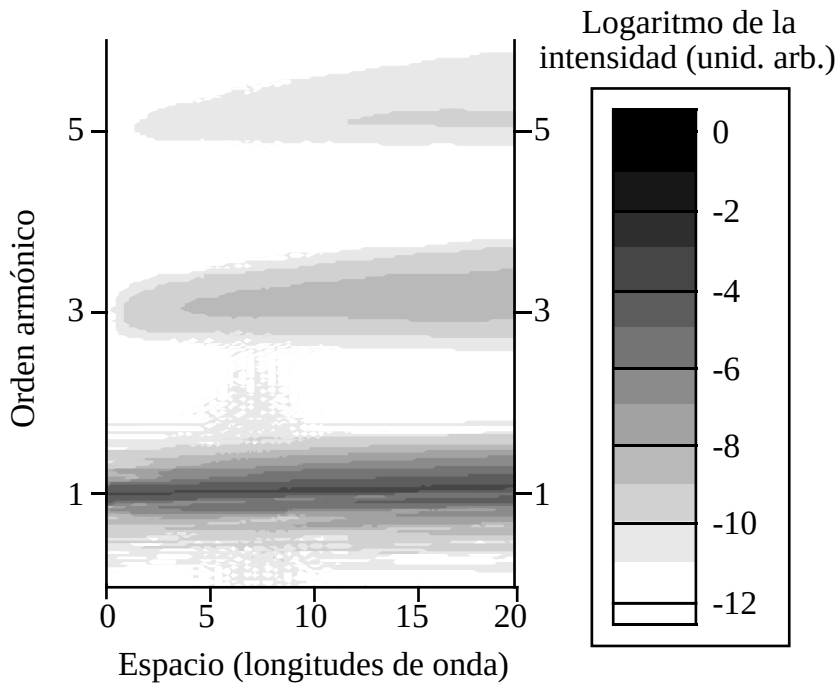


Figure 4.13: Spatial evolution of the harmonics in a medium with a maximum density of $N_0 = 0.1N_c$ and an incident pulse of amplitude of $E_0 = 0.08$ a.u.

with a wavelength longer than the incident one. In turn, the pulse tail propagates through a medium whose density, and therefore whose refraction index, varies smoothly. Since that index is smaller than unity, the wavelength is longer than the vacuum wavelength. This phase modulation and the changes in the "instantaneous wavelength" affect the frequency of the transmitted pulse. We can see the time evolution of the transmitted field in figure 4.15. The maximum amplitude of the pulse is slightly lower than the incident one, as is expected due to the reflection, which is not very high for these undercritical densities (figure 4.3b). In both plots, we see the blueshift near the pulse peak and the small redshift in its tail. This broadens the spectra of the peaks and, since the blueshift is much more important when the field is close to the maximum, the mean frequency of the pulse is increased.

The literature contains several references to frequency shifts during the propa-

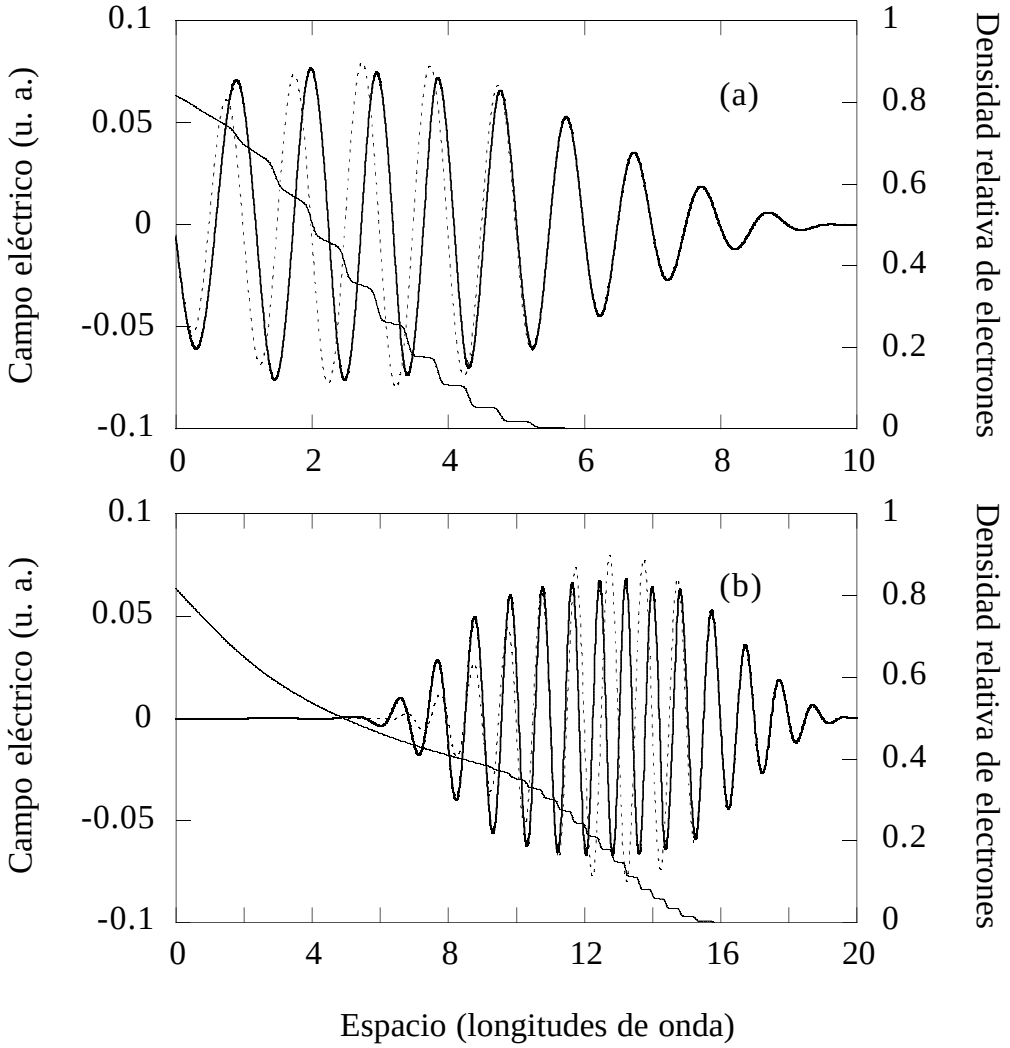


Figure 4.14: Propagation of a pulse of maximum amplitude of $E_0 = 0.08$ a.u. through a medium with maximum density $N_0 = 0.4N_c$. Plot (a) shows the field inside the medium (thick solid line), the field as it would propagate in vacuum (dotted line) and the free electron density profile in the medium (thin solid line) ten cycles after the pulse reaches the boundary. Plot (b) shows the same twenty cycles after the pulse reaches the boundary.

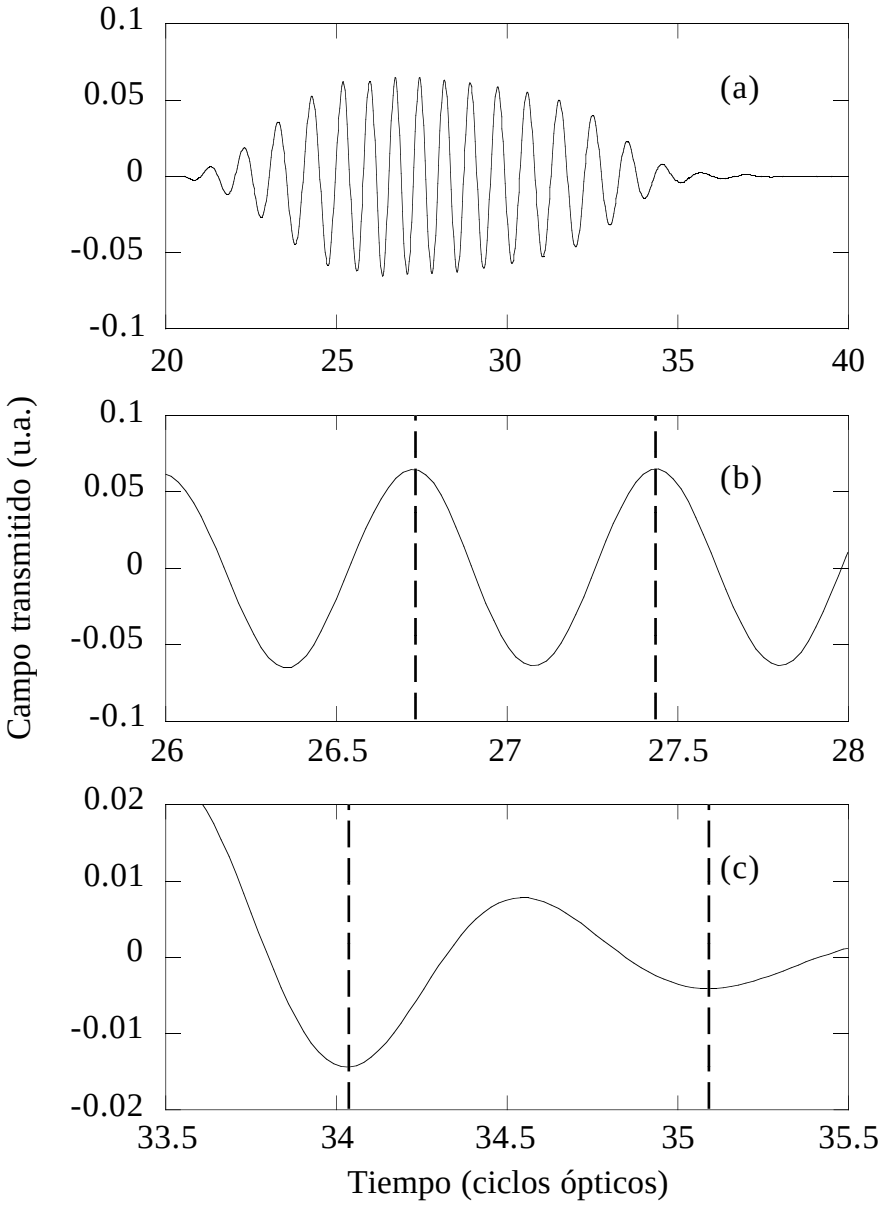


Figure 4.15: Transmitted pulse in the previous case when the pulse crosses a slab with a thickness of $20\lambda_0$ (a). Plots (a) and (b) show details of the zone close to the pulse maximum and tail, respectively.

gation of not very intense fields through low-density ionizing media, both of theoretical [107, 110, 116, 119, 120, 121] and experimental [122, 123, 124] interest.

When the field is very intense, the frequency shifts are different. In this case the ionization is very fast, as we have already explained, and occurs during the leading part of the pulse. The electrons are dragged by this front due to the ponderomotive force and the rest of the pulse finds a lower density. The effect is opposite to the one described above and the mean shift tends to lower frequencies. A small redshift is then visible [85, 116]. The same inhomogeneity generates the waveshocks in overdense plasmas. A different situation arises when the pulse impinges onto an ionization front generated not by the pulse but by other means, which moves with relativistic velocity in the opposite direction. In this case there is a strong blueshift because the initial frequency cannot propagate through the medium and changes to a final value given by the plasma dispersion relationship $\omega_f^2 = \omega_0^2 + \omega_p^2$ [125, 126, 127]. One further effect which appears in the case of intense fields is the Doppler shift, which also affects the radiation from moving electrons, as stated in section 1.5. However, its contribution is usually less important than the previous ones.

### 4.3.2 Phase mismatch effects

In addition to frequency shifts, phase mismatch effects due to the ionization process and the existence of free electrons appear. As we already know, these effects are also very important. The phase mismatch will deteriorate the visibility of the harmonics and these will disappear after a more or less short propagation length. In the case of a not very dense medium, this length can be many wavelengths and the phase mismatch depends on the product of the free electron density multiplied by the propagation length [113]. For dense media, this no longer holds.

Figure 4.16 shows the propagation of the low harmonics when the density is

higher than in figure 4.13. As the density is increased, the harmonics are created closer to the boundary and are broadened faster, visibility rapidly being lost. For overcritical densities the variation is not significant because the main part of the pulse is reflected and the ionization is only visible in a very thin layer of the slab. The rest of the pulse is then propagated through a medium with low free electron density.

Hence, when the medium is dense the transmitted harmonics undergo a strong phase mismatch, while the reflected ones are generated in a very thin layer in which the ionization is important and then propagate in vacuum. This is why the reflected harmonics will be of better quality and will be more visible.

### 4.3.3 Harmonic filtering in overdense plasmas [128]

In the previous section, we have explored an effect related to the frequency of the propagating field in a weakly-dense plasma, the blueshift. When the medium is overdense, the incident pulse cannot propagate through it and is almost completely reflected, its amplitude decreasing exponentially inside the medium. When the field is intense enough to generate harmonics through the mechanism of relativistic magnetic force, and depending on the medium density, some harmonic frequencies may be higher than the plasma frequency and can propagate freely inside the medium. Hence, the lowest harmonics may be reflected whilst the transmitted field has only high harmonics, the medium behaving like a low frequency filter. This effect has been observed in numerical simulations [129] and also experimentally [130] and can be used to estimate the electron density in the medium directly.

This is true in the case of a preformed plasma, but if the plasma is generated by the pulse and the medium is initially transparent, the field can penetrate it until the free electron density exceeds the critical value for its frequency, as we have mentioned. The transmitted field will be lower or higher, depending on the

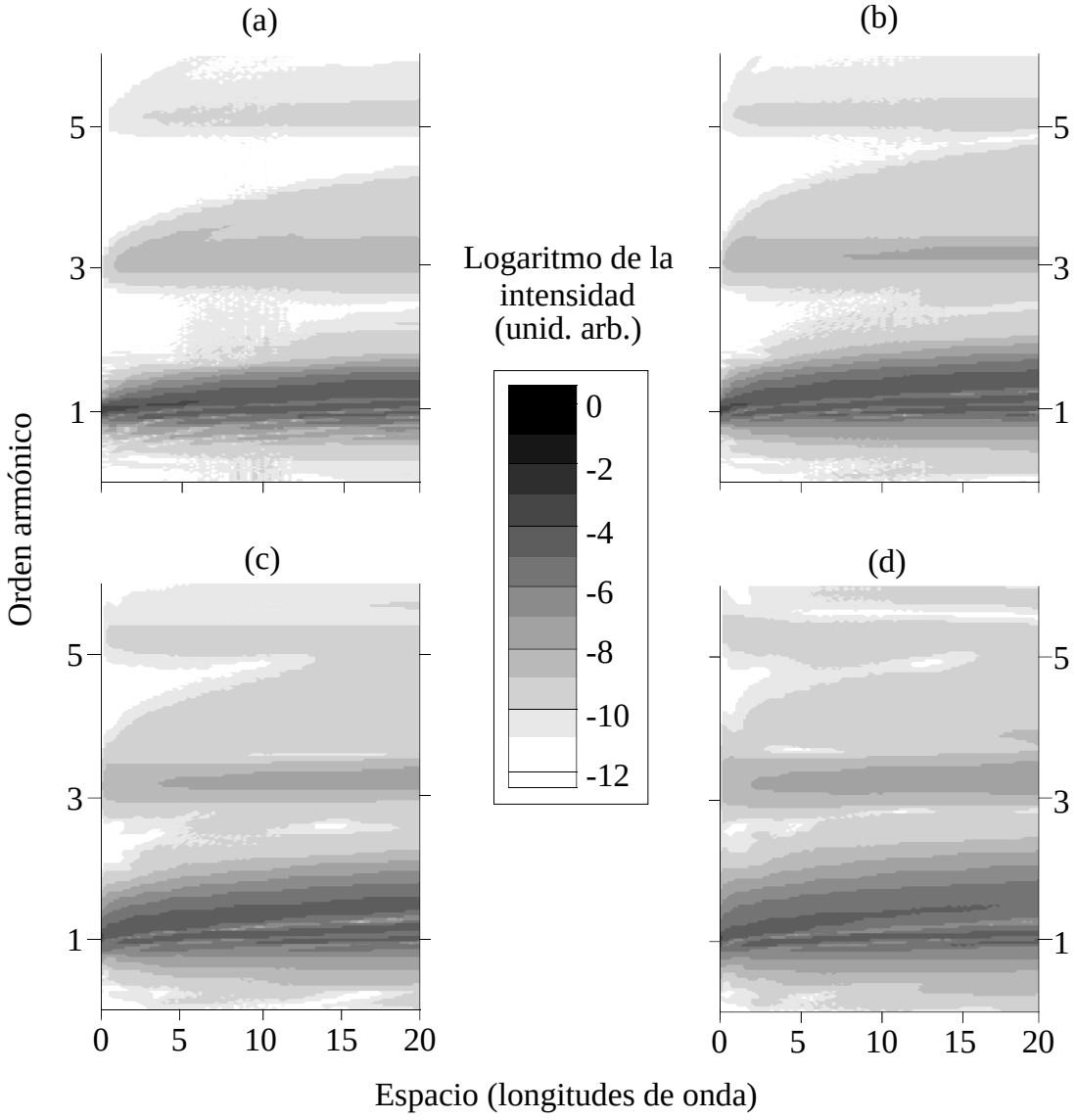


Figure 4.16: Propagation of the harmonics due to the ionization for densities of $N_0 = 0.4N_c$ (a), $N_c$ (b), $2N_c$ (c) and $5N_c$ (d). The field amplitude is always $E_0 = 0.08$ a.u.

rate of ionization of the medium. In addition, we must take into account that the ionization is not homogeneous, especially when the medium is thick enough. In this case, there is a very thin, completely ionized layer which attenuates the transmitted field amplitude. As a result, the pulse is initially absorbed but its evanescent part which crosses the ionized layer, as soon as its intensity becomes so low that it is no longer able to ionize the medium, propagates through a transparent bulk and is not completely filtered.

Let us begin with a preionized slab, which is the easiest one. The thickness of the slab is equal to the wavelength of the incident pulse, whose frequency is $\omega_0 = 0.05$ a.u. Figure 4.17 shows the spectrum of the transmitted field when $E_0 = 0.5$ a.u. and $N_0 = 7N_c$ (a), and $E_0 = 4$ a.u. and $N_0 = 15N_c$. The critical density for the harmonics is $N_c^{(m)} = \omega_m^2/4\pi = m^2 N_c$, and so in case (a) the medium is overdense for the fundamental frequency but underdense for all its odd harmonics, while in case (b) it is also overdense for the third harmonic and underdense for the higher ones. The results of simulations agree perfectly in both cases and the harmonics are quite visible, especially in the case of the more intense laser and denser medium.

Figure 4.18 shows the transmitted pulses whose spectra have been shown previously. At the beginning there is no propagated field, but then a shorter and less intense pulse appears whose frequency is the corresponding harmonic. The peak of the transmitted pulse corresponds approximately to the peak of the incident pulse, which is logical since it is precisely when the field is maximum that the surface oscillations are greater and the harmonics more intense (the delay of roughly three optical cycles appears because we measure the transmitted pulse at a point two wavelengths distant from the right surface of the slab, whose thickness is one wavelength).

Let us now study the case when the medium is not previously ionized but the

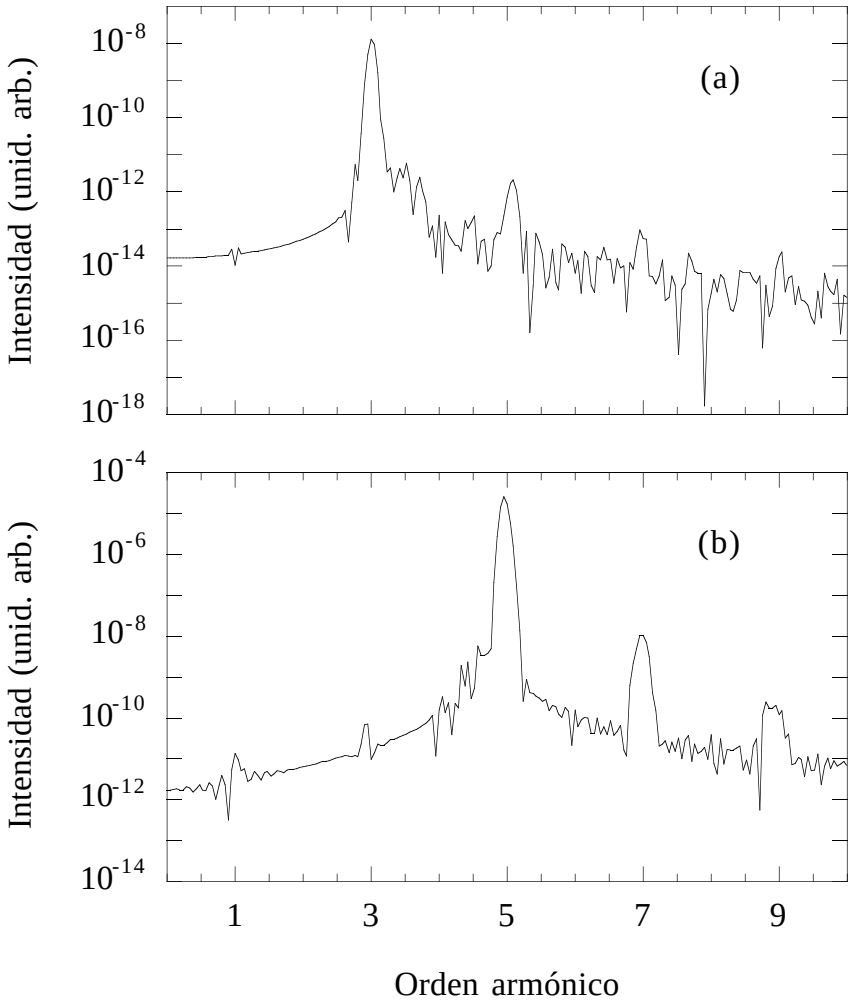


Figure 4.17: Spectrum of the field transmitted through a preionized slab of thickness $\lambda_0$. The medium density and the maximum amplitude of the incident pulse are, respectively, $N_0 = 7N_c$, $E_0 = 0.5$ a.u. (a); $N_0 = 15N_c$, $E_0 = 4$ a.u. (b).

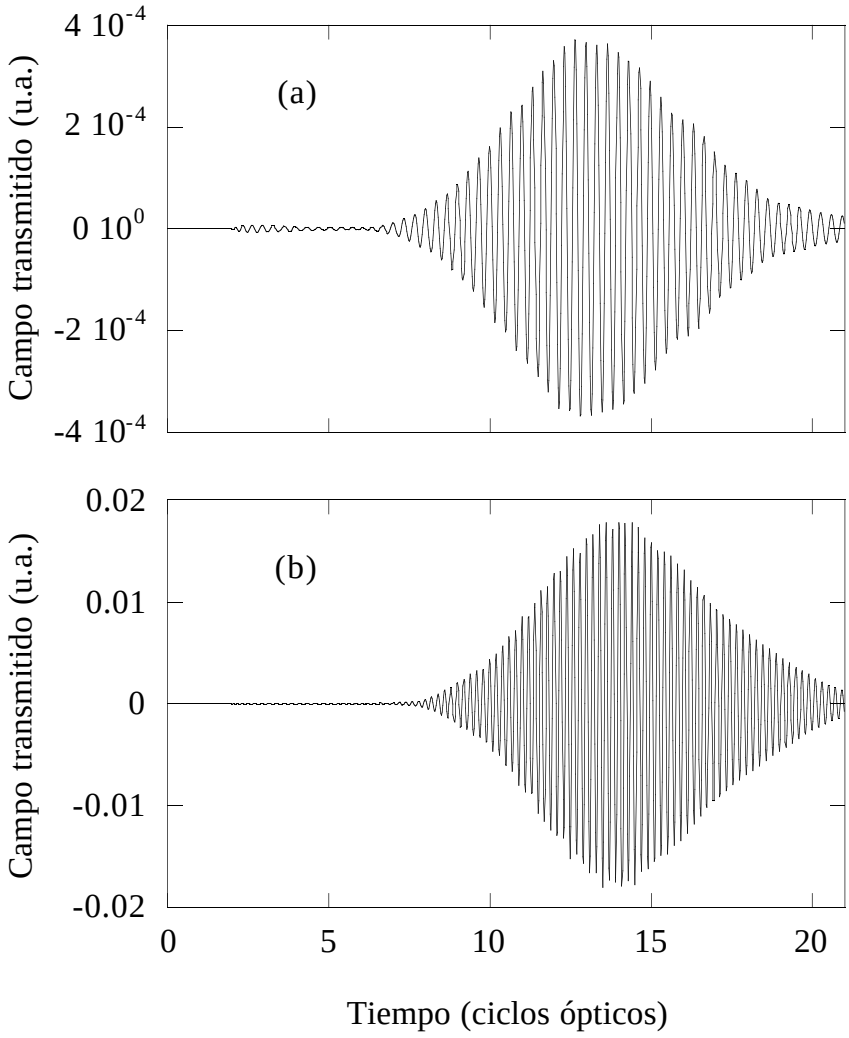


Figure 4.18: Transmitted pulses whose spectra are depicted in figure 4.17.

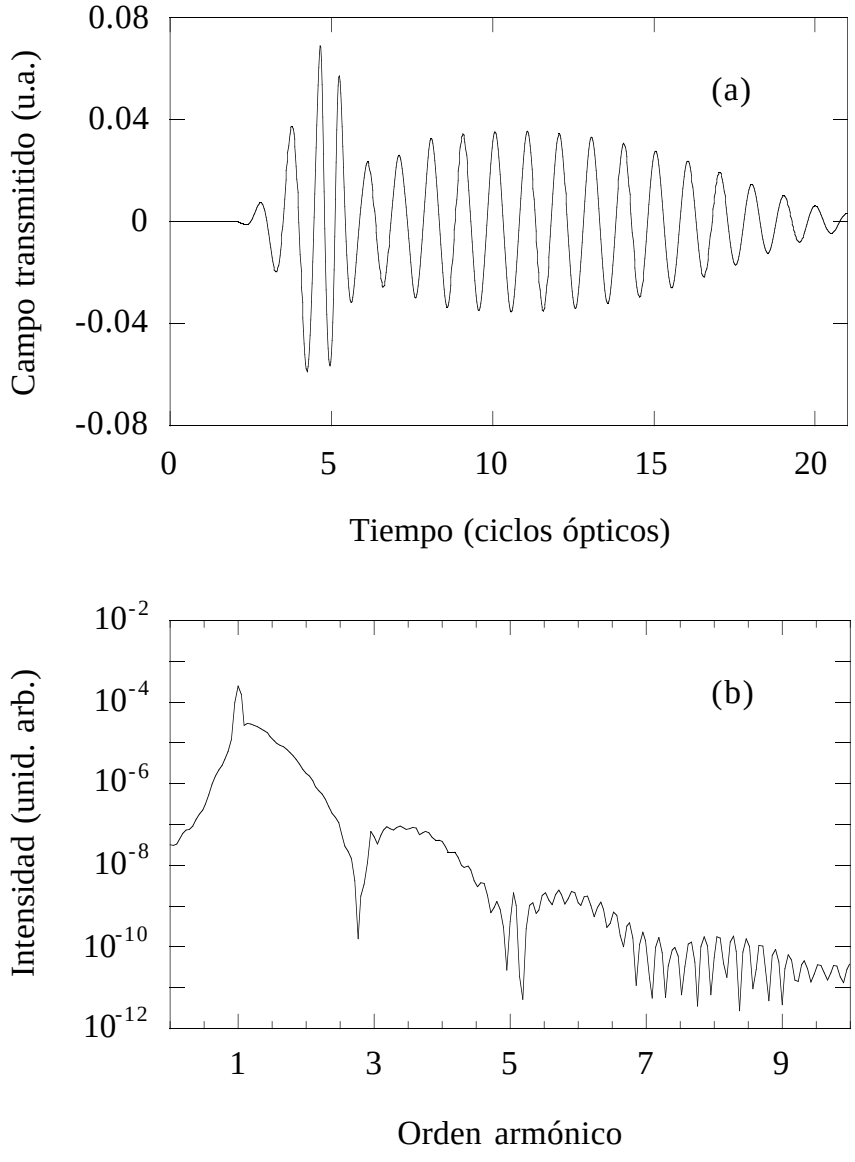


Figure 4.19: Transmitted pulse (a) and its spectrum (b) for an amplitude of $E_0 = 0.5$ a.u. impinging on an initially transparent slab of thickness $\lambda_0$ and density $N_0 = 7N_c$.

pulse itself generates the plasma. Figure 4.19 shows the transmitted pulse and its spectrum when $E_0 = 0.5$ a.u. and $N_0 = 7N_c$. We see that the pulse propagates, although its amplitude varies in a strange way and the spectrum does not show any sign of filtering, the typical broadened and blueshifted ionization peaks appearing. Figure 4.20 shows the evolution of the electron density corresponding to this case, affording a better description of what is happening. The incident pulse enters the medium without any opposition because the initial amplitude is not able to ionize it (this corresponds to the initial peak of the transmitted pulse). However, as soon as the amplitude increases, the medium begins to ionize, not homogeneously but in a decreasing way along the medium. When the pulse reaches its maximum, a stationary regime is attained with a completely ionized layer of small thickness. If this thickness is lower than the penetration depth, the evanescent wave can go through it and propagate freely because its amplitude is not high enough to completely ionize the bulk and it only undergoes phase mismatch effects, but not a strong attenuation. That is precisely what occurs in this case.

If we increase the field amplitude up to $E_0 = 4$ a.u., we obtain the results depicted in figures 4.21 and 4.22. The pulse begins to propagate but, as soon as it ionizes the medium, the transmitted wave has a frequency which is three times the initial one. This is also visible in the spectrum, which shows a third harmonic two orders of magnitude more intense than the fundamental one, which has been filtered. In the density plot, we see that the ionization is slow until the peak of the pulse, whose evanescent part is intense enough to ionize the whole slab. In this situation, the overdense region inside the plasma exceeds the penetration depth of the incident field but does not affect the propagation of the higher harmonics, which are mainly generated at the plasma surface.

One last example, which is even more interesting, is shown in figures 4.23 and 4.24. In this case, the field amplitude is still $E_0 = 4$ a.u. but the medium is denser,

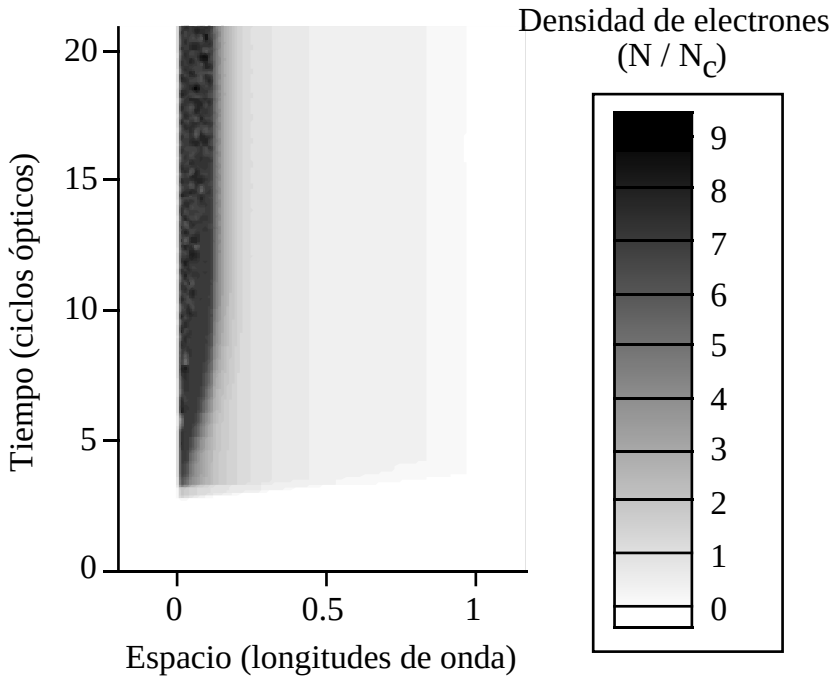


Figure 4.20: Evolution in space and time of the free electron density corresponding to the parameters in figure 4.19.

$N_0 = 15N_c$. Observing the spectrum, one could conclude that there is no perfect filtering of the first and third harmonics, regardless of the high density of the slab. However, upon inspection of the transmitted field, we see that the problem is in fact more complicated and that the transmitted field has a time-dependent frequency, called *chirped*, although in this case the variation is not smooth: initially the transmitted field is governed by the fundamental frequency component $\omega_0$; after some cycles it shows a steplike transition to a frequency of $3\omega_0$, and finally another step transition to $5\omega_0$. The mechanism underlying this step-chirping is the time evolution of the filtering property of the target as the ionization increases the charge density to overcritical values, first for the fundamental frequency and then for the third harmonic.

This time-dependent filter can be easily understood with the help of figure 4.24. The first part of the pulse enters the medium, ionizing a very thin slice. This part

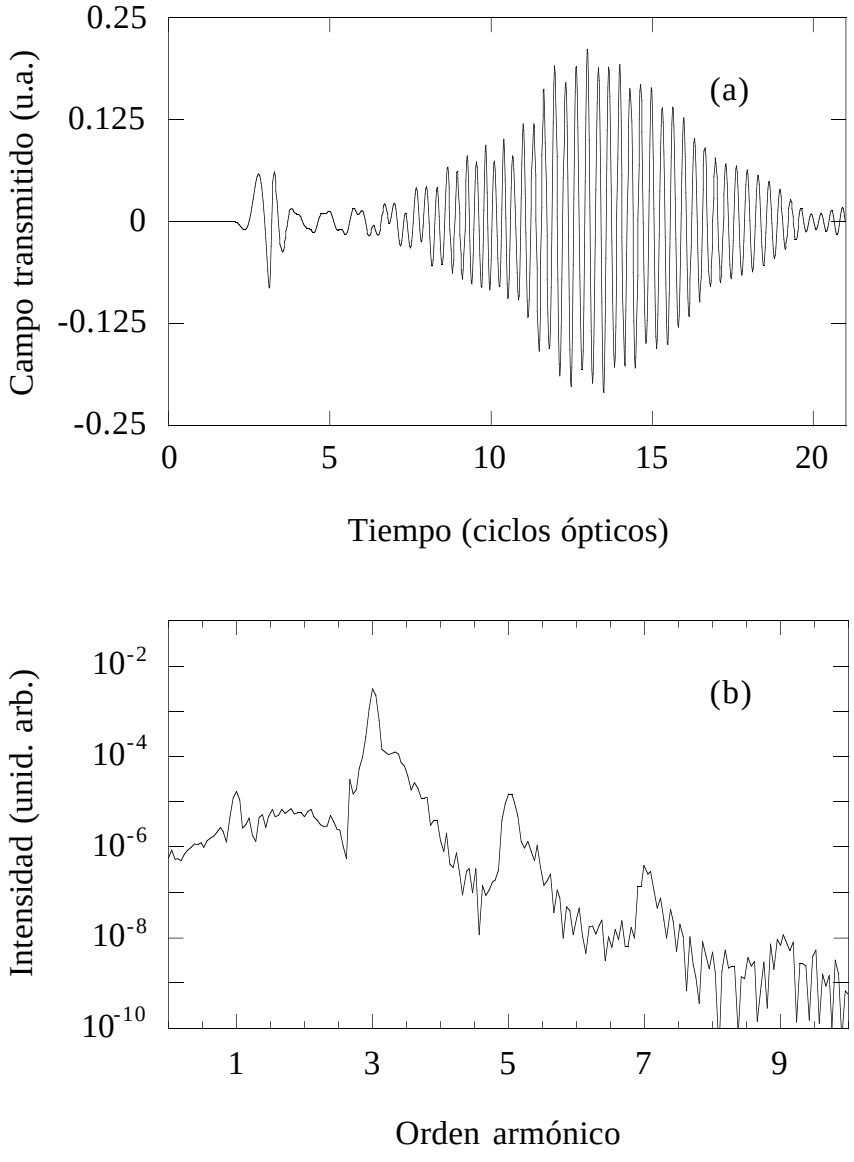


Figure 4.21: Transmitted pulse (a) and its spectrum (b) for an amplitude of $E_0 = 4$ a.u. impinging on an initially transparent slab of thickness $\lambda_0$ and density $N_0 = 7N_c$.

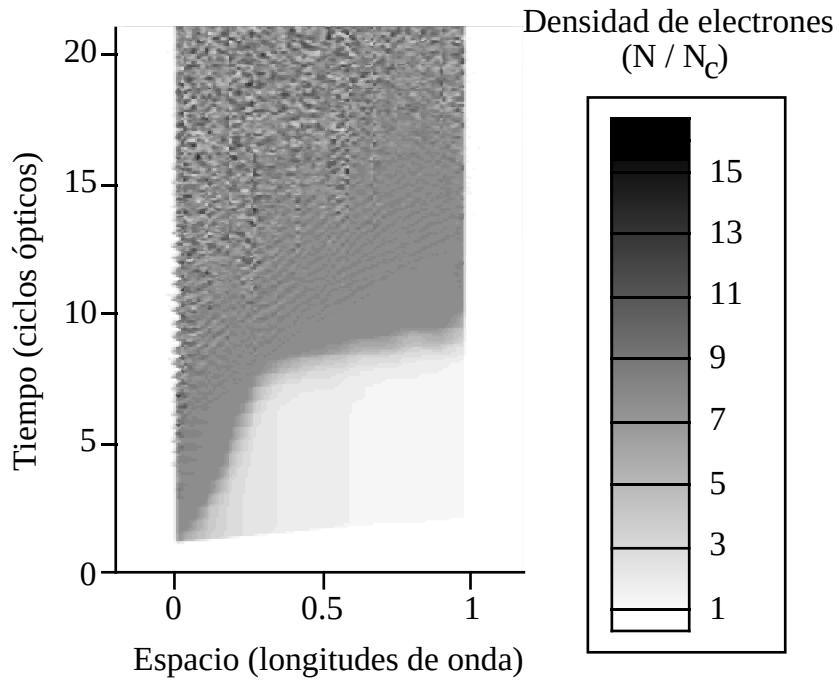


Figure 4.22: Evolution in space and time of the free electron density corresponding to the parameters in figure 4.21.

corresponds to the first intense burst in the transmitted pulse. In approximately two cycles, the amplitude of the incident field has grown enough to ionize a length greater than the penetration depth for the first harmonic, which is then reflected. This point corresponds to the first shift in frequency from $\omega_0$ to $3\omega_0$. The third harmonic, generated at the surface, propagates inside the target until the eighth cycle, when the surface layer becomes overcritical for this harmonic along a distance which exceeds the penetration depth. This point is observed at the tenth cycle of the transmitted field. After this, the plasma filters the fundamental and third harmonic, being transparent to the fifth and higher harmonics.

Another important point that we wish to highlight is that the transmitted pulses are more intense when the slab is not preionized, which is logical since the medium is initially transparent and its final effective thickness is less than the slab thickness. This has to be taken into account when estimating the transmittivity

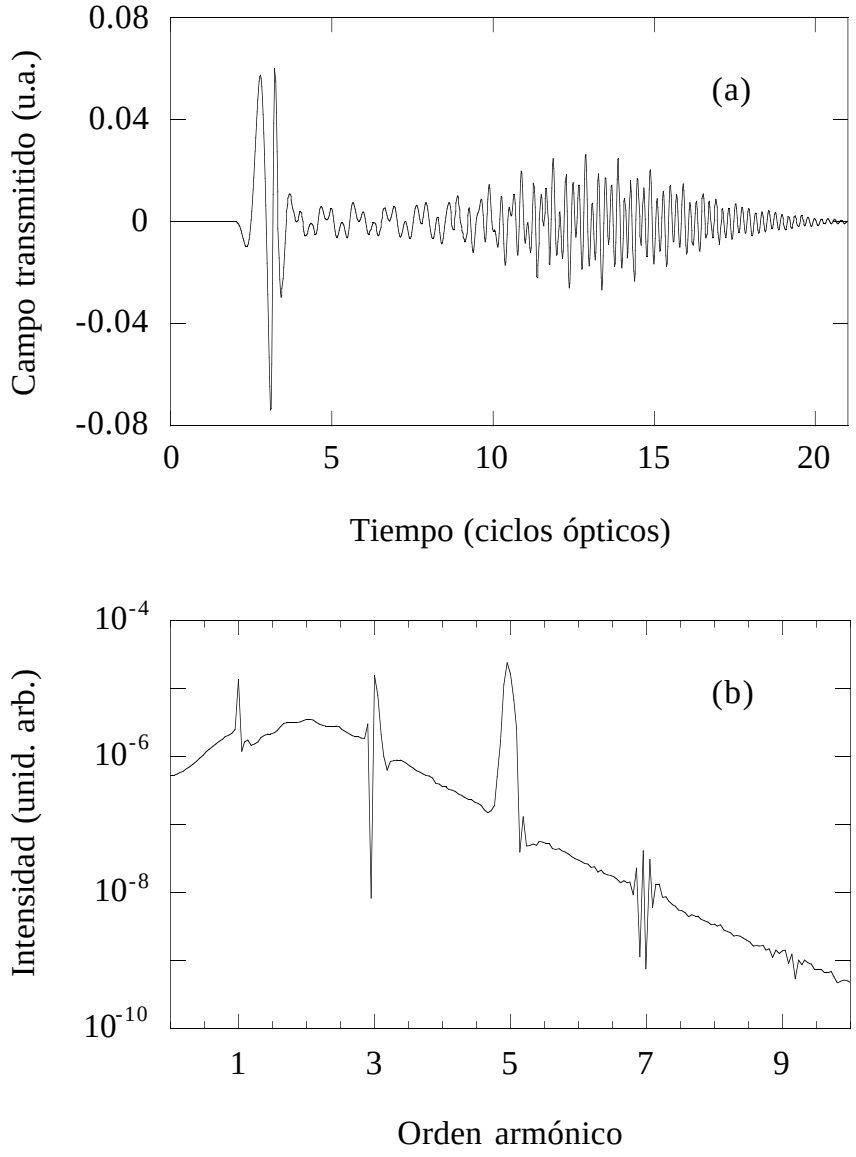


Figure 4.23: Transmitted pulse (a) and its spectrum (b) for an amplitude of $E_0 = 4$ a.u. impinging on an initially transparent slab of thickness $\lambda_0$ and density $N_0 = 15N_c$.

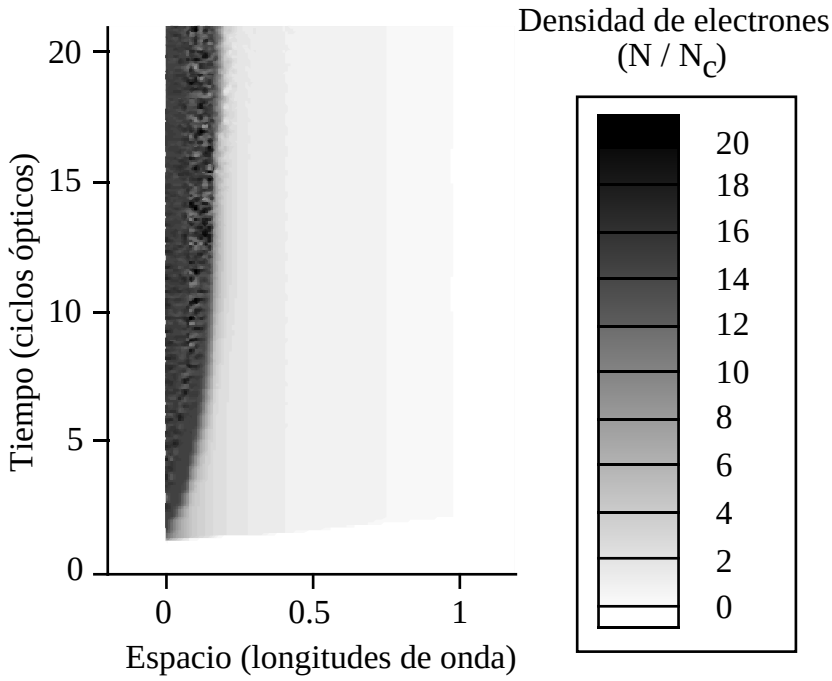


Figure 4.24: Evolution in space and time of the free electron density corresponding to the parameters in figure 4.23.

in experiments, some of which have shown a transmitted field that is much more intense than the expected value [131, 132]. This high transmittivity may also be affected by relativistic effects such as self-induced transparency due to the decrease in the effective plasma frequency caused by the growth of the electrons' inertial mass, or the hole-boring due to transversal effects, or even to the presence of strong magnetic fields created during the ionization process. However, none of these factors is able to explain such a high transmittivity for laser intensities below $10^{18}\mathrm{W/cm^2}$, which are in principle insufficient to yield these relativistic effects.

We have therefore seen that the ionization dynamics is important not only for the generation of harmonics but also for propagation in the ionized medium. This latter example of harmonic filtering can be useful to obtain pulses with special features in their temporal profile and in their frequency, and it is also a good method for measuring plasma densities.

# Conclusions

Along this work, we have examined the interaction between an intense electromagnetic field and ionizing media in an attempt to gain further insight into the generation and propagation of harmonics in such media. Our study comprises a purely theoretical aspect developed on the basis of numerical solutions of the evolution equations corresponding to each model. These models have consisted of rather drastic simplifications of reality but, nevertheless, the results obtained with them are consistent, at least qualitatively, with the results from more complicated models and even with experimental results.

Let us summarize the conclusions that can be drawn from our work

**Regarding harmonic generation in atoms [95, 96]**

We have proposed a new model which improves the standard two-level atom with the inclusion of ionization and coherent recombination.

- We have checked the importance of the time-dependence of the ionization rates in harmonic generation, a factor which had not been previously taken into account in the study of this process. The fast variation of the population of the states generates new oscillations in the dipole which result in high order harmonics. This mechanism is essential for understanding the intermediate frequencies in the spectrum.

- The addition of recombination by means of a semiclassical approach has

revealed the important role played by bound-bound transitions in the atomic harmonic spectra, even when the ionization is important, especially in the tunnelling regime. Such transitions can be said to act as resonators of the oscillations induced by the recombination of free states, amplifying them and increasing the intensity of the harmonics.

**Regarding the simulation of the interaction between intense fields and solids [104]**

- We have developed a particle code to study the evolution of a plasma. In this code, we solve Maxwell equations using the retarded potentials, thus conserving causality.

- We have implemented photoionization in our code, which has permitted us to study the dynamics of the generation of a plasma, hitherto not tackled.

- We have observed the importance of some relativistic effects which appear in simulations as a consequence of the inclusion of the retarded Liénard-Wiechert potentials. To our knowledge, these effects had not been previously mentioned.

- A simple code, which we call *fixed charge*, has been developed to study the propagation of a pulse through an ionizing medium. This model permits us to separate the effect of ionization from other effects related to collective phenomena in a plasma.

**Regarding harmonic generation in a plasma [114, 115, 118]**

Harmonics generated in a plasma can be due to two different processes: ionization and the relativistic motion of electrons. Study of both mechanisms leads us to the following conclusions:

- On studying the harmonics generated by inhomogeneous time-dependent ionization in extended media, we see that they can be detected not only in the field transmitted through underdense gases but also in the fields reflected in near-critical and overdense media.

- The relative importance of both processes has been studied, establishing the regimes in which each of them is more important. These regimes can be discriminated by the value of the ratio between the ionization time and the duration of the pulse. If the field is not intense enough to generate harmonics by the relativistic motion of electrons, ionization plays the main role since it is the only mechanism able to generate harmonics. By contrast, when the field does have enough intensity to generate relativistic harmonics, ionization is important if the time during which it is produced is at least 1/5 of the duration of the pulse. In this case, the usual assumption of considering a preformed plasma is incorrect.

**Regarding the effects of propagation [128]**

- In the case of the harmonics generated by ionization, we observed a blueshift as they propagate through the medium and a loss of visibility due to phase mismatch effects, which renders the harmonics invisible after a few wavelengths. The reflected harmonics, which propagate in vacuum, do not undergo phase mismatch and are observed more easily than the transmitted ones.

- In the case of highly dense preionized targets, we saw that the harmonics generated by the relativistic motion of electrons can be filtered and do not appear in the transmitted field if the target is thick enough. In the case of non-preionized targets, the filtering is time-dependent and changes as the pulse ionizes the medium and the free electron density increases. This results

in a transmitted pulse whose frequency is increased stepwise.

# Bibliography


[1] N. B. Delone and V. P. Krainov, *Multiphoton Processes in Atoms*, (Springer-Verlag, Berlin, 1994).

[2] A. Einstein, Ann. Physik **17**, 132 (1905). English translation in A. B. Arons and M. B. Peppard, Am. J. Phys. **33**, 367 (1965).

[3] L. V. Keldysh, Sov. Phys. JETP **20**, 1307 (1965).

[4] *Atoms in Intense Laser Fields*, M. Gavrila ed. (Academic Press, Boston, 1992).

[5] K. Burnett, V. C. Reed and P. L. Knight, J. Phys. B: At. Mol. Opt. Phys. **26**, 561 (1993).

[6] P. Moreno, *Tesis Doctoral: Generación de armónicos en H and $H_2^+$ sometidos a pulsos láser intensos*, (Universidad de Salamanca, 1996).

[7] M. Protopapas, C. H. Keitel and P. L. Knight, Rep. Prog. Phys. **60**, 389 (1997).

[8] L. A. Lompré, G. Mainfray, C. Manus and J. Thebault, Phys. Rev. A **15**, 1604 (1977).

[9] P. Agostini, F. Fabre, G. Mainfray, G. Petite and N. Rahman, Phys. Rev. Lett. **42**, 1127 (1979).

[10] L. D. Landau and E. M. Lifshitz, *Mecánica Cuántica No-Relativista*, (Reverté, Barcelona, 1972).

[11] M. Büttiker and R. Landauer, Phys. Rev. Lett. **49**, 1739 (1982).

[12] K. Rzazewski and L. Roso, Laser Physics **3**, 310 (1993).

[13] P. W. Milonni and B. Sundaram, in *Progress in Optics XXXI*, E. Wolf ed. (Elsevier, Amsterdam, 1993).

[14] V. P. Krainov, J. Opt. Soc. Am. B **14**, 425 (1997).

[15] M. V. Ammosov, N. B. Delone and V. P. Krainov, Sov. Phys. JETP **64**, 1191 (1986).

[16] F. H. M. Faisal, J. Phys. B **6**, L89 (1973).

[17] H. R. Reiss, Phys. Rev. A **22**, 1786 (1980).

[18] G. Arfken, *Mathematical Methods for Physicists*, (Academic Press, San Diego, 1985).

[19] L. Mandel and E. Wolf, *Optical Coherence and Quantum Optics*, (Cambridge University Press, Cambridge, 1995).

[20] F. A. Ilkov, J. E. Decker and S. L. Chin, J. Phys. B: At. Mol. Opt. Phys. **25**, 4005 (1992).

[21] G. E. Bayfield and P. M. Koch, Phys. Rev. Lett. **33**, 258 (1974).

[22] M. Dörr, R. M. Potvliege and R. Shakeshaft, Phys. Rev. Lett. **64**, 2003 (1990).

[23] H. A. Bethe, and E. E. Salpeter, *Quantum Mechanics of One- and Two-Electron Atoms*, (Plenum, New York, 1977).

[24] R. Shakeshaft, R. M. Potvliege, M. Dörr and W. E. Cooke, Phys. Rev. A **42**, 1656 (1990).

[25] D. Bauer, Phys. Rev. A **55**, 2180 (1997).

[26] S. Augst, D. D. Meyerhofer, D. Strickland and S. L. Chin, J. Opt. Soc. Am. B **8**, 858 (1991).

[27] P. A. Franken, A. E. Hill, C. W. Peters and G. Weinrich, Phys. Rev. Lett. **7**, 118 (1961).

[28] J. A. Armstrong, N. Bloembergen, J. Ducuing and P. S. Pershan, Phys. Rev. **127**, 1918 (1962).

[29] Z. Chang, A. Rundquist, H. Wang, M. M. Murnane and H. C. Kapteyn, Phys. Rev. Lett **79**, 2967 (1997).

[30] See P. Salières, A. L'Huillier, Ph. Antoine and M. Lewenstein, to appear in Adv. in At., Mol. and Opt. Phys., and references therein.

[31] J. D. Jackson, *Classical Electrodynamics*, (John Wiley and Sons, New York, 1975).

[32] P. M. Morse and H. Feshbach *Methods of Theoretical Physics*, (McGraw Hill, New York, 1953).

[33] G. Scharf, *From Electrostatic to Optics. A Concise Electrodynamics Course*, (Springer-Verlag, Berlin, 1994).

[34] P. L. Knight and P. W. Milonni, Phys. Rep. **66**, 21 (1980).

[35] B. W. Shore, *The Theory of Coherent Atomic Excitation*, (John Wiley and Sons, New York, 1990).

[36] B. Sundaram and P. W. Milonni, Phys. Rev. A **41**, 6571 (1990).

[37] J. D. Cresser, Phys. Rep. **94**, 47 (1983).

[38] L. Mandel and E. Wolf, *Optical Coherence and Quantum Optics*, (Cambridge University Press, Cambridge, 1995).

[39] F. I. Gauthey, C. H. Keitel, P. L. Knight and A. Maquet, Phys. Rev. A **52**, 525 (1995).

[40] K. J. LaGattuta, J. Mod. Opt. **39**, 1181 (1992).

[41] K. Burnett, V. C. Reed, J. Cooper and P. L. Knight, Phys. Rev. A **45**, 3347 (1992).

[42] J. L. Krause, K. J. Schafer and K. C. Kulander, Phys. Rev. A **45**, 4998 (1992).

[43] K. J. LaGattuta, Phys. Rev. A **48**, 666 (1993).

[44] J. Parker, K. T. Taylor, C. W. Clark, and S. Blodgett-Ford, J. Phys. B: At. Mol. Opt. Phys. **29**, L33 (1996).

[45] K. T. Taylor, J. S. Parker, D. Dundas, E. Smyth and S. Vivirito, in *Multiphoton Processes 1996*, P. Lambropoulos and H. Walther eds. (IOP Publishing, London, 1997).

[46] H. B. van Linden van den Heuvell and H. G. Muller, in *Multiphoton Processes*, S. J. Smith and P. L. Knight eds., (Cambridge University Press, Cambridge, 1988).

[47] T. F. Gallagher, Phys. Rev. Lett. **61**, 2304 (1988).

[48] P. B. Corkum, Phys. Rev. Lett **71**, 1994 (1993).

[49] K. C. Kulander and K. J. Schafer, in *Proc. Int. Conf. Multiphoton Processes VI*, D. K. Evans ed. (World Scientific, Singapur, 1993).

[50] P. Moreno, L. Plaja, V. Malyshev and L. Roso, Phys. Rev. A **51**, 4746 (1995).

[51] M. Lewenstein, Ph. Balcou, M. Yu. Ivanov, A. L'Huillier and P. B. Corkum, Phys. Rev. A **49**, 2117 (1994).

[52] K. C. Kulander, Phys. Rev. A **35**, 445 (1987).

[53] K. C. Kulander, Phys. Rev. A **36**, 778 (1988).

[54] P. L. DeVries, J. Opt. Soc. Am. B **7**, 517 (1990).

[55] K. J. LaGattuta, J. Opt. Soc. Am. B **7**, 639 (1990).

[56] A. Sanpera, *PhD Thesis: Theoretical Study of the Photoionization of Isolated Atoms by Intense Laser Pulses*, (Universitat Autònoma de Barcelona, 1992).

[57] U. Schwengelbeck and F. H. M. Faisal, Phys. Rev. A **50**, 632 (1994).

[58] J. Javanainen, J. H. Eberly and Q. Su, Phys. Rev. A **38**, 3430 (1988).

[59] Q. Su and J. H. Eberly, J. Opt. Soc. Am. B **7**, 564 (1990).

[60] Q. Su, J. H. Eberly and J. Javanainen, Phys. Rev. Lett. **64**, 862 (1990).

[61] Q. Su and J. H. Eberly, Phys. Rev. A **44**, 5997 (1991).

[62] Q. Su, *PhD Thesis: Ionization of a model atomic system by short intense laser pulses*, (University of Rochester, 1991).

[63] E. S. Sarachik and G. T. Schappert, Phys. Rev. A **1**, 2738 (1970).

[64] P. Gibbon, IEEE J. Quantum Electronics **33**, 1915 (1997).

[65] C. H. Keitel, C. Szymanowski, P. L. Knight and A. Maquet, J. Phys. B: At. Mol. Opt. Phys. **31**, L75 (1998).

[66] X. F. Li, A. L'Huillier, M. Ferray, L. A. Lompré and G. Mainfray, Phys. Rev. A **39**, 5751 (1989).

[67] A. L'Huillier, X. F. Li and L. A. Lompré, J. Opt. Soc. Am. B **7**, 527 (1990).

[68] A. L'Huillier, Ph. Balcou, S. Candel, K. J. Schafer and K. C. Kulander, Phys. Rev. A **46**, 2778 (1992).

[69] A. L'Huillier, L. A. Lompré, G. Mainfray and C. Manus, en *Atoms in Intense Laser Fields*, M. Gavrila ed. (Academic Press, Boston, 1992).

[70] M. Ll. Pons and L. Plaja, J. Mod. Opt. **43**, 1939 (1996).

[71] A. E. Siegman, *Lasers*, (University Science Books, Mill Valley, 1986).

[72] M. Born and E. Wolf, *Principles of Optics*, (Pergamon Press, Oxford, 1989).

[73] U. Mohideen, H. W. K. Tom, R. R. Freeman, J. Bokor and P. H. Bucksbaum, J. Opt. Soc. Am. B **12**, 2190 (1992).

[74] W. L. Kruer *The Physics of Laser Plasma Interactions*, (Addison-Wesley, New York, 1988).

[75] *Superstrong Fields in Plasmas*, M. Lontano, G. Mourou, F. Pegoraro and E. Sindoni eds., (AIP Conference Proceedings 426, New York, 1998).

[76] J. N. Bardsley, B. M. Penetrante and M. H. Mittleman, Phys. Rev. A **40**, 3823 (1989).

[77] P. Sprangle, E. Esarey and A. Ting, Phys. Rev. A **41**, 4463 (1990).

[78] N. H. Burnett, H. A. Baldis, M. C. Richardson and G. D. Enright, Appl. Phys. Lett. **31**, 172 (1977).

[79] R. L. Carman, D. W. Forslund and J. M. Kindel, Phys. Rev. Lett. **46**, 29 (1981).

[80] R. L. Carman, C. K. Rhodes and R. F. Benjamin, Phys. Rev. A **24**, 2649 (1981).

[81] P. A. Norreys, M. Zepf, S. Moustaizis, A. P. Fews, J. Zhang, P. Lee, M. Bakazeros, C. N. Danson, A. Dyson, P. Gibbon, P. Loukakos, D. Neely, F. N. Walsh, J. S. Wark and A. E. Dangor, Phys. Rev. Lett. **76**, 1832 (1996).

[82] S. C. Wilks, W. L. Kruer and W. B. Mori, IEEE Trans. Plasma Sci. **21**, 120 (1993).

[83] S. V. Bulanov, N. M. Naumova and F. Pegoraro, Phys. Plasmas **1**, 745 (1994).

[84] P. Gibbon, Phys. Rev. Lett. **76**, 50 (1996).

[85] R. Lichters, J. Meyer-ter-Vehn and A. Pukhov, Phys. Plasmas **3**, 3425 (1996).

[86] D. von der Linde and K. Rzazewski, Appl. Phys. B **63**, 499 (1996).

[87] K. Rzazewski, private communication.

[88] L. Allen and J. H. Eberly, *Optical Resonance and Two-level Atoms*, (Dover Publications, New York, 1987).

[89] L. Plaja, *PhD Thesis: A Theoretical Study on Optical High-Order Harmonic Generation in Three Matter Models*, (Universitat Autònoma de Barcelona, 1993).

[90] F. Gauthey, *Thèse de Doctorat: Modélisation théorique de la réponse d'un atome soumis à un champ laser très intense à l'aide de systèmes simples*, (Université Paris 6, 1996).

[91] J. B. Watson, A. Sanpera, X. Chen and K. Burnett, Phys. Rev. A **53**, R1962 (1996).

[92] A. Sanpera, J. B. Watson, M. Lewenstein and K. Burnett, Phys. Rev. A **54**, 4320 (1996).

[93] W. H. Press, S. A. Teukolsky, W. T. Vetterling and B. P. Flannery, *Numerical Recipes in C: The Art of Scientific Computing*, (Cambridge University Press, Cambridge, 1992).

[94] V. P. Krainov and Z. S. Mulyukov, Laser Phys. **4**, 544 (1994).

[95] E. Conejero Jarque and L. Plaja, J. Opt. Soc. Am. B **13**, 2724 (1996).

[96] E. Conejero Jarque and L. Plaja, J. Phys. B: At. Mol. Opt. Phys., **31**, 1687 (1998).

[97] M. Protopapas, D. G. Lappas, C. H. Keitel and P. L. Knight, Phys. Rev. A **53**, R2933 (1996).

[98] J. B. Watson, A. Sanpera, K. Burnett and P. L. Knight, Phys. Rev. A **55**, 1224 (1997).

[99] D. Richards, J. Phys. B: At. Mol. Opt. Phys. **29**, 2925 (1996).

[100] W. Becker, S. Long and J. K. McIver, Phys. Rev. A **50**, 1540 (1994).

[101] C. K. Birdsall and A. B. Langdon, *Plasma Physics via Computer Simulation*, Plasma Physics Series (IOP Publishing, Bristol, 1991).

[102] J. M. Dawson, Rev. Mod. Phys. **55**, 403 (1983).

[103] *Proceedings of the 16th International Conference on the Numerical Simulation of Plasmas*, V. Decyk ed. (Santa Barbara, 1998).

[104] L. Plaja and E. Conejero Jarque, accepted for publication in Phys. Rev. E.

[105] L. D. Landau and E. M. Lifshitz, *Teoría Clásica de los Campos*, (Reverté, Barcelona, 1981).

[106] K. Huang, *Statistical Mechanics*, (John Wiley and Sons, New York, 1987).

[107] S. C. Rae and K. Burnett, Phys. Rev. A **46**, 1084 (1992).

[108] K. L. Bell, H. B. Gilbody, J. G. Hughes, A. E. Kingston and F. J. Smith, J. Phys. Chem. Ref. Data **12**, 891 (1983).

[109] M. A. Lennon, K. L. Bell, H. B. Gilbody, J. G. Hughes, A. E. Kingston, M. J. Murray and F. J. Smith, J. Phys. Chem. Ref. Data **17**, 1285 (1988).

[110] B. M. Penetrante, J. N. Bardsley, W. M. Wood, C. W. Siders and M. C. Downer, J. Opt. Soc. Am. B **9**, 2032 (1992).

[111] G. J. Pert, Phys. Rev. E **51**, 4778 (1995).

[112] F. Brunel, J. Opt. Soc. Am. B **4**, 521 (1990).

[113] S. C. Rae and K. Burnett, J. Phys. B: At. Mol. Opt. Phys. **26**, 1509 (1993).

[114] V. Malyshev, E. Conejero Jarque and L. Roso, J. Opt. Soc. Am. B **14**, 163 (1997).

[115] E. Conejero Jarque, V. Malyshev and L. Roso, J. Mod. Opt. **44**, 563 (1997).

[116] A. Bendib, A. Tahraoui, K. Kalache, P. Chessa and P. Mora, Opt. Commun. **142**, 146 (1997).

[117] W. P. Leemans, C. E. Clayton, W. B. Mori, K. A. Marsh, P. K. Kaw, A. Dyson, C. Joshi and J. M. Wallace, Phys. Rev. A **46**, 1091 (1992).

[118] E. Conejero Jarque and L. Plaja, submitted for publication.

[119] E. Yablonovitch, Phys. Rev. A **10**, 1888 (1974).

[120] E. Yablonovitch, Phys. Rev. Lett. **60**, 795 (1988).

[121] E. V. Vanin, A. V. Kim, A. M. Sergeev and M. C. Downer, JETP Lett. **58**, 900 (1993).

[122] W. M. Wood, G. Focht and M. C. Downer, Opt. Lett. **13**, 984 (1988).

[123] W. M. Wood, C. W. Siders and M. C. Downer, Phys. Rev. Lett. **67**, 3523 (1991).

[124] C. W. Siders, N. C. Turner III, M. C. Downer, A. Babine, A. Stepanov and A. M. Sergeev, J. Opt. Soc. Am. B **13**, 330 (1996).

[125] S. C. Wilks, J. M. Dawson and W. B. Mori, Phys. Rev. Lett. **61**, 337 (1988).

[126] W. B. Mori, Phys. Rev. A **44**, 5118 (1991).

[127] R. L. Savage Jr., C. Joshi and W. B. Mori, Phys. Rev. Lett. **68**, 946 (1992).

[128] E. Conejero Jarque and L. Plaja, submitted for publication.

[129] R. Lichters and J. Meyer-ter-Vehn, en *Multiphoton Processes 1996*, P. Lambropoulos and H. Walther eds. (IOP Publishing, London, 1997).

[130] W. Theobald, R. Häßner, C. Wülker and R. Sauerbrey, Phys. Rev. Lett. **77**, 298 (1996).

[131] D. Giulietti, L. A. Gizzi, A. Giulietti, A. Macchi, D. Teychenné, P. Chessa, A. Rousse, G. Cheriaux, J. P. Chambaret and G. Darpentigny, Phys. Rev. Lett. **79**, 3194 (1997).

[132] J. Fuchs, J. C. Adams, F. Aminaroff, S. D. Baton, P. Gallant, L. Gremillet, A. Héron, J. C. Kieffer, G. Laval, G. Malka, J. L. Miquel, P. Mora, H. Pépin and C. Rosseaux, Phys. Rev. Lett. **80**, 2326 (1998).